Analysis of Pole-Type Structures of Fibre-Reinforced Plastics by Finite Element Method

by

Zhi-Min Lin

A Thesis

Submitted to the Faculty of Graduate Studies

in Partial Fulfillment of the Requirements

for the Degree of

Doctor of Philosophy

Department of Civil and Geological Engineering

University of Manitoba

Winnipeg, Manitoba, Canada

ISBN 0-612-13300-1

Canada

Name _____

Dissertation Abstracts International is arranged by broad, general subject categories. Please select the one subject which most nearly describes the content of your dissertation. Enter the corresponding four-digit code in the spaces provided.

Applied Mechanics
SUBJECT TERM

0346
SUBJECT CODE

U·M·I

Subject Categories

THE HUMANITIES AND SOCIAL SCIENCES

COMMUNICATIONS AND THE ARTS
Architecture 0729
Art History 0377
Cinema 0900
Dance 0378
Fine Arts 0357
Information Science 0723
Journalism 0391
Library Science 0399
Mass Communications 0708
Music 0413
Speech Communication 0459
Theater 0465

EDUCATION
General 0515
Administration 0514
Adult and Continuing 0516
Agricultural 0517
Art 0273
Bilingual and Multicultural 0282
Business 0688
Community College 0275
Curriculum and Instruction 0727
Early Childhood 0518
Elementary 0524
Finance 0277
Guidance and Counseling 0519
Health 0680
Higher 0745
History of 0520
Home Economics 0278
Industrial 0521
Language and Literature 0279
Mathematics 0280
Music 0522
Philosophy of 0998
Physical 0523
Psychology 0525
Reading 0535
Religious 0527
Sciences 0714
Secondary 0533
Social Sciences 0534
Sociology of 0340
Special 0529
Teacher Training 0530
Technology 0710
Tests and Measurements 0288
Vocational 0747

LANGUAGE, LITERATURE AND LINGUISTICS
Language
- General 0679
- Ancient 0289
- Linguistics 0290
- Modern 0291

Literature
- General 0401
- Classical 0294
- Comparative 0295
- Medieval 0297
- Modern 0298
- African 0316
- American 0591
- Asian 0305
- Canadian (English) 0352
- Canadian (French) 0355
- English 0593
- Germanic 0311
- Latin American 0312
- Middle Eastern 0315
- Romance 0313
- Slavic and East European 0314

PHILOSOPHY, RELIGION AND THEOLOGY
Philosophy 0422
Religion
- General 0318
- Biblical Studies 0321
- Clergy 0319
- History of 0320
- Philosophy of 0322

Theology 0469

SOCIAL SCIENCES
American Studies 0323
Anthropology
- Archaeology 0324
- Cultural 0326
- Physical 0327

Business Administration
- General 0310
- Accounting 0272
- Banking 0770
- Management 0454
- Marketing 0338

Canadian Studies 0385
Economics
- General 0501
- Agricultural 0503
- Commerce-Business 0505
- Finance 0508
- History 0509
- Labor 0510
- Theory 0511

Folklore 0358
Geography 0366
Gerontology 0351
History
- General 0578
- Ancient 0579
- Medieval 0581
- Modern 0582
- Black 0328
- African 0331
- Asia, Australia and Oceania 0332
- Canadian 0334
- European 0335
- Latin American 0336
- Middle Eastern 0333
- United States 0337

History of Science 0585
Law 0398
Political Science
- General 0615
- International Law and Relations 0616
- Public Administration 0617

Recreation 0814
Social Work 0452
Sociology
- General 0626
- Criminology and Penology 0627
- Demography 0938
- Ethnic and Racial Studies 0631
- Individual and Family Studies 0628
- Industrial and Labor Relations 0629
- Public and Social Welfare 0630
- Social Structure and Development 0700
- Theory and Methods 0344

Transportation 0709
Urban and Regional Planning 0999
Women's Studies 0453

THE SCIENCES AND ENGINEERING

BIOLOGICAL SCIENCES
Agriculture
- General 0473
- Agronomy 0285
- Animal Culture and Nutrition 0475
- Animal Pathology 0476
- Food Science and Technology 0359
- Forestry and Wildlife 0478
- Plant Culture 0479
- Plant Pathology 0480
- Plant Physiology 0817
- Range Management 0777
- Wood Technology 0746

Biology
- General 0306
- Anatomy 0287
- Biostatistics 0308
- Botany 0309
- Cell 0379
- Ecology 0329
- Entomology 0353
- Genetics 0369
- Limnology 0793
- Microbiology 0410
- Molecular 0307
- Neuroscience 0317
- Oceanography 0416
- Physiology 0433
- Radiation 0821
- Veterinary Science 0778
- Zoology 0472

Biophysics
- General 0786
- Medical 0760

EARTH SCIENCES
Biogeochemistry 0425
Geochemistry 0996
Geodesy 0370
Geology 0372
Geophysics 0373
Hydrology 0388
Mineralogy 0411
Paleobotany 0345
Paleoecology 0426
Paleontology 0418
Paleozoology 0985
Palynology 0427
Physical Geography 0368
Physical Oceanography 0415

HEALTH AND ENVIRONMENTAL SCIENCES
Environmental Sciences 0768
Health Sciences
- General 0566
- Audiology 0300
- Chemotherapy 0992
- Dentistry 0567
- Education 0350
- Hospital Management 0769
- Human Development 0758
- Immunology 0982
- Medicine and Surgery 0564
- Mental Health 0347
- Nursing 0569
- Nutrition 0570
- Obstetrics and Gynecology 0380
- Occupational Health and Therapy 0354
- Ophthalmology 0381
- Pathology 0571
- Pharmacology 0419
- Pharmacy 0572
- Physical Therapy 0382
- Public Health 0573
- Radiology 0574
- Recreation 0575
- Speech Pathology 0460
- Toxicology 0383

Home Economics 0386

PHYSICAL SCIENCES
Pure Sciences
Chemistry
- General 0485
- Agricultural 0749
- Analytical 0486
- Biochemistry 0487
- Inorganic 0488
- Nuclear 0738
- Organic 0490
- Pharmaceutical 0491
- Physical 0494
- Polymer 0495
- Radiation 0754

Mathematics 0405
Physics
- General 0605
- Acoustics 0986
- Astronomy and Astrophysics 0606
- Atmospheric Science 0608
- Atomic 0748
- Electronics and Electricity 0607
- Elementary Particles and High Energy 0798
- Fluid and Plasma 0759
- Molecular 0609
- Nuclear 0610
- Optics 0752
- Radiation 0756
- Solid State 0611

Statistics 0463

Applied Sciences
Applied Mechanics 0346
Computer Science 0984
Engineering
- General 0537
- Aerospace 0538
- Agricultural 0539
- Automotive 0540
- Biomedical 0541
- Chemical 0542
- Civil 0543
- Electronics and Electrical 0544
- Heat and Thermodynamics 0348
- Hydraulic 0545
- Industrial 0546
- Marine 0547
- Materials Science 0794
- Mechanical 0548
- Metallurgy 0743
- Mining 0551
- Nuclear 0552
- Packaging 0549
- Petroleum 0765
- Sanitary and Municipal 0554
- System Science 0790

Geotechnology 0428
Operations Research 0796
Plastics Technology 0795
Textile Technology 0994

PSYCHOLOGY
General 0621
Behavioral 0384
Clinical 0622
Developmental 0620
Experimental 0623
Industrial 0624
Personality 0625
Physiological 0989
Psychobiology 0349
Psychometrics 0632
Social 0451

ANALYSIS OF POLE TYPE STRUCTURES OF FIBRE-REINFORCED PLASTICS BY FINITE ELEMENT METHOD

BY

ZHI-MIN LIN

A Thesis submitted to the Faculty of Graduate Studies of the University of Manitoba in partial fulfillment of the requirements of the degree of

DOCTOR OF PHILOSOPHY

ABSTRACT

Fibre-reinforced plastics (FRP) are becoming increasingly popular in the engineering applications as alternative to conventional engineering materials. The unique characteristics of FRP, such as their light weight, their resistance to corrosion, and the lower cost of construction and maintenance, are very promising in the application of FRP in civil engineering. One such application is the replacement of power transmission poles, traditionally made of either concrete, steel, or wood, by FRP poles.

This thesis deals with the finite element analysis of fiber-reinforced plastic poles. Using the principle of stationary potential energy and Novozhilov's derivations of nonlinear strains, tapered FRP poles are treated as conical shells and a semi-analytical finite element model based on the theory of shell of revolution is developed. The computer program based on the finite element model developed can be used to perform: a) a linear static analysis, b) a linear buckling (bifurcation) analysis, c) a linear $P-\Delta$ analysis, d) a geometrically nonlinear (large deflection) analysis of beam-column-type bending, and e) an ovalization analysis.

Solution methods of the nonlinear system of equations are discussed. Based on the augmented equation method, external and internal potential control schemes are proposed and evolved into incremental work control and incremental strain energy control. These controls are proven to have good capability to traverse a limit point.

For slender poles, the nonlinear behaviour of beam-column type bending is more important. This type of nonlinear analysis requires the proper handling of the rigid-body rotation. A method is proposed to include the rigid-body mode in the analysis.

The ovalization of cylindrical poles is investigated numerically. The analysis involves the inclusion of all second-order Fourier terms in the displacement functions. It is demonstrated in this thesis that ovalization can significantly decrease the load carrying capacities of cylindrical poles.- The linear stability and the $P-\Delta$ analyses are considered to be simplifications of the nonlinear analysis of beam-column type bending. Assumptions and conditions which enable the simplifications are also discussed. The linear analysis is the simplest analysis and is applicable for small displacements. Behaviors of FRP poles with different material configurations, geometries, loading and boundary conditions are investigated using the linear analysis. The numerical results from the proposed analyses are compared with limited experimental data and with analytical results.

Acknowledgements

The author wishes to express his deepest gratitude to his advisor, Prof. D. Polyzois, for suggesting this research topic and providing constant supervision and guidance during this study. Invaluable support received from Prof. Polyzois is greatly appreciated.

The author is extremely thankful to Prof. A. H. Shah for serving as co-advisor and dedicating his expertise to this thesis. Suggestions, inspirations and encouragement from Prof. Shah are specially appreciated.

Sincere thanks are extended to Prof. M. L. Ayari for his fruitful suggestions and serving as the committee member.

The author deeply appreciates the assistance received from Prof. Q. Zhang when pursuing this graduate study program.

Grateful acknowledgements are due to Mr. W. Haldane-Wilson for conducting the experimental work of fibre-reinforced plastic poles; Mr. K. Church, FAROEX Ltd., for donating test specimens; Mr. C. Wang, Manitoba Hydro, for his keen interests in this research study.

Financial support in the form of a research assistantship from the NSERC research grant of Prof. Polyzois, a research grant from Manitoba Hydro, a graduate fellowship from The University of Manitoba, and a teaching assistantship from the Department of Civil & Geological Engineering enable the author to pursue his graduate studies. They are kindly acknowledged.

The author wishes to convey sincere thanks to his wife, Li Qiao, for her understanding and moral support during the course of this study. Special thanks are due to the author's daughter, Yujie, for her patience and cheerful encouragement.

Finally, the author respectfully dedicates this thesis to his parents who taught him persistence and honesty which helped him to achieve his success.

Zhimin Lin
Winnipeg, Canada
September 25, 1995

Table of Contents

Chapter 1. Introduction

1.1. Background to the Research Investigation

The use of fibre-reinforced plastics (FRP) in civil engineering applications has grown rapidly over the last few years. This growth is mainly contributed to some excellent characteristics, strength, stiffness, and low weight, of the fibres used (Schwartz 1984). The outstanding characteristics combined with the flexibility in design capability, ease of fabrication and transportation, and corrosion resistance of FRP have distinguished them as the material of the 21th century.

Application of FRP began in the 1940s (Ballinger 1990). The early applications of FRP was for military airplanes and equipment because of the weight advantage these materials provide. Today, industries such as aircraft, automobile, sports goods, electronics and others are quite dependent on the use of fibre-reinforced plastics. The cost of FRP has dropped significantly over the last few years to the point where they are now comparable to conventional materials, such as steel and aluminum. This lower cost promises even more broader range of applications of FRP in other industries, such as agricultural machineries, telecommunication structures, transportation equipment, storage tanks etc.

Fibre-reinforced plastics are also becoming more popular in the civil engineering community. FRP gratings, for example, are used for walkways, stair steps (Plecnik 1992), as well as filtration system for facilities such as water treatment plants, swimming pools, and aquariums mainly because of their corrosion resistant characteristic. Buildings with FRP members as primary load carrying structure components, have been also built (Green 1987). The electromagnetic transparency of FRP makes them ideal for radomes in protecting radar installations from severe weather conditions. Oil companies utilize FRP products in a number of applications ranging from simple roof trusses to very sophisticated structures such as offshore oil drilling platforms. Concrete bridges with FRP tendons have been built in Japan, China, Canada, and the United States (Mufti, et al 1991). Significant research on this area is also widespread. Research topics involve both theoretical and experimental investigations of long term and short term strength, large deformation and stability, failure mechanism, the influence of the lay-up of fibres, numerical analysis method and computer-aided design.

The application of FRP in the construction of poles has been limited to fiberglass light poles. The majority of poles, however are still being constructed from traditional materials such as wood,

concrete, and steel. The motivation for the replacement of traditional poles is manifold. First, the shortage in long wood poles with large capacity, along with a numbers of environmental concerns have motivated the search for alternatives. Secondly, poles made of either wood, concrete or steel are subject to deterioration under environmental attacks. Regular maintenance is necessary in order to prolong serviceability. For example, continuous exposure of wood poles to weather, fungi, woodpeckers, accidents, etc., result in structures with capacities that often deteriorate very significantly with time in service. The service life of wooden poles is approximately 20 years (Vanderbuilt and Criswell, 1988) and any extension of this service life requires continuous and systematic inspection and expensive follow-up care. The main disadvantage of using concrete poles is their high weight which drastically increases the transportation and erection costs which can be as much as 60% higher than those of wooden poles. Chemical influences on the concrete surfaces due to environmental impact can also influence the capacity and service life of concrete poles. Concrete poles develop cracks and the steel reinforcement corrodes. Steel poles need to be painted or galvanized which, coupled with low temperatures, could result in a brittle behaviour. Fibre-reinforced plastic poles, on the other hand, are light-weight and corrosion resistant. While the material cost of FRP poles may be high, the overall cost of FRP poles, including manufacturing, transportation, erection and maintenance, could be much less than that of traditional poles. Therefore, FRP poles are very good candidates for replacing traditional poles.

The major weaknesses of FRP poles are a high initial cost and a low stiffness. Reduction of the initial cost is a long term process and involves multi-disciplinary efforts. The problem associated with a lower stiffness, such as excessive deformation and instability is more technical and must be addressed before any consideration for practical use of FRP poles is given.

Under a large deflection, the classical linear beam-column theory may no longer be adequate for the analysis and design of FRP poles. A rigorous geometric nonlinear analysis which takes into account the large displacement has to be performed in order to predict accurately the mechanical behaviour of those poles. Due to the complexity of material properties, layer lay-ups, fibre orientations, combination of loads and boundary conditions, the pure analytical method is incapable of providing acceptable solutions effectively. Semi-analytical and semi-numerical methods, on the other hand, are proved to be very effective.

To achieve, approximately, a uniform strength, transmission poles whose basic loading consists of both an axial load and a transverse load, are tapered. The taper angles are very small (less than

3°), while the height-to-radius ratios range from 20 to 100. Thus, the overall behaviour of transmission poles is that of a beam-column type. The analyses of the beam-column behaviour of FRP poles, such as linear buckling, nonlinear post-buckling and large deformation, are primary issues.

Except for wooden poles, concrete, steel and FRP poles are hollow sections. The relatively small thickness-to-radius ratio and the high stress near the ground level of FRP poles may result in distortion of the cross-section which in turn could significantly influence their load carrying capacity. A typical distortion is the so-called ovalization, which further increases the stress level and induces local buckling. The beam-column theory can not account for the deformation of the cross-section. This kind of behaviour which leads to a reduction in the load bearing capacity can be modeled using shell theory. Ovalization may become the leading factor in determining the ultimate load of FRP poles and must be included in the analysis of FRP poles.

1.2. Review of Related Literature

The application of FRP for transmission poles was proposed in mid 1970's (Tang and Adams 1973). Untreated full-size wood poles used in transmission lines were laminated with reinforced plastics over their entire length. Static and dynamic mechanical tests were conducted. Tests showed that full-length-jacketed poles exhibited an increase in bending stiffness of approximately 16 percent in comparison with that of unjacketed poles. The principal advantages of composite poles seemed to be greater strength, resistance to deterioration, and better appearance.

A market research for a possible application of FRP lighting poles was carried out by Marting and Richter (1974). Technical research was also conducted. Two aluminum poles and seven FRP poles were tested. Test results showed that the load-deflection of fibre glass poles was near linear up to failure which, in this case, was due to local section collapse (buckling) a few inches above ground level on the compression side of the pole. Marting and Richter also concluded that fibre glass poles can be designed so that their stiffness and strength are equal to those of their aluminum counterparts with little or possibly no weight penalties. However, this level of performance can only be attained through reinforcement orientation and effective pole size design.

A similar technical testing and market research study was conducted jointly by the Canadian Electrical Association (CEA) and ABCD plastics (Escher; G.A. 1982). Issues for design and manufacturing of FRP transmission poles were discussed. Through the market research study, the report concluded that FRP poles for electrical distribution and transmission purpose have an unat-

tractive competitive position in comparison to wood poles but not to concrete utility poles.

In 1988, Bell initiated its own investigation of fibre-reinforced plastic poles. Tests were carried out at the Centre de Recherche du Reseau Exterior (CERRE) (Mclure and Boire 1992). The prototype tested was a truncated hollow circular cone made of fibre glass reinforced polyester unsaturated resin and fabricated by centrifugal casting. The tests demonstrated that the product could safely resist loads comparable to those of wood poles under the same conditions, and its behaviour was truly elastic even for very large deflections. In the tests, stiffness was insufficient, but researchers pointed out that this could be increased without difficulty. Failure of the poles was mainly caused by ovalization of the cross-section, degenerating in local instability in the compression zone.

The theoretical investigation of fibre-reinforced plastic poles are very limited. To analyze FRP poles, the theory of shell of revolution may be used since tapered FRP poles can be considered as rotational shells. The governing equations of rotational shells can be derived by the principle of virtual work and the principle of stationary potential energy. The derivation of the governing equations may involve the first and second variation of a functional. The definitions of the first and second variation of a functional can be found in the book by Gelfand and Formin (1963).

Navaratna et al (1968) were among the early researchers to use the finite element method to analyze the stability of shells of revolution. The approach used by Navaratna et al to develop the geometric stiffness matrix was followed by Gould and Basu (1977) for linear buckling analysis and incremental deformation analysis of rotational shells. Ugural and Cheng (1968) investigated the linear buckling of composite cylindrical shells under pure bending. Holston (1968) investigated the buckling of filament-wound cylinder under axil compression. Gould (1985) dedicated the subject of finite element analysis of shells of revolution in his book. Fourier series were employed to represent displacement functions of rotational shells. Noor et al (1991) assessed a group of computational methods for multilayered composite cylinders. The finite element models they surveyed are mostly two or three dimensional elements. Khdeir et al (1989) studied the vibration and buckling of cross-ply circular cylindrical shells with various shell theories. The different approaches of inclusion of transverse shear strains were discussed.

Most of the research work discussed above falls into the category of linear analysis. Wood and Zienkiewicz (1977) discussed general procedures for geometric nonlinear analysis of beams, frames, arches and axisymmetric shells. Bushnell (1984) presented a thorough study of governing

equations of shells for computerized linear as well nonlinear analysis. He does not, however, address the application of these governing equations to FRP shells. Some work on the nonlinear dynamic analysis of shells of revolution using matrix displacement method was conducted by Stricklin et al (1971). A self-correction method for the solution procedures of nonlinear structural analysis was later proposed by Stricklin and Haisler (1977). The fundamental finite element formulations for large deformation analysis can be found in the paper by Bathe et al (1975).

1.3. Objectives and Scope of the Research Investigation

The objective of this research study was to develop a semi-analytical and semi-numerical model for the analysis of tapered hollow FRP poles. The principle of stationary potential energy is employed to establish equilibrium and stability conditions. To account for not only the beam-column-type but also the shell-type behaviour, the theory of shell of revolution is utilized. Novozhilov's strain expressions (Novozhilov, 1961) are used in the formulations of strain energy. Geometric nonlinearity is considered and arbitrary large displacements are permitted in the analyses. The finite element method is used in the longitudinal (axial) dimension only. Analyses tasks such as linear static, linear buckling, $P-\Delta$ effect, post-buckling, large deformation and ovalization are performed using the developed computer programs.

This thesis consists of eight chapters. Chapter 1 is an introduction which presents the background of the research, review of related literature and the objectives of the research program. Chapter 2 describes the fundamental formulations for nonlinear analysis of FRP poles. These formulations form the basis for the analyses discussed in Chapter 3 through Chapter 7. Chapter 3 is dedicated to the solution method of nonlinear system of equations. Emphasis is placed on the selection of increment control schemes which are the cornerstone of the primary solution method, the augmented equation method. Control schemes based on the potential energy are proposed and example of a one-dimensional problem is presented. Chapter 4 covers the nonlinear analysis of beam-type bending of FRP poles. Examples with post-buckling and large deformation behaviours of various poles are presented. Chapter 5 is concerned with the ovalization of FRP poles. Chapter 6 deals with the linear stability of FRP poles and includes the $P-\Delta$ analyses. These analyses are considered to be simplifications of the nonlinear analysis discussed in Chapter 4. Chapter 7 involves the linear static analysis. Many examples are presented to demonstrate the behaviour of FRP poles with different material configurations, geometries, loadings and boundary conditions. Comparisons of the results from the linear analysis are made with the results from the nonlinear analysis in some selected cases.The numerical results from the proposed analysis are also com-

pared with the experimental and analytical results. Finally, in Chapter 8 the general conclusions and recommendations for future research are presented.

Chapter 2. Fundamental Formulations

2.1. Basic Constitutive Equations for FRP

Composite materials are materials composed of two or more chemically distinct constituents. Fibre-Reinforced Plastics are composites where matrix resin and fibres are combined to form a completely new material. The matrix resin is a type of polymer which binds the fibres together. Its mechanical properties are the same as those of a typical polymer, hence the term "plastic". The primary function of the matrix is to bind and protect the fibres which bear the strength of the whole composite. Isophthalic polyester is a common type of resin used in the industry today. However, other esters of different characteristics may be used depending on the application requirements.

The fibres are the constituent that carry the loads applied to the material. They provide the stiffness, strength, and as the name implies, reinforcement to the matrix. These fibres can be: carbon/graphite, glass, nylon, and/or aramid fibres. The most widely used type of fibres is glass, which is also the least expensive.

Fibre-reinforced plastic poles may be made through the filament winding method which involves wrapping of continuous fibres and/or rovings over a mandrel in a single machine-controlled operation (Schwartz 1984). A number of layers of the same or different patterns are placed on the mandrel, and the repetitive patterns and reinforcement spacing are subject to close control. The fibres may be impregnated with resin before winding (wet winding). The process is completed by curing the resin and removing the mandrel.

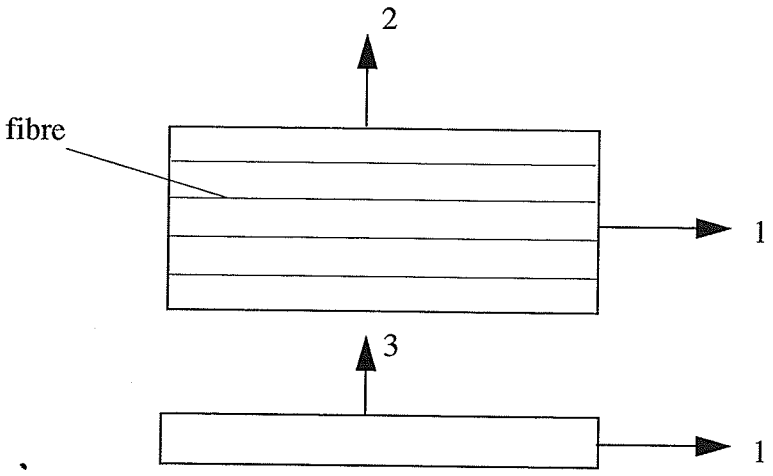

Fig. 2-1. A single layer of fibre-reinforced plastics

The FRP poles discussed hereinafter are made of a combination of several laminas. The fibres in each lamina are unidirectional but not necessarily with the same alignment as in the other laminas. A single layer of the composite can be treated as an orthotropic lamina with respect to its material coordinates (1, 2, 3) (Fig. 2-1). The stress-strain relationship is (Agawal 1980):

$$\begin{bmatrix} \sigma_1^m \\ \sigma_2^m \\ \tau_{23}^m \\ \tau_{31}^m \\ \tau_{12}^m \end{bmatrix} = \begin{bmatrix} Q_{11} & Q_{12} & 0 & 0 & 0 \\ Q_{12} & Q_{22} & 0 & 0 & 0 \\ 0 & 0 & Q_{44} & 0 & 0 \\ 0 & 0 & 0 & Q_{55} & 0 \\ 0 & 0 & 0 & 0 & Q_{66} \end{bmatrix} \begin{bmatrix} \varepsilon_1^m \\ \varepsilon_2^m \\ \gamma_{23}^m \\ \gamma_{31}^m \\ \gamma_{12}^m \end{bmatrix} \tag{2-1}$$

or

$$\{\sigma^m\} = \boldsymbol{Q}\{\varepsilon^m\} \tag{2-2}$$

where $\boldsymbol{Q}$ is the material constant matrix. Superscript "m" denotes that the stresses or strains are expressed in material coordinates. The normal strain ε_3^m is considered to be very small and its contribution to the strain energy can be neglected.

The six material constants can be expressed in terms of the engineering material constants (Agarwal 1980, Jone 1975):

$$Q_{11} = \frac{E_L}{1 - \nu_{LT}\nu_{TL}} \tag{2-3}$$

$$Q_{22} = \frac{E_T}{1 - \nu_{LT}\nu_{TL}} \tag{2-4}$$

$$Q_{12} = \frac{\nu_{LT}E_T}{1 - \nu_{LT}\nu_{TL}} = \frac{\nu_{TL}E_L}{1 - \nu_{LT}\nu_{TL}} \tag{2-5}$$

$$Q_{44} = G_{TT'} = \frac{E_T}{2(1 + \nu_{TT'})} \tag{2-6}$$

$$Q_{55} = G_{LT} = G_{LT'} \tag{2-7}$$

$$Q_{66} = G_{LT} \tag{2-8}$$

where L denotes the fibre longitudinal direction ($L = 1$), T denotes the fibre transverse direction ($L = 2$) and T' ($T' = 3$) denotes the normal (to the lamina) direction. Only five engineering material constants are needed to determine these six material constants. They are: E_L, the longitudinal elastic modulus; E_T, the transverse elastic modulus; ν_{LT}, the major Poisson's ratio; $\nu_{TT'}$, the Poisson's ratio in transverse directions; and G_{LT}, the shear modulus (longitudinal and transverse directions). The minor Poisson's ratio ν_{TL} can be determined by $\nu_{TL} = \nu_{LT}(E_T/E_L)$ (Agarwal 1980).

Ideally, these five engineering material constants should be obtained through standard tests. Due to the infinite number of design configurations of FRP, a simple method of determining the engineering material constants using the constituent material properties is desirable. The rule of mixture reported by Jones (1975) can be well employed to fulfill this task. That is,

$$E_L = V_f E_f + V_m E_m \tag{2-9}$$

$$E_T = \frac{E_m E_f}{V_m E_f + V_f E_m} \tag{2-10}$$

$$G_{TL} = \frac{G_m G_f}{V_m G_f + V_f G_m} \tag{2-11}$$

$$\nu_{LT} = V_f \nu_f + V_m \nu_m \tag{2-12}$$

where V_f is the fibre volume fraction, V_m is the matrix volume fraction; E_f and E_m are the elastic modulus of fibres and matrix, respectively; G_f and G_m are shear modulus of fibres and matrix, respectively; and ν_f and ν_m are Poisson's ratio of fibres and matrix, respectively. If the material properties of fibres and matrix are available, four engineering material constants can be computed from Eqns. (2-9) through (2-12).

In the following analyses, stresses and strains are referred to in the structural coordinates (x, y, z). For a typical lamina, the relationship of the material (local) coordinates and the structural coordinates (if assumed to be global xyz) is shown in Fig. 2-2. The z axis coincides with the '3' axis, while the '1' axis is rotated an angle θ with respect to the axis x. Accordingly, the stress-strain relationship is found as:

$$\{\sigma\} = \boldsymbol{D}\{\varepsilon^*\} \tag{2-13}$$

or

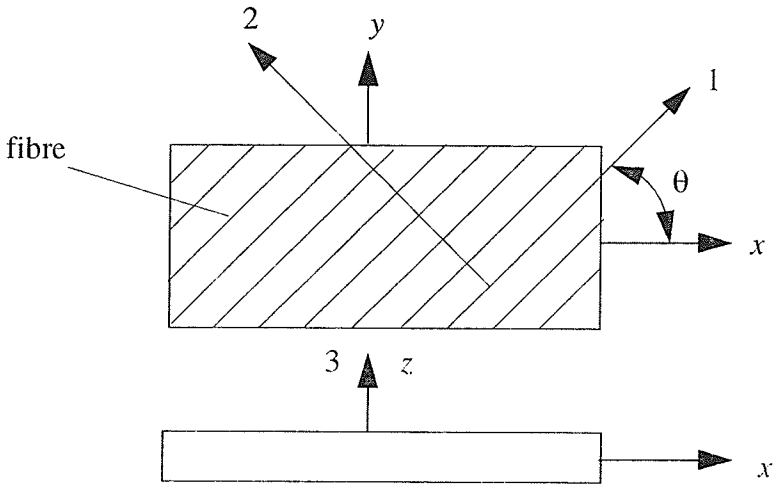

Fig. 2-2. Material coordinates and structural coordinates

$$\begin{bmatrix} \sigma_x \\ \sigma_y \\ \tau_{yz} \\ \tau_{zx} \\ \tau_{xy} \end{bmatrix} = \boldsymbol{D} \begin{bmatrix} \varepsilon_x \\ \varepsilon_y \\ \gamma_{yz} \\ \gamma_{zx} \\ \gamma_{xy} \end{bmatrix} \tag{2-14}$$

where $\boldsymbol{D}$ is the stress-strain transformation matrix whose development is given in Appendix A.

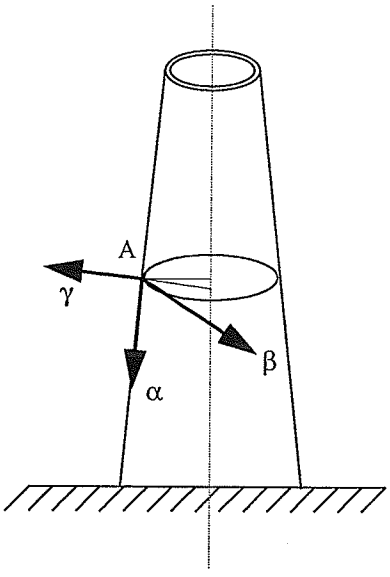

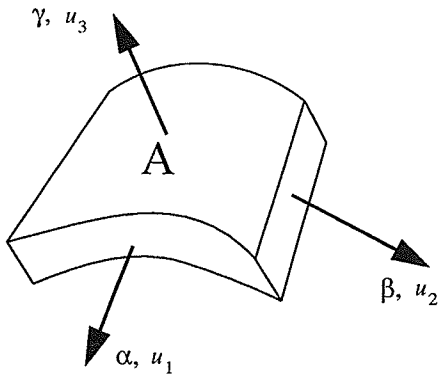

Displacements in Global Coordinates

Fig. 2-3. FRP pole as shell of revolution

2.2. Strains and Stresses of Conical Shells

To optimize the use of materials, the FRP poles are assumed to be conical shells (Fig. 2-3). For rotational shells, the use of curvilinear coordinates is the most convenient way of expressing the geometric variables, such as displacements and strains. The coordinates α, β, γ and the corresponding displacements u_1, u_2, u_3 are illustrated in Fig. 2-3, where α and β are surface coordinates and γ is normal to the surface. The strain vector in Eqn. (2.14) can be expressed as the sum of linear strain vector $\{\varepsilon^L\}$ and nonlinear strain vector $\{\varepsilon^N\}$; i.e.:

$$\{\varepsilon^*\} = \{\varepsilon^L\} + \{\varepsilon^N\}. \tag{2-15}$$

The strain vectors ε^L and ε^N consist of five strain components as follows:

$$\{\varepsilon^L\} = \left[e_{11}\ e_{22}\ e_{23}\ e_{31}\ e_{12}\right]^T \quad \text{and} \quad \{\varepsilon^N\} = \left[\varepsilon_{11}\ \varepsilon_{22}\ \varepsilon_{23}\ \varepsilon_{31}\ \varepsilon_{12}\right]^T. \tag{2-16}$$

The strain components in orthogonal curvilinear coordinates (Novozhilov 1961) are:

$$e_{11} = \frac{1}{H_1}\frac{\partial u_1}{\partial \alpha} + \frac{1}{H_1 H_2}\frac{\partial H_1}{\partial \beta}u_2 + \frac{1}{H_1 H_3}\frac{\partial H_1}{\partial \gamma}u_3, \qquad e_{12} = \frac{H_2}{H_1}\frac{\partial}{\partial \alpha}\left(\frac{u_2}{H_2}\right) + \frac{H_1}{H_2}\frac{\partial}{\partial \beta}\left(\frac{u_1}{H_1}\right) \tag{2-17}$$

and

$$\varepsilon_{11} = \frac{1}{2}\left[e_{11}^2 + \left(\frac{1}{2}e_{12} + \omega_3\right)^2 + \left(\frac{1}{2}e_{13} - \omega_2\right)^2\right] \tag{2-18}$$

$$\varepsilon_{12} = e_{11}\left(\frac{1}{2}e_{12} - \omega_3\right) + e_{22}\left(\frac{1}{2}e_{12} + \omega_3\right) + \left(\frac{1}{2}e_{13} - \omega_2\right)\left(\frac{1}{2}e_{23} + \omega_1\right) \tag{2-19}$$

where ω_1, ω_2 and ω_3 are:

$$\omega_1 = \frac{1}{2H_2H_3}\left[\frac{\partial}{\partial \beta}(H_3u_3) - \frac{\partial}{\partial \gamma}(H_2u_2)\right] \tag{2-20}$$

$$\omega_2 = \frac{1}{2H_1H_3}\left[\frac{\partial}{\partial \gamma}(H_1u_1) - \frac{\partial}{\partial \alpha}(H_3u_3)\right] \tag{2-21}$$

$$\omega_3 = \frac{1}{2H_1H_2}\left[\frac{\partial}{\partial \alpha}(H_2u_2) - \frac{\partial}{\partial \beta}(H_1u_1)\right] \tag{2-22}$$

and H_i $(i = 1, 2, 3)$ are Lame coefficients of the shell. For conical shells,

$$H_1 = 1.0 \tag{2-23}$$

$$H_2 = r + \gamma\cos\psi \tag{2-24}$$

$$H_3 = 1.0 \tag{2-25}$$

where r is the radius of the mid-surface; ψ is the taper angle (Fig. 2- 4); and u_1, u_2 and u_3 are displacements in α, β and γ directions, respectively (Fig. 2-3). The rest of the strain terms, e_{22}, e_{23}, ε_{22}, ε_{23}, etc., can be obtained by cycling (α, β, γ) and subscript (1, 2, 3) in Eqs. (2-17), (2-18) and (2-19).

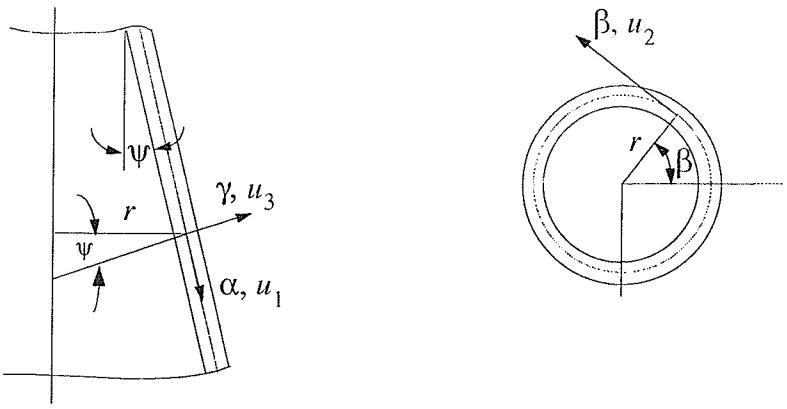

Fig. 2-4. Geometry of FRP pole

The following points should be made regarding Novozhilov's strain expressions. First, Novozhilov's strains are expressed in curvilinear coordinates and are referenced with respect to the original configuration. Second, there is no restrictions for the range of displacements in Novozhilov's strain expressions. Hence, Novozhilov's strains can be used for large displacement analyses. Third, Novozhilov's strains are general and applicable to thin as well as thick shells.

Fibre-reinforced plastic poles are usually more flexible than steel and wood poles. The displacement could be large but it is assumed that the stress-strain relationship is still linear. That is,

$$\{\sigma\} = \boldsymbol{D}\{\varepsilon^*\} \tag{2-26}$$

This is the same equation as Eqn. (2-13).

2.3. Finite Element Formulations

In this study, the principle of stationary potential energy is employed to derive equilibrium and stability conditions of the system. If the system is conservative, the total potential energy is

$$\Pi = U - W \tag{2-27}$$

where U is the strain energy of the system, W is the work done by the external conservative loads. Alternatively we say that $-W$ is the potential of the external loads. The reference state where $U = 0$ and $W = 0$ is the undeformed state.

The principle of stationary potential energy states that at an equilibrium position, the first variation of the total potential energy of a conservative system vanishes; i.e.,

$$\delta\Pi = \delta U - \delta W = 0 \tag{2-28}$$

where variation is taken with respect to displacement variables. Eqn. (2-28) does not give any information about whether the equilibrium is stable or unstable. Second or higher than second variations are needed (Chen and Lui 1987) to determine stability. Generally, if $\delta^2\Pi > 0$, the equilibrium is stable; if $\delta^2\Pi < 0$, the equilibrium is unstable; and if $\delta^2\Pi = 0$, the equilibrium is said to be neutral or a higher variation $\delta^3\Pi$ is required to determine whether the equilibrium is stable or not.

In the finite element method, the displacement functions are usually assumed to depend on the element nodal displacements $\boldsymbol{q}_e$, that is,

$$u_i = [\boldsymbol{F}_i(\alpha, \beta, \gamma)]\boldsymbol{q}_e \tag{2-29}$$

where $\boldsymbol{F}_i$ $(i = 1, 2, 3)$ is a function of the coordinates α, β and γ. It is well known that the linear strains in an element can be expressed in terms of node displacements $\boldsymbol{q}_e$ as follows:

$$\{\varepsilon^L\} = \boldsymbol{B}^L\boldsymbol{q}_e, \qquad \text{and} \qquad \{\delta\varepsilon^L\} = \boldsymbol{B}^L\delta\boldsymbol{q}_e \tag{2-30}$$

where the linear strain matrix $\boldsymbol{B}^L$ is independent of nodal displacements. The relationship of nonlinear strains and nodal displacements developed in Appendix B can be obtained using the Novozhilov's formulations as follows:

$$\{\varepsilon^N\} = \frac{1}{2}\left[\boldsymbol{B}^N(\boldsymbol{q}_e)\right]\boldsymbol{q}_e, \qquad \text{and} \qquad \{\delta\varepsilon^N\} = \left[\boldsymbol{B}^N(\boldsymbol{q}_e)\right]\delta\boldsymbol{q}_e. \tag{2-31}$$

Noting that matrix $\boldsymbol{B}^N$ is function of q_e, the element strain energy and its variation are:

$$U_e = \frac{1}{2}\int_v (\{\varepsilon^L\} + \{\varepsilon^N\})^T \boldsymbol{D} (\{\varepsilon^L\} + \{\varepsilon^N\})\, dv \tag{2-32}$$

$$\delta U_e = \int_v \{\delta\varepsilon^L\}^T \boldsymbol{D} \{\varepsilon^L\}\, dv + \int_v \{\delta\varepsilon^L\}^T \boldsymbol{D} \{\varepsilon^N\}\, dv + \int_v \{\delta\varepsilon^N\}^T \boldsymbol{D} \{\varepsilon^L\}\, dv + \int_v \{\delta\varepsilon^N\}^T \boldsymbol{D} \{\varepsilon^N\}\, dv \tag{2-33}$$

where v is the volume of an element. Letting

$$\int_v \{\delta\varepsilon^L\}^T \boldsymbol{D} \{\varepsilon^L\}\, dv = \delta q_e^T [K_e] q_e, \qquad \int_v \{\delta\varepsilon^L\}^T \boldsymbol{D} \{\varepsilon^N\}\, dv = \delta q_e^T [H_e(q_e)] q_e \tag{2-34}$$

$$\int_v \{\delta\varepsilon^N\}^T \boldsymbol{D} \{\varepsilon^L\}\, dv = \delta q_e^T [G_e(q_e)] q_e, \qquad \int_v \{\delta\varepsilon^N\}^T \boldsymbol{D} \{\varepsilon^N\}\, dv = \delta q_e^T [J_e(q_e)] q_e \tag{2-35}$$

and substituting Eqs. (2-30) and (2-31) into Eqs. (2-34) and (2-35), we find that

$$\boldsymbol{K}_e = \int_v (\boldsymbol{B}^L)^T \boldsymbol{D} \boldsymbol{B}^L dv \tag{2-36}$$

$$\boldsymbol{H}_e = \frac{1}{2}\int_v (\boldsymbol{B}^L)^T \boldsymbol{D} \left[\boldsymbol{B}^N(q_e)\right] dv \tag{2-37}$$

$$\boldsymbol{G}_e = \int_v \left[\boldsymbol{B}^N(q_e)\right]^T \boldsymbol{D} \boldsymbol{B}^L dv \tag{2-38}$$

$$\boldsymbol{J}_e = \frac{1}{2}\int_v \left[\boldsymbol{B}^N(q_e)\right]^T \boldsymbol{D} \left[\boldsymbol{B}^N(q_e)\right] dv \tag{2-39}$$

where $\boldsymbol{K}_e$ is the linear element stiffness matrix which is independent of nodal displacement q_e, and matrices $\boldsymbol{H}_e$, $\boldsymbol{G}_e$ and $\boldsymbol{J}_e$ are functions of nodal displacement q_e, called nonlinear element stiffness matrices.

The total strain energy of the system upon assembling Eqn. (2-32) can be written as

$$U = \frac{1}{2} q^T \boldsymbol{A} q \tag{2-40}$$

where matrix $\boldsymbol{A}$ is the system strain energy matrix and is defined as

$$A = \left[K + H(q) + \frac{1}{2}G(q) + \frac{1}{2}J(q)\right] \tag{2-41}$$

Eqns. (2-40) and (2-41) can be proved as follows. By expending Eqn. (2-32), the element strain energy is

$$U_e = \frac{1}{2}\left[\int_v (\varepsilon^L)^T D\varepsilon^L dv + \int_v (\varepsilon^L)^T D\varepsilon^N dv + \int_v (\varepsilon^N)^T D\varepsilon^L dv + \int_v (\varepsilon^N)^T D\varepsilon^N dv\right] \tag{2-42}$$

Substituting Eqns. (2-30) and (2-31) into above equation, yields,

$$U_e = \frac{1}{2}q_e^T\left[\int_v (B^L)^T DB^L dv + \frac{1}{2}\int_v (B^L)^T DB^N dv + \frac{1}{2}\int_v [B^N]^T DB^L dv + \frac{1}{4}\int_v [B^N]^T DB^N dv\right]q_e \tag{2-43}$$

or

$$U_e = \frac{1}{2}q_e^T\left[K_e + H_e + \frac{1}{2}G_e + \frac{1}{2}J_e\right]q_e \tag{2-44}$$

The total strain energy of the system Eqn (2-40) can be obtained by assembling the element strain energy.

The variation of the total strain energy of a system is

$$\delta U = \delta q^T K_S q \tag{2-45}$$

where the static stiffness matrix is defined as

$$K_S = K + H(q) + G(q) + J(q) \tag{2-46}$$

where K, H, G, J are global stiffness matrices. The following system equation is obtained using the standard finite element procedures (Weaver and Johnston 1985):

$$R = f \tag{2-47}$$

where R is the internal force vector, and f is the nodal load vector. R and f are defined as:

$$R = [K + H(q) + G(q) + J(q)]q \tag{2-48}$$

$$f = \lambda P \tag{2-49}$$

In Eqs. (2-48) and (2-49), q is the system nodal displacement vector; P is a prescribed load vector; and λ is a load parameter which, when multiplied with P, will describe the actual load. The contribution of the nonlinear strain ε^N to the strain energy may be significant, hence, Eq. (2-47) is the full governing equation without simplification. Eq. (2-47) can be rearranged in the form:

$$\chi = R - \lambda P = \{0\}. \tag{2-50}$$

Generally, the Newton-Raphson iteration method is employed to solve the above nonlinear equations. Different control schemes, namely, load control, displacement control (Batoz and Dhatt 1979, Lock and Sabir 1973), arc-length control (Riks 1979, Crisfield 1981), etc., have been proposed and successfully implemented in various computer programs. In most schemes, the tangent stiffness matrix K_T has to be evaluated where

$$K_T = \left[\frac{\partial \chi}{\partial q}\right] = \left[\frac{\partial R}{\partial q}\right]. \tag{2-51}$$

From Eq. (2-48), it can be noted that it is sufficient to find the derivative of $[M(q)q]$ to evaluate the derivative of K_T. Thus, for an $n \times n$ matrix $M(q)$

$$\frac{\partial}{\partial q}[M(q)q] = M^*(q) + M(q) \tag{2-52}$$

where $M^*(q)$ is also an $n \times n$ matrix and

$$m^*_{ij} = \sum_{k=1}^{n} \frac{\partial m_{ik}}{\partial q_j} q_k \tag{2-53}$$

Applying Eqs. (2-52) and (2-53) to matrix H and using Eqs. (2-37) and (2-38), yields,

$$H^* = H \qquad \text{and} \qquad G = 2H^T \tag{2-54}$$

Since computing nonlinear matrices such as H, G and H^* are time intensive, the above two equations can be used to reduce computational time.

2.4. Displacement Functions

The displacement vector $\{u\}$ can be expressed as $\{u\} = \left[u_1\ u_2\ u_3\right]^T$ which is a function of the coordinates (α, β, γ). In the γ direction, each displacement u_1, u_2, u_3 can be assumed to be the sum of a constant part, which is the mid-surface displacement, and a variable part, which is a func-

tion of γ. For the nonlinear analysis, u_1, u_2, u_3 are assumed to be linearly dependent on γ as $u_i = v_i + \gamma\phi_i$ $(i = 1, 2, 3)$, where v_i is the mid-surface displacement and ϕ_i is a rotation-type variable. Using

$$\{\bar{u}\} = \left[v_1 \ \phi_1 \ v_2 \ \phi_2 \ v_3 \ \phi_3\right]^T \tag{2-55}$$

each component of the vector $\{\bar{u}\}$ can be expanded into Fourier series in β (circumferential) direction; that is,

$$\begin{bmatrix} v_1 \\ \phi_1 \\ v_2 \\ \phi_2 \\ v_3 \\ \phi_3 \end{bmatrix} = \begin{bmatrix} v_1^o \\ \phi_1^o \\ v_2^o \\ \phi_2^o \\ v_3^o \\ \phi_3^o \end{bmatrix} + \sum_{l=1}^{M_l} \begin{bmatrix} v_{1l}^a \cos l\beta \\ \phi_{1l}^a \cos l\beta \\ v_{2l}^a \sin l\beta \\ \phi_{2l}^a \sin l\beta \\ v_{3l}^a \cos l\beta \\ \phi_{3l}^a \cos l\beta \end{bmatrix} + \sum_{l=1}^{M_l} \begin{bmatrix} v_{1l}^b \sin l\beta \\ \phi_{1l}^b \sin l\beta \\ v_{2l}^b \cos l\beta \\ \phi_{2l}^b \cos l\beta \\ v_{3l}^b \sin l\beta \\ \phi_{3l}^b \sin l\beta \end{bmatrix}. \tag{2-56}$$

In Eq. (2-56), the first vector on the right hand side represents the axial symmetric displacements corresponding to the zeroth-order Fourier series; the second vector includes the symmetric (about $\beta = 0$) displacements; the third vector includes the antisymmetric (about $\beta = 0$) displacements. M_l is the highest harmonic to be chosen. For linear static analysis, displacements of different orders are uncoupled due to the orthogonality of the trigonometric functions (Zienkiewicz 1971) so M_l can be chosen up to any particular order of interest. For a nonlinear analysis, displacements of different orders are coupled and only finite orders are retained depending on the machine capacity of time and space.

2.5. Discussion

The principle of stationary potential energy is employed for the analysis of FRP hollow tapered poles. Novozhilov's derivations of strains of general shells are used in the formulation process for the nonlinear finite element analysis. The use of Novozhilov's derivations results in a concise and compact expression for nonlinear strains and their first variations. The evaluation of the tangent stiffness matrices is discussed. It is shown that $\boldsymbol{H}^* = \boldsymbol{H}$ and $\boldsymbol{G} = 2\boldsymbol{H}^T$. These two equations can be used to reduce computational time. The programming of nonlinear stiffness matrices can also be systematically manipulated.

The formulations discussed in this chapter form the basis for the analyses presented in the following chapters. Chapter 3 deals with the solution methods of nonlinear equations, such as Eqn. (2-50). Chapter 4 covers the nonlinear analysis of beam-column-type bending of the FRP poles. Three nonlinear stiffness matrices are included in that analysis. Conceptually, the highest order of harmonic M_l is one for beam-type bending, but in order to account for rigid body rotation and to conform to the assumption of beam theory, special second-order terms are derived and included in the displacement function (Eqn. (2-56)). The ovalization analysis is discussed in chapter 5. All the second-order harmonic terms are included in order to model the dominant behaviour of ovalization. The $P-\Delta$ analysis and the linear buckling analysis are dealt with in Chapter 6. A number of assumptions made to arrive to these simplified analyses are also discussed in Chapter 6. The linear analysis is covered in Chapter 7. This is the simplest analysis where all nonlinear terms are neglected.

Chapter 3. Solution Method of Nonlinear System of Equations

Since the major obstacle in performing a nonlinear analysis is the solution of the nonlinear equations, a great deal of effort has been exerted since 1960 to develop procedures to solve such problems. Methods developed include the pseudo-force method (Stricklin and Haisler 1977) for the formulation of nonlinear equations; the self-correcting method (Haisler and Stricklin 1977); and the dynamic relaxation method (Park 1982) for the solution of nonlinear equations.

The major difficulty in solving nonlinear system of equations is to traverse a limit point of the equilibrium path. The traditional load control is incapable of traversing a load limit point. If such problem is encountered, the displacement control is usually adopted. But, displacement control do fail at a displacement limit point. Innovative control methods were proposed since 1970. Among them, the arc length control (Riks 1979) is the basic method. The circular arc length control (Crisfield 1981) is a variation of the arc length control. The equation used for controlling the incremental step is called constraint equation. The Newton-Raphson iteration form of the constraint equation is called the augmented equation. Naturally, the method based on the augmented equation is called the augmented equation method

In this Thesis, the augmented equation method is employed to solve the nonlinear system of equations. The classical load and displacement control schemes are discussed first. Then the advanced arc length control (Riks 1979) scheme and some related control schemes are briefly introduced. A suggestion is made that the coefficients in the augmented equation may be considered as weighing factors. These weighing factors can be determined according to the control scheme being used. To explore more simple control methods, control schemes based on the potential energy are proposed and the implementation of these control schemes are discussed in detail in this chapter.

3.1. Load Control and Displacement Control

The nonlinear system of equations developed in Chapter 2 by the finite element method has the following form (Eqn. (2-50)):

$$\{\chi\} = \boldsymbol{R} - \lambda \boldsymbol{P} = \{\mathbf{0}\} \tag{3-1}$$

The Newton-Raphson iteration method is commonly employed to solve this nonlinear system of equations. If an approximate solution q_k at the kth iteration has been obtained, the increment δq_k is to be sought by solving

$$\delta\{\chi\} + \{\chi\} = \{0\} \tag{3-2}$$

where

$$\delta\{\chi\} = \left[\frac{\partial}{\partial q}\{\chi\}\right]\delta q_k - P\delta\lambda_k = \left[\frac{\partial R}{\partial q}\right]\delta q_k - P\delta\lambda_k \tag{3-3}$$

Substitution of the tangent stiffness matrix (Eqn (2-48)) into Eqn. (3.2), yields,

$$K_T\delta q_k - P\delta\lambda_k = -R + \lambda_k P \tag{3-4}$$

In a standard load control scheme, λ is prescribed as a fixed value $\bar{\lambda}$. The displacement incremental vector δq_k can be solved from the equation

$$K_T\delta q_k - P\delta\lambda_k = -R + \bar{\lambda}P \tag{3-5}$$

and a new improved solution is obtained from

$$q_{k+1} = q_k + \delta q_k \tag{3-6}$$

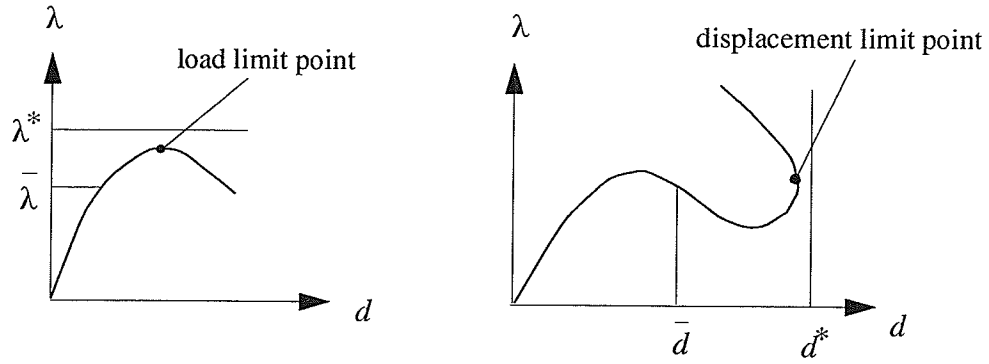

(a) load control

(b) displacement control

Fig. 3-1. Load control displacement control

The load control scheme is easy to manipulate and incorporate into a computer program but it will fail in the vicinity of a limit point (Riks 1979). This is because the tangent stiffness matrix K_T becomes singular at a limit point, as shown in Fig. 3-1 (a). In this figure, d represents a component of displacement vector and λ^* represents a value of λ which does not intersect with the equilib-

rium path. To overcome this difficulty, a number of algorithms based on the displacement control scheme were proposed by Zienkiewicz (1971), Lock and Sabir (1973), and others. Zienkiewicz (1971) proposed an incremental displacement method based on the concept of linearized superposition. Lock and Sabir (1973) presented an algorithm based on the Gauss elimination method for large deflection geometric nonlinear plane and curved structures. Batoz and Dhatt (1979) advocated a displacement incremental method by using multiple right-hand sides for solving linear and nonlinear equations. Although displacement control can be used to traverse limit point effectively, it could fail at a displacement turning point (Riks 1979, Crisfield 1981). This is illustrated in Fig.3-1 (b), where d^* represents a value of the displacement component, which does not intersect with the equilibrium path.

3.2. Arc Length Control and Augmented Equation Method

To control the progress of the computation along the equilibrium path better, a parameter control, namely, the arc length control, was proposed by Riks (1979) and Wempner (1971). The arc length control consists of appending a constraint equation to the basic system of equilibrium equations (Eqn. (3-1)). That is,

$$\frac{\partial q^T}{\partial \eta}\Delta q + \frac{\partial \lambda}{\partial \eta}\Delta\lambda = \Delta\eta \tag{3-7}$$

This equation defines a hyperplane in an (n+1) Euclidean space. The concept of arc length control can be demonstrated for a one degree-of-freedom system as shown in Fig. 3-2.

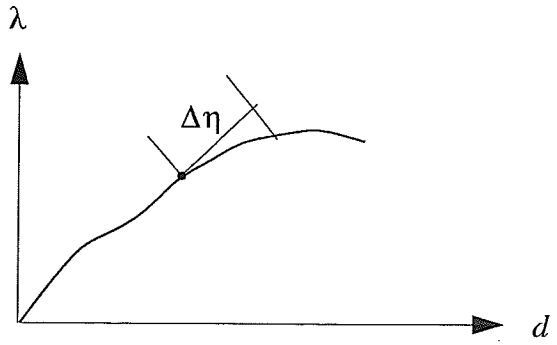

Fig. 3-2. Arc length control

In general, a constraint equation can be abstracted as:

$$f_c = 0 \tag{3-8}$$

The Newton-Raphson iteration method is applied to this constraint equation, yields

$$\delta f_c + f_c = 0 \tag{3-9}$$

In view of Eqn. (3-4), there are (n+1) unknowns in a system of (n) equations. Iteration of the constraint equation will serve the (n+1)th equation. In general, the iteration of constraint equation can be expressed as:

$$s\delta\lambda - g^T \delta q = R_0 \tag{3-10}$$

where s is a coefficient corresponding to $\delta\lambda$, g is a coefficient vector in which g_i ($i = 1, 2, ..., n$) is corresponding to δq_i, R_0 is the residual of the constraint. Hence, the Newton-Raphson iteration equations with (n+1) unknowns can be written as:

$$\begin{bmatrix} s & -g^T \\ -P & K_T \end{bmatrix} \begin{bmatrix} \delta\lambda \\ \delta q \end{bmatrix} = \begin{bmatrix} R_0 \\ -R \end{bmatrix} + \lambda \begin{bmatrix} 0 \\ P \end{bmatrix} \tag{3-11}$$

Eqn. (3-11) forms the basis of the augmented equation method. Load control and displacement control are the special cases of this method. Since the introduction of arc length control method, several other control schemes have been proposed. Among these control schemes are state control, spherical arc length control, cylindrical arc length control (Crisfield 1981), and hyperelliptical arc length control. The trend is to abandon the single variable controls (Load control and single displacement control) and switch to whole state controls such as those mentioned earlier.

3.3. Refining the Augmented Equation

In state control schemes, the incremental control parameter such as $\Delta\eta$ varies with the total degree-of-freedom of a system. Even the length unit of the displacement used in the computer program can influence the determination of the control parameter. To minimize this effect, Fellipa (1986) proposed a generic control scheme which uses three coefficients, a, b, v, and one coefficient matrix, S, to make the control parameter scaled and dimensionless. This control scheme can be written as

$$\frac{a^2}{v^2} \Delta q^T S \Delta q + b^2 (\Delta\lambda)^2 = (\Delta l)^2 \tag{3-12}$$

where a and b are dimensionless scalars, S is a symmetric non-negative matrix that scales the

state vector, v is a reference value with the dimension $\sqrt{\Delta q^T S \Delta q}$, Δl is a dimensionless control parameter. Coefficients a and b may not be simultaneously zero. Fellipa suggested that useful choice for S could be I or diag (K_T) (or even K_T if positive definite).

3.4. Weighing Factors in Augmented Equation

The terms s and g_i ($i = 1, 2, ..., n$) in the augmented equation (Eqn. (3-10)) may be considered as a group of weighing factors. Weighing factors are given to different variables according to their importances. That is,

$$w_\lambda \delta\lambda + \sum_i^n w_i \delta q_i = R_0 \tag{3-13}$$

where w_λ is the weighing factor of $\delta\lambda$ and w_i ($i = 1, 2, ..., n$) are weighing factors of δq_i. These weighing factors are determined according to the control schemes. For load control, $w_\lambda = 1.0$, $w_i = 0.0$ ($i = 1, 2, ..., n$) and $R_0 = \bar{\lambda} - \lambda^{(k)}$. For displacement control (where q_j is the displacement variable to be controlled), $w_\lambda = 0.0$, $w_i = 0.0$ ($i \neq j$), $w_j = 1.0$, and $R_0 = \bar{q}_j - q_j^{(k)}$.

Two conclusions may be drawn from the above discussion. First, multiple control schemes can be implemented in a single computer program because different controls are merely different cases of Eqn. (3-13). In other words, to implement different controls, one needs only to change the weighting factors w_λ, w_i ($i = 1, 2, ..., n$) and the incremental control parameter R_0. Second, weighing factors can be selective and only those which have the most influence on the solution are retained. Since every control has its own advantages, it is possible to use different control schemes s at different stages of equilibrium path finding. The user of the computer program can also have some flexibility on selecting different control schemes at different situations.

3.5. External and Internal Potential Controls

The problem of traversing limit point has been solved by Riks (1979), Crisfield (1981), and others. The arc length control, although a number of variations have emerged, is still the core method of traversing limit point. To use the arc length control, the derivative of q with respect to the path need to be evaluated. This task can be very involved. The physical meaning of the other controls, such as the spherical arc length control and the hyperelliptical arc length control are not so obvious as to be appreciated by design engineers. In the following discussions, two control methods, the external and internal potential controls, which are based on the potential energy, are proposed. The incremental work control and the incremental strain energy control are then derived. The latter two control methods are closely related to the former two, i.e., to the external

and internal potential controls.

The first step in developing the proposed control method is to consider the external potential energy $-W$ as the control and a solution is obtained for an increment. For the next increment, the external potential is specified as,

$$-W = -\overline{W} \tag{3-14}$$

or

$$F = W - \overline{W} = 0 \tag{3-15}$$

Assuming $W^{(k)}$ is the result of W at the kth iteration, then $\delta F = \delta W^{(k)}$. The iteration equation is then written as,

$$\delta F + F = 0 \tag{3-16}$$

or

$$\delta W^{(k)} + W^{(k)} = \overline{W} \tag{3-17}$$

Since

$$W^{(k)} = \lambda^{(k)} \boldsymbol{P}^T \boldsymbol{q}^{(k)} \tag{3-18}$$

and

$$\delta W^{(k)} = \delta\lambda^{(k)} \boldsymbol{P}^T \boldsymbol{q}^{(k)} + \lambda^{(k)} \boldsymbol{P}^T \delta \boldsymbol{q}^{(k)} \tag{3-19}$$

Eqn. (3-17) becomes

$$\left[\boldsymbol{P}^T \boldsymbol{q}^{(k)} \;\; \lambda^{(k)} \boldsymbol{P}^T\right] \begin{bmatrix} \delta\lambda^{(k)} \\ \delta \boldsymbol{q}^{(k)} \end{bmatrix} = \overline{W} - W^{(k)} \tag{3-20}$$

This is the augmented equation of external potential control. Using Eqn. (3-20) and Eqn. (3-10), for external potential control,

$$s = \boldsymbol{P}^T \dot{\boldsymbol{q}}^{(k)} \tag{3-21}$$

and

$$g^T = -\lambda^{(k)} P^T \tag{3-22}$$

Next, the internal potential energy U is considered to be the control and a solution is obtained for an increment. For the next increment, the internal potential is

$$U = \bar{U} \tag{3-23}$$

or

$$F = U - \bar{U} = 0 \tag{3-24}$$

where $\bar{U}$ is a fixed value which indicates a goal of internal potential energy to be reached in the next increment step. Assuming that $U^{(k)}$ is the result of U at kth iteration, then $\delta F = \delta U^{(k)}$. The iteration equation can be written as

$$\delta F + F = 0 \tag{3-25}$$

or

$$\delta U^{(k)} + U^{(k)} = \bar{U} \tag{3-26}$$

From Eqns. (2-40) and (2-45)

$$\delta U^{(k)} = (q^{(k)})^T K_s^T \delta q^{(k)} \tag{3-27}$$

and

$$U^{(k)} = \frac{1}{2} (q^{(k)})^T A q^{(k)} \tag{3-28}$$

Thus, Eqn. (3-25) becomes

$$\begin{bmatrix} 0 & (q^{(k)})^T K_s^T \end{bmatrix} \begin{bmatrix} \delta\lambda^{(k)} \\ \delta q^{(k)} \end{bmatrix} = \bar{U} - U^{(k)} \tag{3-29}$$

This is the augmented equation of internal potential control. Using Eqn. (3-29) and Eqn. (3-10), for internal potential control

$$s = 0 \tag{3-30}$$

and

$$g^T = -(q^{(k)})^T K_s^T \tag{3-31}$$

An advantage of using external and internal potential controls is the obvious physical interpretation. The solution of the system of equations is advanced by advancing the potential energy. Another advantage is that the information needed, such as matrices K_s and A, is available when the tangent stiffness matrix has been formed.

3.6. Incremental Work Control and Incremental Strain Energy Control

In many problems the actual work done by the external loads increases monotonically within the displacement range of interest. Typical examples are poles under transverse load (Example 4-1), under axial load (Timoshenko and Gere 1961), and under combined axial and transverse loads (Example 4-2). In these examples, the increment of the actual work done by an external load is always positive. This characteristic can be utilized to form the following constrain equation:

$$\Delta W_a^{(k)} = \Delta \overline{W}_a \tag{3-32}$$

where $\Delta W_a^{(k)}$ is the increment of the actual work done (referenced to the last incremental step) by the external loads if the equilibrium path is to be advanced. $\Delta \overline{W}_a$ is a specified value which controls the incremental step. If the incremental step is small, $\Delta W_a^{(k)}$ can be approximated as

$$\Delta W_a^{(k)} = \frac{1}{2}(\lambda^{(k)} + \lambda^{(0)}) P^T (q^{(k)} - q^{(0)}) \tag{3-33}$$

Letting $\delta W_a^{(k)}$ be the variation of $\Delta W_a^{(k)}$,

$$\delta W_a^{(k)} = \frac{1}{2}\delta\lambda^{(k)} P^T (q^{(k)} - q^{(0)}) + \frac{1}{2}(\lambda^{(k)} + \lambda^{(0)}) P^T \delta q^{(k)} \tag{3-34}$$

Using the Newton-Raphson iteration form of Eqn. (3-32),

$$\delta W_a^{(k)} + \Delta W_a^{(k)} - \Delta \overline{W}_a = 0 \tag{3-35}$$

yields

$$\left[\frac{1}{2}P^T (q^{(k)} - q^{(0)}) \;\; \frac{1}{2}(\lambda^{(k)} + \lambda^{(0)}) P^T\right] \begin{bmatrix} \delta\lambda^{(k)} \\ \delta q^{(k)} \end{bmatrix} = \Delta \overline{W}_a - \Delta W_a^{(k)} \tag{3-36}$$

This is the augmented equation of incremental work control.

In a similar manner, the internal potential control can be adapted into incremental internal potential control or incremental strain energy control. Instead of specifying the absolute value of internal potential energy, an increment, $\Delta\bar{U}$, is specified which is referenced to the last incremental step. That is,

$$\Delta U^{(k)} = \Delta\bar{U} \tag{3-37}$$

where $\Delta U^{(k)}$ can be either determined according to Eqn. (2-40) as

$$\Delta U^{(k)} = \frac{1}{2}(q^{(k)})^T A^{(k)} q^{(k)} - \frac{1}{2}(q^{(0)})^T A^{(0)} q^{(0)} \tag{3-38}$$

or approximated by using Eqn. (2-45) as

$$\Delta U^{(k)} = (q^{(k)} - q^{(0)})^T K_s^T q^{(k)} \tag{3-39}$$

Letting $\delta U^{(k)}$ be the variation of $\Delta U^{(k)}$,

$$\delta U^{(k)} = (q^{(k)})^T K_s^T \delta q^{(k)} \tag{3-40}$$

Using the Newton-Raphson iteration form of Eqn. (3-37),

$$\delta U^{(k)} + \Delta U^{(k)} - \Delta\bar{U} = 0 \tag{3-41}$$

and

$$\begin{bmatrix} 0 & (q^{(k)})^T K_s^T \end{bmatrix} \begin{bmatrix} \delta\lambda^{(k)} \\ \delta q^{(k)} \end{bmatrix} = \Delta\bar{U} - \Delta U^{(k)} \tag{3-42}$$

This is the augmented equation of incremental strain energy control.

3.7. Solution Procedure for Regular Point

Although the tangent stiffness matrix K_T in Eqn. (3-11) is symmetric, the augmented tangent stiffness matrix is not because often $P \neq g$. In addition, the augmented tangent stiffness is no longer banded if arc-length-type control or state-type control are used. To take advantage of the symmetric and banded nature of the tangent stiffness matrix, Eqn. (3-11) can be solved separately using the following procedure.

From Eqn. (3-11),

$$s\delta\lambda - g^T\delta q = R_0 \tag{3-43}$$

and

$$\delta q = K_T^{-1}(-R + \lambda P + P\delta\lambda) \tag{3-44}$$

Thus,

$$\delta\lambda = \frac{R_0 + g^T K_T^{-1}(-R + \lambda P)}{s - g^T K_T^{-1} P} \tag{3-45}$$

Equation (3-45) is solved first and then δq is obtained from Eqn. (3-44).

3.8. Solution Procedure for Limit Point

The solution procedure represented by Eqns. (3-44) and (3-45) is based on the fact that the tangent stiffness matrix is nonsingular. Theoretically, the tangent stiffness matrix K_T is exactly singular at a limit point. However, if certain decomposition methods, such as LU decomposition and LDL^T decomposition, are used to decompose the tangent stiffness, K_T can not be numerically singular because of the many degrees-of-freedoms. Relying on this factor, Batoz and Dhatt (1979) and Crisfield (1981) implemented procedures in their computer programs to traverse the limit points in a manner similar to that used in the solution of regular points. These researchers point out that they have not encountered a case in which K_T is exactly singular.

For singular or ill-conditioned tangent stiffness matrix, the fictitious spring method can be used. This method which was first proposed by Sharifi and Popov (1971) consists of inserting a penalty number s^o in the ith diagonal element of the tangent stiffness matrix. The modified stiffness matrix is equal to $K_T + s^o E_i$, where $E_i = e_i e_i^T$, e_i is a vector whose ith element is unity and the rest of the elements are zeros. Expressing

$$\eta = \lambda^{(k+1)} - \lambda^{(k)} \tag{3-46}$$

and

$$d = q^{(k+1)} - q^{(k)} \tag{3-47}$$

then, Eqn. (3-11) can be written as

$$\begin{bmatrix} s & -g^T \\ -P & K_T \end{bmatrix} \begin{bmatrix} \eta \\ d \end{bmatrix} = \begin{bmatrix} R_0 \\ -R \end{bmatrix} + \lambda \begin{bmatrix} 0 \\ P \end{bmatrix} \tag{3-48}$$

The solution vector d is expressed as

$$d = d_R + \sigma_P d_P + \sigma_e d_e \tag{3-49}$$

where σ_P and σ_e are two coefficients to be determined later. d_R, d_P, and d_e are solutions of the following equations:

$$(K_T + s^o E_i)\, d_R = -R + \lambda P \tag{3-50}$$

$$(K_T + s^o E_i)\, d_P = P \tag{3-51}$$

$$(K_T + s^o E_i)\, d_e = s^o e_i \tag{3-52}$$

Inserting Eqns. (3-50), (3-51), and (3-52) into the second equation of Eqn. (3-48), produce the residual:

$$-P\eta + K_T d = (-R + \lambda P) + \left[\sigma_P - \frac{(R_0 + g^T d)}{s}\right] P + s^o \left[\sigma_e - e_i^T d\right] e_i \tag{3-53}$$

s is, temporarily, assumed to be nonzero and will be eliminated in subsequent steps. σ_P and σ_e can be determined by enforcing the condition that the expressions in square brackets vanish; i.e.,

$$\left[\sigma_P - (R_0 + g^T d)/s\right] = 0 \tag{3-54}$$

and

$$\left[\sigma_e - e_i^T d\right] = 0 \tag{3-55}$$

Substituting the expression of d (Eqn. (3-49)) into Eqns. (3-54) and (3-55) produces,

$$\begin{bmatrix} s - g^T d_P & -g^T d_e \\ -e_i^T d_P & 1 - e_i^T d_e \end{bmatrix} \begin{bmatrix} \sigma_P \\ \sigma_e \end{bmatrix} = \begin{bmatrix} R_0 + g^T d_R \\ e_i^T d_R \end{bmatrix} \tag{3-56}$$

For the control schemes where $s \neq 0$, η is obtained from the first equation of Eqn. (3-48); i.e.,

$$\eta = \frac{(R_0 + g^T d)}{s} \tag{3-57}$$

For the control schemes where $s = 0$, η can not be obtained Eqn. (3-57). However, the following procedure is recommended by Fellipa (1986) to guarantee a solution for η. Multiplying the second equation of Eqn. (3-48) by d^T, yields,

$$\eta = \frac{d^T K_T d - d^T(-R + \lambda P)}{d^T P} \tag{3-58}$$

Using Eqn. (3-49) and Eqns. (3-50), (3-51) and (3-52),

$$K_T d = (-R + \lambda P) + \sigma_p P - s^o E_i d + s^o \sigma_e e_i \tag{3-59}$$

Substituting Eqn. (3-59) into Eqn. (3-58), results in

$$\eta = \sigma_p + s^o \frac{\sigma_e d_i - d_i^2}{d^T P} \tag{3-60}$$

The solutions of the displacement incremental vector, d (Eqn. (3-49)), and the load incremental parameter, η (Eqns. (3-57) or (3-60)), enable one iteration to be completed. A new improved solution of the nonlinear equations are obtained and the next iteration may proceed.

3.9. Example

To demonstrate the applicability of the control schemes discussed and proposed in this chapter, the Misses truss (Fig. 3-3), which is one dimensional nonlinear problem (Sokol and Witkowski 1994), is used here. First, the strain energy and external potential energy are determined. Second, the static stiffness matrix and tangent stiffness matrix are derived. Then, the formulations of the augmented equation method of external potential control, internal potential control, incremental work control and incremental strain energy control are presented. The nonlinear load-displacement curves are obtained using these control schemes.

The axial strain of the bar is

$$\varepsilon = \frac{L_0 - L_t}{L_0} = 1 - \frac{\sqrt{1 + (0.3 - t)^2}}{1.044} \tag{3-61}$$

where $t = V/L$.

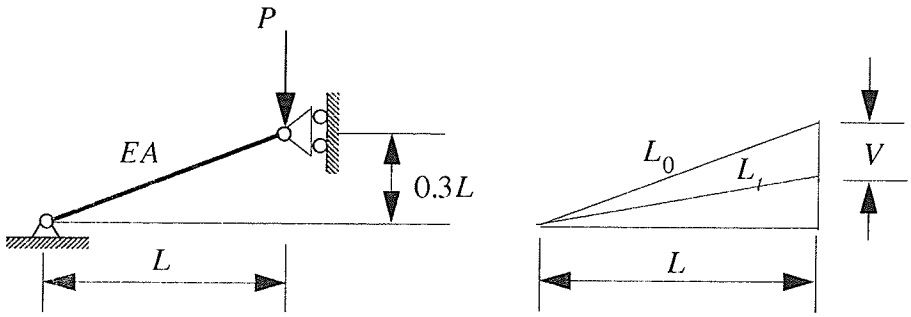

Fig. 3-3. Misses Truss

The strain energy is

$$U = \frac{1}{2}\int_v E\varepsilon^2 dv = \frac{EAL}{2}\left(1.044 - \sqrt{1+\tau^2}\right)^2 \tag{3-62}$$

where $\tau = 0.3 - t$. The external potential is

$$-W = -\lambda PLt = -(0.3\lambda PL - \lambda PL\tau) \tag{3-63}$$

The following equilibrium condition is derived by using the principle of stationary potential energy,

$$\boldsymbol{K}_s\tau - \lambda \boldsymbol{P} = \boldsymbol{0} \tag{3-64}$$

where $\boldsymbol{K}_s$ is the static stiffness matrix

$$\boldsymbol{K}_s = EA\left(\frac{1}{\sqrt{1+\tau^2}} - \frac{1}{1.044}\right) \tag{3-65}$$

The tangent stiffness matrix is derived as

$$K_T = \frac{\partial}{\partial\tau}(\boldsymbol{K}_s\tau) = EA\left(\frac{1}{\sqrt{1+\tau^2}} - \frac{1}{1.044}\right) - \frac{EA\tau}{\sqrt{(1+\tau^2)^3}} \tag{3-66}$$

If external potential control is used, the Newton-Raphson iteration is

$$\begin{bmatrix} (0.3-P\tau)L & -\lambda LP \\ -P & K_T \end{bmatrix} \begin{bmatrix} \delta\lambda \\ \delta\tau \end{bmatrix} = -\begin{bmatrix} 0 & 0 \\ -P & K_s \end{bmatrix} \begin{bmatrix} \lambda \\ \tau \end{bmatrix} + \begin{bmatrix} \overline{W} - W^{(k)} \\ 0 \end{bmatrix} \tag{3-67}$$

If internal potential control is used, the Newton-Raphson iteration is

$$\begin{bmatrix} 0 & -K_s L\tau \\ -P & K_T \end{bmatrix} \begin{bmatrix} \delta\lambda \\ \delta\tau \end{bmatrix} = \begin{bmatrix} 0 & 0 \\ -P & K_s \end{bmatrix} \begin{bmatrix} \lambda \\ \tau \end{bmatrix} + \begin{bmatrix} \overline{U} - U^{(k)} \\ 0 \end{bmatrix} \tag{3-68}$$

If incremental work control is used, the Newton-Raphson iteration is

$$\begin{bmatrix} \left(-\frac{1}{2}\right)PL(\tau^{(k)}-\tau^{(0)}) & -\frac{1}{2}(\lambda^{(k)}-\lambda^{(0)})LP \\ -P & K_T \end{bmatrix} \begin{bmatrix} \delta\lambda \\ \delta\tau \end{bmatrix} = -\begin{bmatrix} 0 & 0 \\ -P & K_s \end{bmatrix} \begin{bmatrix} \lambda \\ \tau \end{bmatrix} + \begin{bmatrix} \overline{\Delta W} + \overline{\Delta W}^{(k)} \\ 0 \end{bmatrix} \tag{3-69}$$

where

$$\overline{\Delta W}^{(k)} = \frac{1}{2}(\lambda^{(k)}-\lambda^{(0)})LP(\tau^{(k)}-\tau^{(0)}) \tag{3-70}$$

If incremental strain energy control is used, the Newton-Raphson iteration is

$$\begin{bmatrix} 0 & -K_s L\tau \\ -P & K_T \end{bmatrix} \begin{bmatrix} \delta\lambda \\ \delta\tau \end{bmatrix} = \begin{bmatrix} 0 & 0 \\ -P & K_s \end{bmatrix} \begin{bmatrix} \lambda \\ \tau \end{bmatrix} + \begin{bmatrix} \overline{\Delta U} - \Delta U^{(k)} \\ 0 \end{bmatrix} \tag{3-71}$$

where

$$\Delta U^{(k)} = -(\tau^{(k)}-\tau^{(0)})K_s\tau \tag{3-72}$$

A short computer program is required to obtain the solution of the Newton-Raphson Equations. The nonlinear curve obtained using the proposed control schemes is drawn in Fig. 3-4. The incremental work control and the incremental strain energy control can be used to obtain the load-deflection curve from $V/L = 0$ to $V/L = 0.3$. The curve from $V/L = 0.3$ to $V/L = 0.6$, however, is antisymmetric to the line $V/L = 0.3$. The portion of the curve where $V/L \geq 0.6$, as shown in Fig. 3-4, is computed using displacement control. After the curve becomes too steep, the load control scheme is preferable.

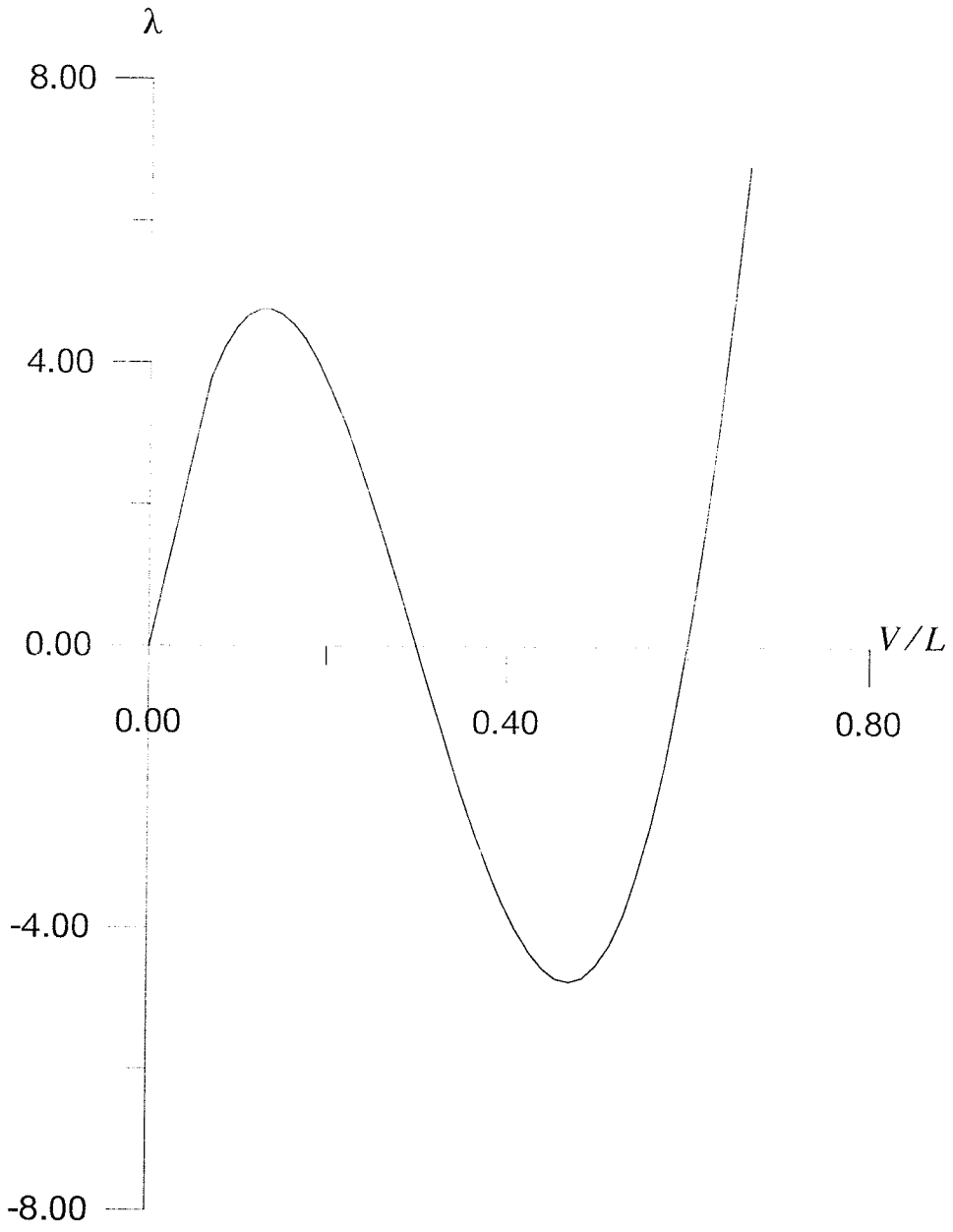

Fig. 3-4. Load deflection curve of Misses truss

The curves of the external potential, $-W$, and the internal potential, U, are shown in Fig. 3-5. The internal potential U (equal to the real work done by the external load P) increases, monotonically, from $V/L = 0$ to $V/L = 0.3$. From $V/L = 0.3$ to $V/L = 0.6$, the curves of the external potential, $-W$, and the internal potential, U, must be antisymmetric and symmetric about the line $V/L = 0.3$, respectively. This is owing to the factor that the structure is symmetric (about $V/L = 0.3$) and the load is antisymmetric (about $V/L = 0.3$) from $V/L = 0$ to $V/L = 0.6$.

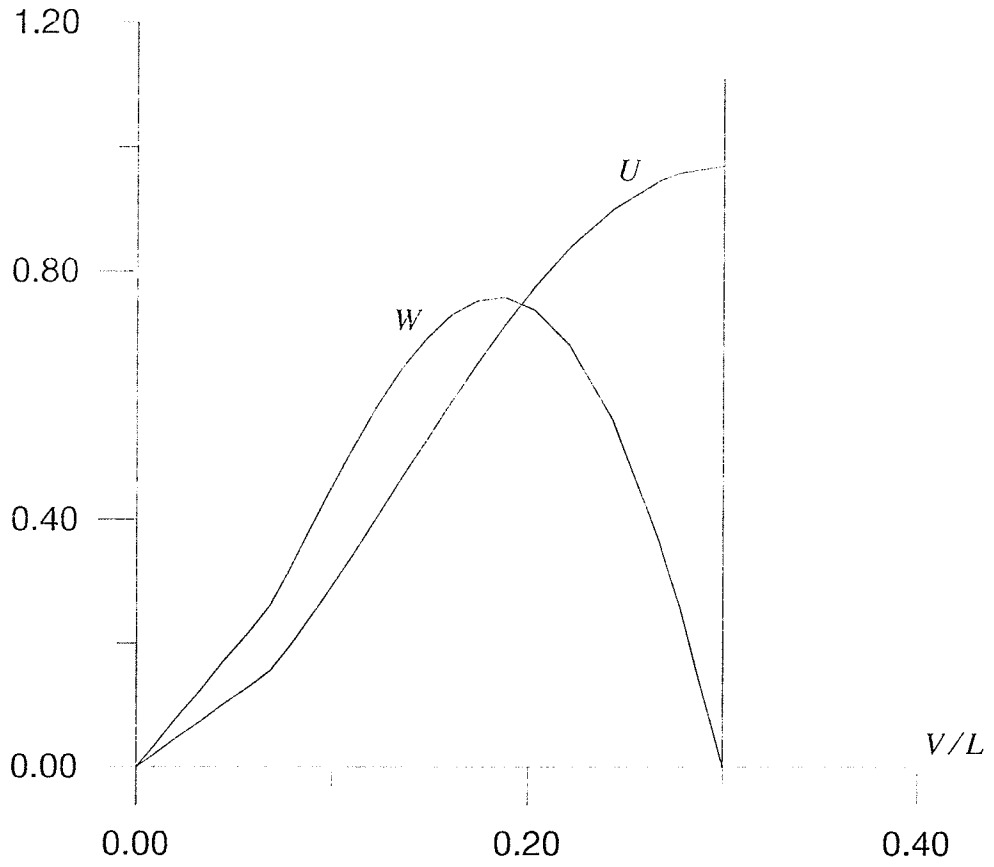

Fig. 3-5. External potential and internal potential

Through this example, as well as through other examples presented in the following chapters, it is shown that the incremental work control and the incremental strain energy control perform well in traversing limit points. The incremental strain energy control performs better than the incremental work control, but is more difficult to program.

3.10. Discussion

In this chapter, four control schemes based on the potential energy are proposed. The external potential control and internal potential control have intuitive physical interpretation. The nonlinear curve is advanced by controlling the absolute value of the external potential energy or the internal potential energy. For external potential control, the formulation and programing are simple. But for stability problems, the absolute value of external potential energy usually has a maximum (or minimum) point (Fig. 3-5). This maximum (or minimum) point indicates that the external potential energy does not usually increase monotonically. The internal potential energy, on the other

hand, has a broad range within which its absolute value increases monotonically. If the range is broad enough to include the domain of the nonlinear solution desired, it could be an advantage to use internal potential control. However, to use these two controls, the absolute value of the external potential energy and the internal potential energy need to be computed. From Eqns. (3-28) and (3-29), the two matrices, K_s and A, are involved in the formulation of internal potential control. Each of the matrices K_s and A is composed of four matrices (Eqns. (2-41) and (2-49)). The multiplication of these matrices (Eqn. (3-28)) involves many computations. If Eqn. (3-39) is used in the incremental strain energy control, the computation of the absolute value of internal potential energy ($U^{(k)}$) can be avoided. This can be seen from Eqns. (3-39) and (3-42) where only matrix K_s is involved in the formulation of the incremental strain energy control. There is no difficulty to compute the absolute value of the external potential energy (see Eqn. (3-18). But if incremental work control is used the displacement range within which the actual work increases monotonically could be broadened because the actual work done by external load is equal to the internal strain energy (Fig. 3-5). This feature enables the incremental work control to be used effectively in many practical engineering problems where the external load produces positive work.

It should be noted that Bathe and Dvorkin (1983) have proposed a scheme called increment of external work (or work constraint). In their procedure, Bathe and Dvorkin specify a constant increment of external work for the first iteration, i.e.,

$$\frac{1}{2}(\lambda^{(1)}+\lambda^{(0)})\boldsymbol{P}^T\delta\boldsymbol{q}^{(1)} = \Delta\bar{W}_a \tag{3-73}$$

This is equivalent to Eqn. (3-36) of incremental work control if $k = 1$ (first iteration). But, for the next iterations, Bathe and Dvorkin enforce the increment of external work to be zero at each iteration. That is

$$\frac{1}{2}(\lambda^{(k)}+\lambda^{(k-1)})\boldsymbol{P}^T\delta\boldsymbol{q}^{(k)} = 0 \tag{3-74}$$

This is different from Eqn. (3-36) in the incremental work control proposed in this thesis. Bathe and Dvorkin conclude by comparing work constraint with arc length control that the work constraint provides a better capability to traverse load limit point while the arc length control demonstrates fast convergence in the region away from limit point.

The methods discussed in this chapter are based on the augmented equation method. Different control schemes lead to different augmented equations. In this aspect, the augmented equation method is actually a family of methods. Its advantage lies in the fact that similar procedures can be

used for different control schemes. It is suggested in this Thesis that the augmented equation derived from different controls can be considered as a group of weighing factors. This method enables various controls to be incorporated in one program and provides the flexibility of using these controls according to the stages of path finding.

Experience has been gained through the use of the control schemes proposed in this Thesis. In brief, the incremental work control and the incremental strain energy control can be applied in a wide range of engineering problems including the analysis of FRP poles. These control methods are simple, easy to understand and manipulate. In addition to these two control schemes, if other control schemes, such as load control, displacement control, and arc length control, are incorporated in the augmented equation method, the power of the solution method can be further reinforced.

Chapter 4. Nonlinear Analysis of Beam-Type Bending

The common height of transmission poles is in the range of 10 to 30 meters. In order to reduce cost, such poles must be slender and the wall thickness must be made as small as possible. It is well understood that overall buckling of a member is associated with its slenderness ratio and that local buckling is associated with the wall thickness. Therefore, the issue of stability and large displacement of thin-walled slender poles must be addressed before any consideration for practical use of such poles.

The overall buckling load of a prismatic column with one end fixed and the other end free can be obtained using classic procedures. Under the assumption of small deflection, the Euler buckling load of such a column under a concentrated load is $P_e = (\pi^2 EI)/(4L^2)$, where E is the modulus of elasticity, I is the moment of inertia and L is the length of the column. When the critical load P_{cr} is reached, the deflection of the column is undefined. The post-buckling behaviour can not be obtained by the linear beam-column theory. A nonlinear formulation was used by Timoshenko and Gere (1961) to determine the post-buckling of a prismatic column. Similar formulations were used by Holden (1972) to obtain the load-deflection curve of a prismatic column under distributed axial loading. Bisshopp and Drucker (1945), Wang (1969) and Barten (1945) investigated large deflection of beams under various loadings. All these analytical formulations lead to elliptical integrals. The fundamental assumption made in the beam-column theory is that the profile of the cross-section of a member remains undistorted during loading although it undergoes very large deflection. Any local deformation pertinent to local buckling is not considered according to this assumption.

4.1. Rigid-Body Rotation

For nonlinear analysis, in order to capture the most significant characteristics of slender poles, such as large deformation and overall buckling due to beam-type bending, all the terms with $l \leq 1$ should be included. However, spacial terms for $l = 2$ are needed to satisfy the requirement for the rigid-body rotation of conical shells. The antisymmetric (about $\beta = 0$) part is not included currently in the nonlinear analysis.

When the truncated pole shown in Fig. 4-1, for example, is giving a rigid-body rotation θ about the x-axis, the point P at the reference cross-section moves to P'. In this case the displacements in the coordinate system xyz are:

$$u_x = 0 \qquad (4\text{-}1)$$

$$u_y = -(r+\gamma\cos\psi)\cos\beta(1-\cos\theta) \tag{4-2}$$

$$u_z = -(r+\gamma\cos\psi)\cos\beta\sin\theta. \tag{4-3}$$

However, the rigid-body displacements represented by Eqns. (4-1), (4-2) and (4-3) can be projected into the curvilinear coordinates (α, β, γ) as follows:

$$u_1^r = u_y\cos\beta\sin\psi - u_z\cos\psi \tag{4-4}$$

$$u_2^r = -u_y\sin\beta \tag{4-5}$$

$$u_3^r = u_y\cos\beta\cos\psi + u_z\sin\psi \tag{4-6}$$

Thus,

$$u_1^r = -\frac{1}{2}(r+\gamma\cos\psi)\sin\psi(1+\cos2\beta)(1-\cos\theta) - (r+\gamma\cos\psi)\cos\psi\cos\beta\sin\theta \tag{4-7}$$

$$u_2^r = \frac{1}{2}(r+\gamma\cos\psi)\sin2\beta(1-\cos\theta) \tag{4-8}$$

$$u_3^r = -\frac{1}{2}(r+\gamma\cos\psi)\cos\psi(1+\cos2\beta)(1-\cos\theta) + (r+\gamma\cos\psi)\sin\psi\cos\beta\sin\theta \tag{4-9}$$

where u_1^r, u_2^r and u_3^r are displacements induced by rigid-body rotation. They are expressed in terms of α, β, and γ directions, respectively (Fig. 2-3).

It is evident from Eqns. (4-7), (4-8) and (4-9) that in order to capture the displacements induced by rigid-body rotation θ, special terms related to $\cos2\beta$ and $\sin2\beta$ must be included in the displacement functions. The factor $(1-\cos\theta)$ may be treated as a new displacement variable; i.e.,

$$\Phi_R = (1-\cos\theta). \tag{4-10}$$

Letting

$$u_1^R = -\frac{1}{2}(r+\gamma\cos\psi)\sin\psi\cos(2\beta)\Phi_R \tag{4-11}$$

$$u_2^R = \frac{1}{2}(r+\gamma\cos\psi)\sin(2\beta)\Phi_R \tag{4-12}$$

$$u_3^R = -\frac{1}{2}(r+\gamma\cos\psi)\cos\psi\cos(2\beta)\,\Phi_R \tag{4-13}$$

then these three terms are the second-order Fourier terms which must be included in order to capture the displacements induced by rigid-body rotation. The other terms left over in Eqns. (4-7) through (4-9) are either zeroth-order or first-order Fourier terms which will be automatically included if M_l is chosen to be equal to one.

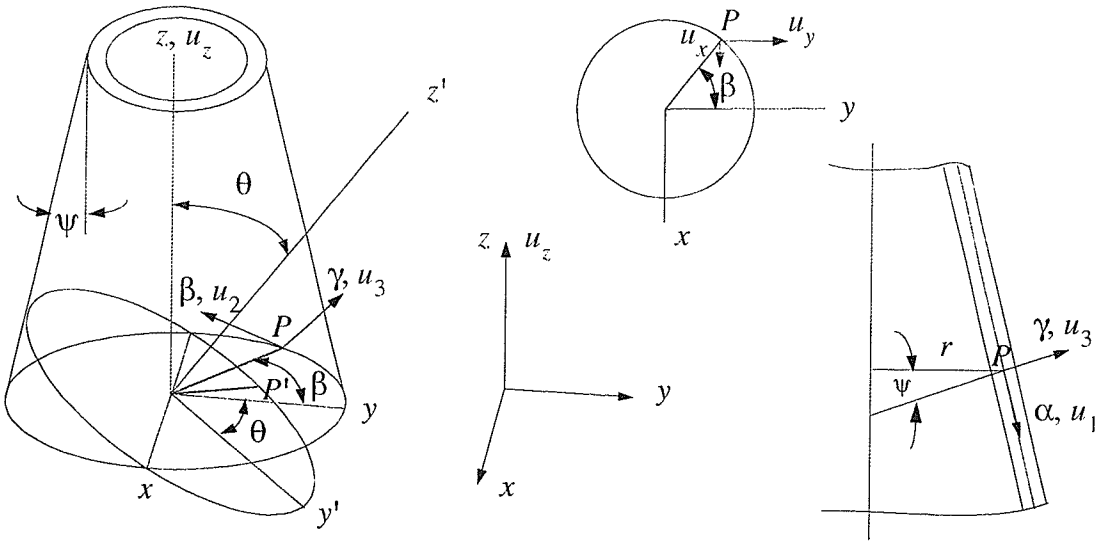

Fig. 4-1. Displacements due to rigid-body rotation

4.2. Finite Element Formulations

Now define:

$$u_1 = v_1 + \gamma\phi_1 + u_1^R \tag{4-14}$$

$$u_2 = v_2 + \gamma\phi_2 + u_2^R \tag{4-15}$$

$$u_3 = v_3 + \gamma\phi_3 + u_3^R \tag{4-16}$$

Substituting v_1 and ϕ_1 from Eqn. (2-56):

$$v_1 = v_1^o + v_{11}^o\cos\beta \tag{4-17}$$

$$\phi_1 = \phi_1^o + \phi_{11}^o\cos\beta \tag{4-18}$$

into Eqn. (4-14), yields:

$$u_1 = [\theta_1][\Gamma_1]\begin{bmatrix} v_1^o \\ \phi_1^o \\ v_{11}^a \\ \phi_{11}^a \\ \Phi_R \\ r\Phi_R \end{bmatrix} \tag{4-19}$$

Similarly

$$u_2 = [\theta_2][\Gamma_2]\begin{bmatrix} v_2^o \\ \phi_2^o \\ v_{21}^a \\ \phi_{21}^a \\ \Phi_R \\ r\Phi_R \end{bmatrix} \tag{4-20}$$

$$u_3 = [\theta_3][\Gamma_3]\begin{bmatrix} v_3^o \\ \phi_3^o \\ v_{31}^a \\ \phi_{31}^a \\ \Phi_R \\ r\Phi_R \end{bmatrix} \tag{4-21}$$

where matrices $[\theta_i]$ $(i = 1, 2, 3)$ are functions of β only, matrices $[\Gamma_i]$ $(i = 1, 2, 3)$ are functions of γ only. These are:

$$[\theta_1] = \begin{bmatrix} 1 & 1 & \cos\beta & \cos\beta & \cos 2\beta \end{bmatrix} \tag{4-22}$$

$$[\theta_2] = \begin{bmatrix} 1 & 1 & \sin\beta & \sin\beta & \sin 2\beta \end{bmatrix} \tag{4-23}$$

$$[\theta_3] = \begin{bmatrix} 1 & 1 & \cos\beta & \cos\beta & \cos 2\beta \end{bmatrix} \tag{4-24}$$

$$\Gamma_1 = \begin{bmatrix} 1 & 0 & 0 & 0 & 0 & 0 \\ 0 & \gamma & 0 & 0 & 0 & 0 \\ 0 & 0 & 1 & 0 & 0 & 0 \\ 0 & 0 & 0 & \gamma & 0 & 0 \\ 0 & 0 & 0 & 0 & \dfrac{-\gamma\cos\psi\sin\psi}{2} & \dfrac{-\sin\psi}{2} \end{bmatrix} \tag{4-25}$$

$$\Gamma_2 = \begin{bmatrix} 1 & 0 & 0 & 0 & 0 & 0 \\ 0 & \gamma & 0 & 0 & 0 & 0 \\ 0 & 0 & 1 & 0 & 0 & 0 \\ 0 & 0 & 0 & \gamma & 0 & 0 \\ 0 & 0 & 0 & 0 & \dfrac{\gamma\cos\psi}{2} & \dfrac{1}{2} \end{bmatrix} \tag{4-26}$$

$$\Gamma_3 = \begin{bmatrix} 1 & 0 & 0 & 0 & 0 & 0 \\ 0 & \gamma & 0 & 0 & 0 & 0 \\ 0 & 0 & 1 & 0 & 0 & 0 \\ 0 & 0 & 0 & \gamma & 0 & 0 \\ 0 & 0 & 0 & 0 & \dfrac{-\gamma\cos\psi\cos\psi}{2} & \dfrac{-\cos\psi}{2} \end{bmatrix} \tag{4-27}$$

The displacement variables Φ_R, v_1^o, ϕ_1^o, etc., are all functions of coordinate α only. Dividing the pole into a number of elements in the α direction, these variables can be interpolated in terms of nodal displacements of an element. Choosing the displacement polynomials and following the standard procedures, the equations for the displacements u_1, u_2 and u_3 can be manipulated in matrix form as follows:

$$u_1 = [\theta_1]\,[\Gamma_1]\,[N_1]\,q_e \tag{4-28}$$

$$u_2 = [\theta_2]\,[\Gamma_2]\,[N_2]\,q_e \tag{4-29}$$

$$u_3 = [\theta_3]\,[\Gamma_3]\,[N_3]\,q_e \tag{4-30}$$

If quadratic form of α is used as shape functions, then an element has three nodes (Fig. 4-2).

Defining the nodal displacements at i, k, j as follows:

$$q_m = \left[v_{1m}^o \;\; \phi_{1m}^o \;\; v_{2m}^o \;\; \phi_{2m}^o \;\; v_{3m}^o \;\; \phi_{3m}^o \;\; v_{11m}^a \;\; \phi_{11m}^a \;\; v_{21m}^a \;\; \phi_{21m}^a \;\; v_{31m}^a \;\; \phi_{31m}^a \;\; \Phi_{Rm} \right]^T \tag{4-31}$$

where $m = i, k, j$, and arrange the element nodal displacement vector as

$$q_e = \begin{bmatrix} q_i \\ q_k \\ q_j \end{bmatrix} \tag{4-32}$$

The shape function matrices $[N_i]$ $(i = 1, 2, 3)$ are functions of α only and can be determined according to the sequence of the nodal displacements in q_e. Expressions of $[N_i]$ $(i = 1, 2, 3)$ are given in Appendix **C**. Upon substituting the displacement functions (Eqns. (4-28), (4-29) and (4-30)) into the formation of linear and nonlinear stiffness matrices (Eqns. (2-36), (2-37), (2-38) and (2-39)), we have finally a nonlinear system equation (Eqn. (2-50)):

$$\chi = R - \lambda P = \{0\} \tag{4-33}$$

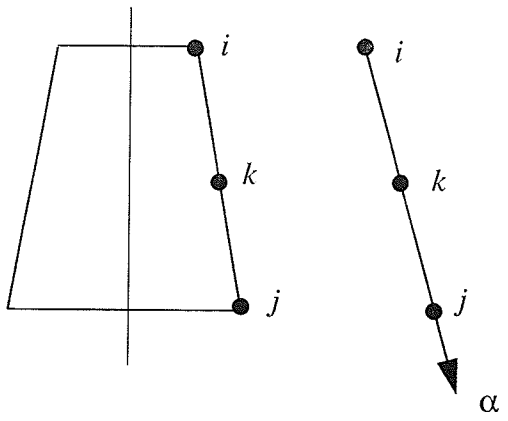

Fig. 4-2. Element and nodes

The finite element model discussed above has been implemented into a computer program. A Newton-Raphson iteration method (Chapter 3) is employed to facilitate the solution of nonlinear equations (Eqn. (4-33)). Following examples demonstrate the applicability of the nonlinear theory and finite element model developed herein.

4.3. Examples

Example 4-1: In this example a homogeneous cylindrical tube (Fig. 4-3) is considered. Material and geometric data are chosen as follows: modulus of elasticity, $E = 24.04GPa$; shear modulus, $G = 9.25GPa$; Poisson's ratio $\nu = 0.3$; $r = 34.29mm$; $t = 5.08mm$; moment of inertia, $I = 0.64 \times 10^6 mm^4$. The load deflection curve obtained from the proposed nonlinear analysis is

shown in Fig. 4-3 along with the curve obtained from the analytical solution developed by Bisshopp and Drucker (1945). These two curves are obtained by applying a transverse load Q only. Very good correlation is observed since both these two curves are almost identical through the whole range of displacements. The linear solution obtained through the basic beam theory is also shown in Fig. 4-3. As shown in Fig. 4-3, for an uniform beam of isotropic material, a linear solution is a good approximation to the nonlinear solution only if the relative displacement (Δ/L) is less than 30%. For design purpose, the linear solution yields conservative results.

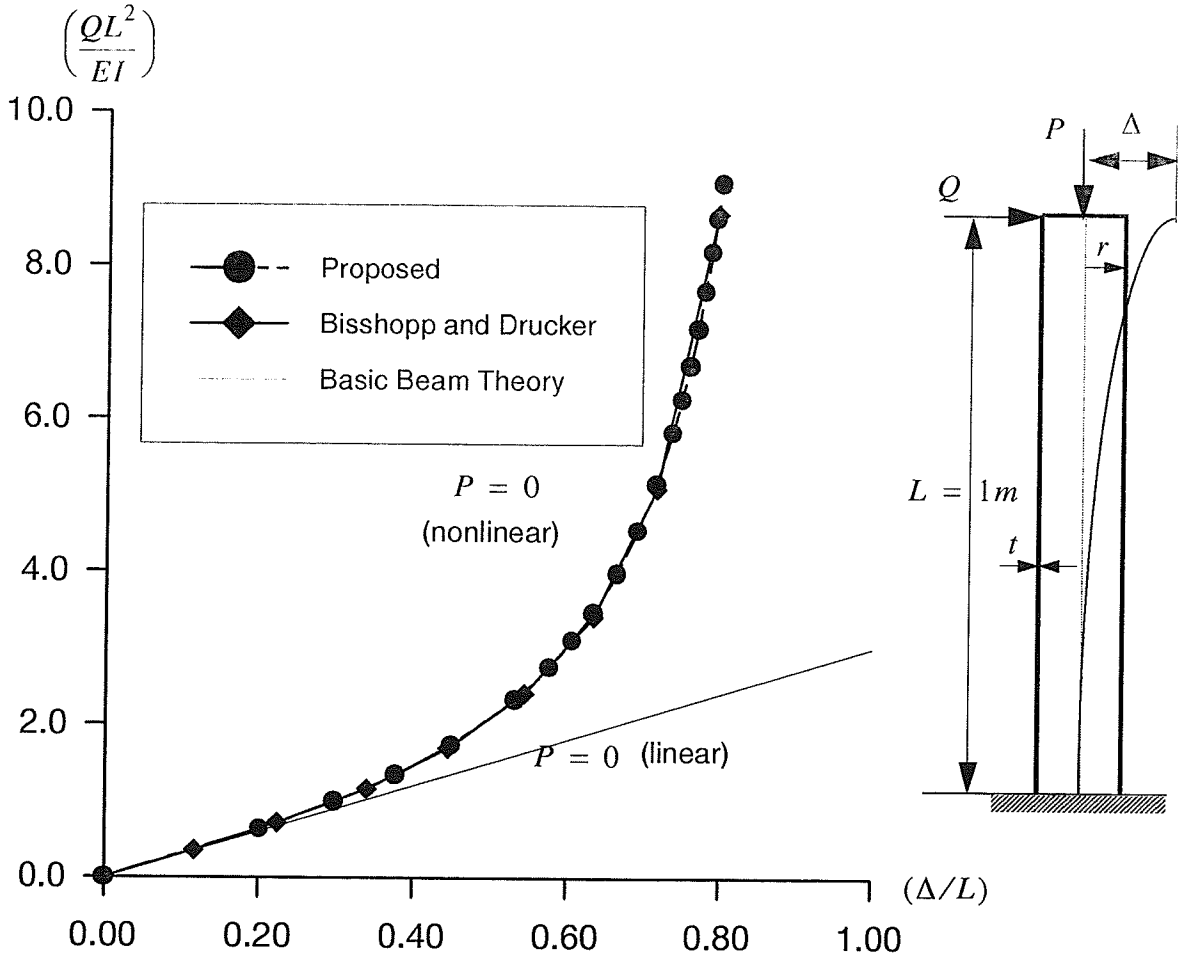

Fig. 4-3. Displacement of the cylindrical tube under lateral load

To examine the behaviour of a tube under combined axial load and bending, an axial load was applied, as shown in Fig. 4-4. In this figure, the lateral deflection of the tube at the free end, Δ, is plotted as a function of the axial load, P. A small transverse load $Q = 0.0056kN$ is applied to obtain a smooth transition from the fundamental to the secondary path (Chen and Lui 1987). The results

are compared with the post buckling results obtained from Timoshenko's formulation (Timoshenko and Gere 1961). The comparison is made at large deflections since only pure axial load is considered in Timoshenko's formulation. P_e in Fig. 4-4 is the Euler load.

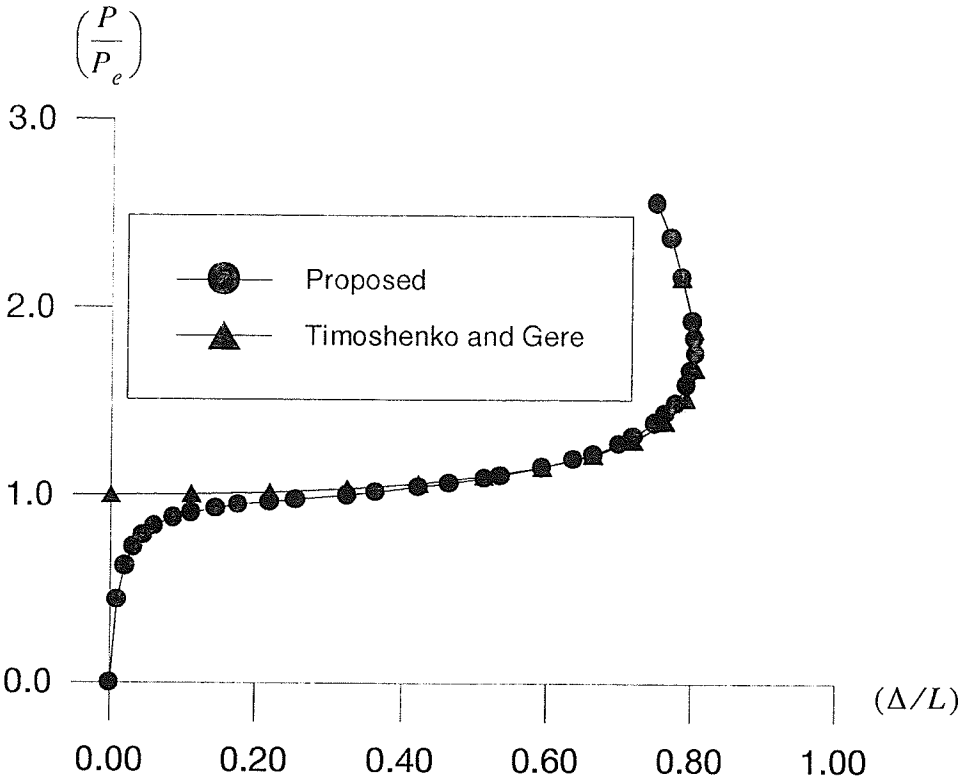

Fig. 4-4. Post buckling curves of the cylindrical tube

Example 4-2: In this example a tapered FRP pole with three layers (Fig. 4-5) is considered. The material properties used are: modulus of elasticity of the fibers in the longitudinal direction, $E_L = 38.0GPa$; modulus of elasticity of the fibres in the transverse direction, $E_T = 6.832GPa$; major Poisson's ratio, $\upsilon_{LT} = 0.3$; minor Poisson's ratio, $\upsilon_{TT} = 0.49$; and in-plane shear modulus, $G_{LT} = 2.293GPa$. The fibres in the middle layers are oriented in meridional direction while the fibres in the inner and outer layers are oriented at ±3 degrees with respect to the circumferential direction.

The results from the nonlinear analysis (solution of Eqn. (4-33)) are compared to those from the linear analysis (solution of Eqn. (7-22) with $l = 1$) in Fig. 4-6. The linear curve is obtained

from the high-order shear theory (Reddy and Liu 1985). Since the axial load P is small compared to the critical load P_{cr} (Chapter 6), a stiffening effect is observed in this portion of the deflection curve. For this example, linear and nonlinear solutions diverge at $\Delta/L \approx 0.25$. At $\Delta/L = 0.3$, the relative difference between the results from the two theories exceeds 20%. These results indicate that the behaviour of FRP poles could be more nonlinear in some cases.

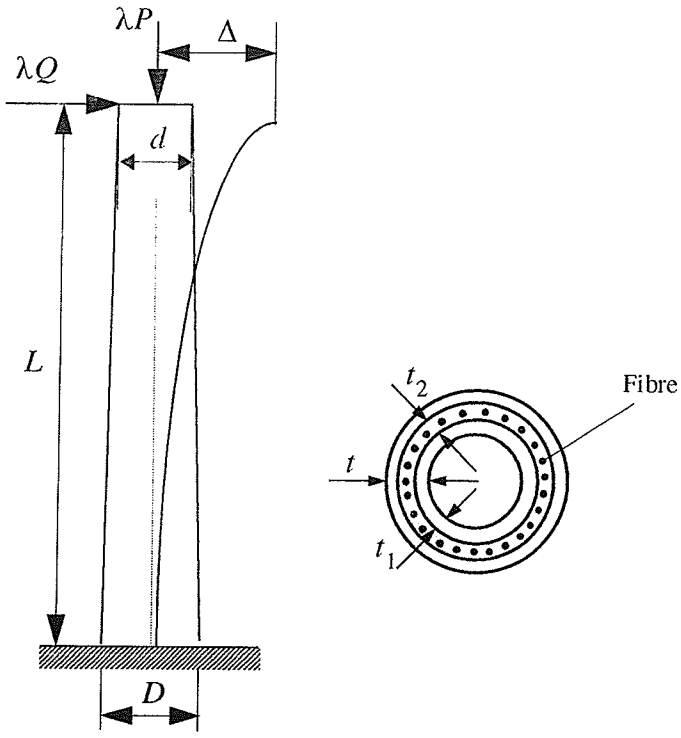

Fig. 4-5. A tapered FRP pole with three layers

4.4. Discussion

To include all the rigid-body modes in the displacement function is difficult (Gould 1985) if curvilinear coordinates are used. Fonder and Clough (1973) proposed a method of explicit addition of rigid-body motion in curved elements. This method is general but requires substantial computations. MeBane and Stricklin (1971) suggest that implicit rigid body motion is sufficient in some finite elements if higher order displacement functions are included. In this chapter, it is proven that in modelling the beam-type bending of the poles, some second-order Fourier terms which are necessary to model the rigid-body rotation must be included in the displacement functions. A special displacement variable $\Phi_R = (1 - \cos\theta)$ is introduced. This approach has been proven to be successful as seen from the examples presented.

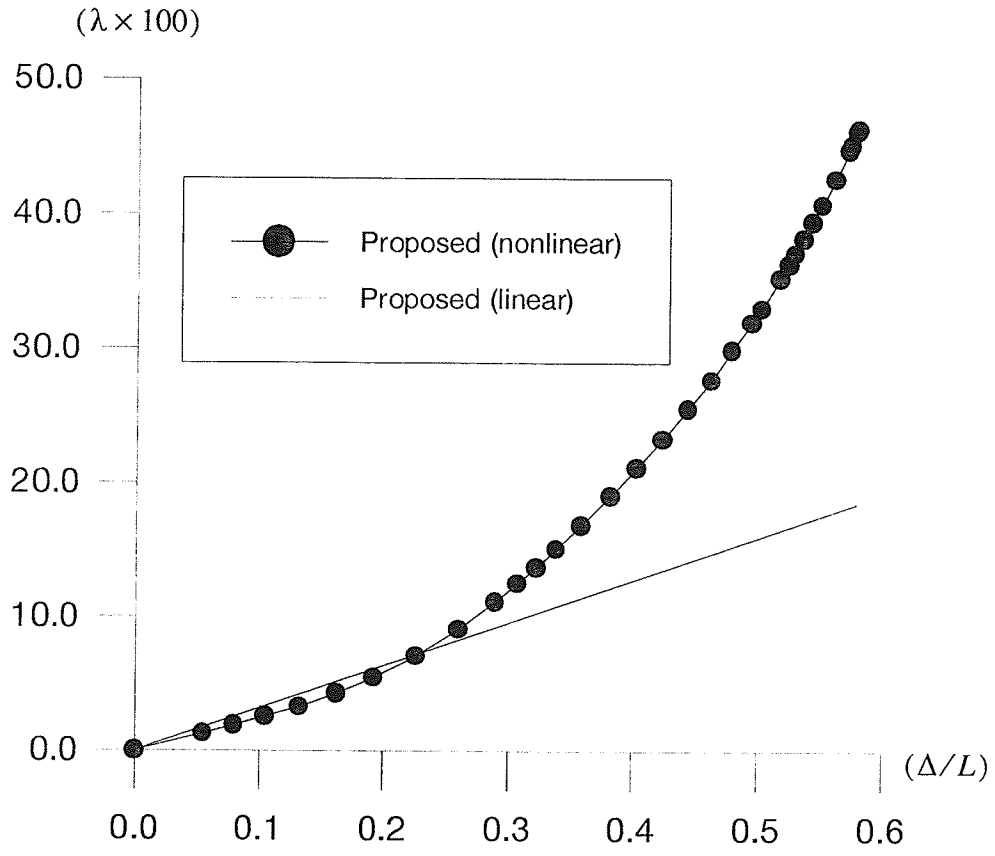

Fig. 4-6. Load deflection curves of the tapered FRP pole

The post-buckling behaviour can be analyzed using the large displacement nonlinear analysis. Very good agreement between the theoretical results and the finite element results has been demonstrated through the examples considered in this chapter. Although transverse shear strains and hoop strains are included in the analysis, for slender poles considered here, no significant effect is observed since the loading conditions considered are simple.

The incremental work control and the incremental strain energy control as proposed in Chapter 3 are used in the solution of nonlinear equations particular to the examples discussed in this chapter. The application of these two control schemes are successful especially for the problems of large displacement and post buckling of beam-type bending of tapered poles because the work done by the external loads monotonically increase as the displacement increases. An automatic

incremental step adjustment procedure is incorporated in the computer program to achieve better efficiency. The computation, however, is intensive. For example, to obtain the curve in Fig. 4-4, ten to twenty hours are needed in an IBM-PC compatible machine running at 33 MHz.

Chapter 5. Ovalization Analysis

5.1. Introduction

It was mentioned in Chapter 1 that FRP poles could fail by ovalization near the supporting base (McClure and Boire 1992). The ovalization of a long cylindrical shell was first studied by Brazier in 1927 (Brush and Almroth 1975) and is referred to as the Brazier effect. Brazier's analysis is restricted to infinitely long shells. If a long cylindrical shell is subjected to a bending moment and bent with a curvature $1/\rho$ (Fig. 5-1), the longitudinal tension and compression stresses will have components directed toward the mid-plane of the tube. The effect of these components is to flatten the tube. The equilibrium path of the bent cylinder may be illustrated in a diagram (Fig. 5-2). The bending moment vs. the curvature is nonlinear. The collapse of the shell occurs at the maximum moment.

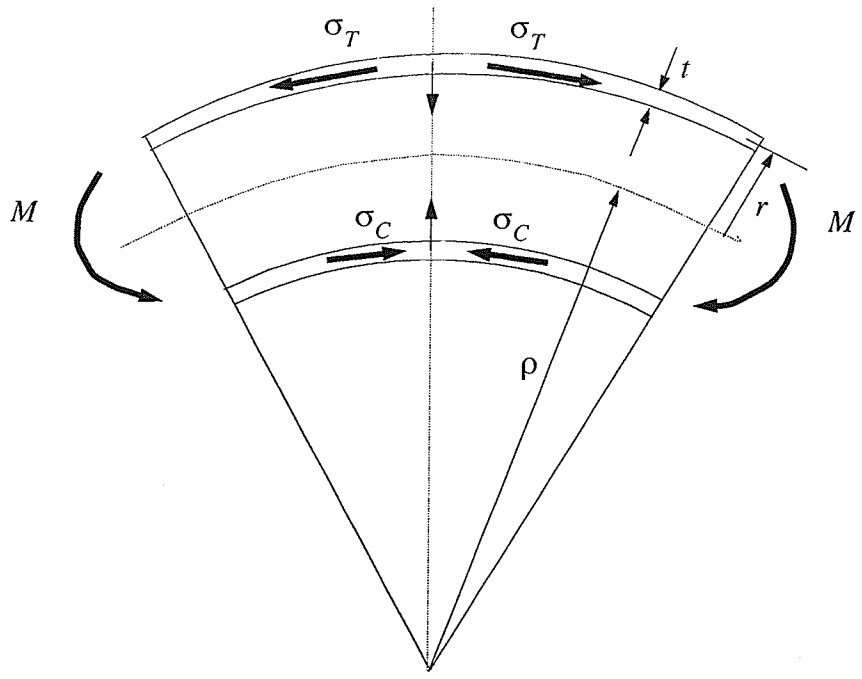

Fig. 5-1. The Brazier effect

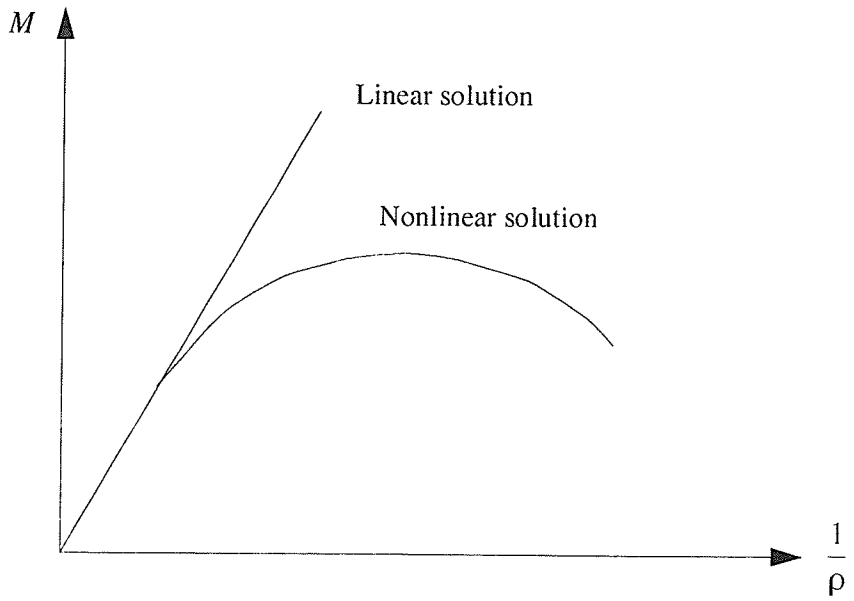

Fig. 5-2. Equilibrium path for bent cylinder

A bent cylinder may be alternatively considered as a curved tube. The phenomena of flattening of a curved tube was observed by Bantling and theoretically investigated by Von Karman (Clark and Reissner 1954). Subsequently the topic was addressed by a few researchers (Clark and Reissner 1954) by using different energy principles and approximate methods. Clark and Reissner (1954) indicated that the flattening effect depends on (a) the ratio of a representative cross-sectional radius r to the center line radius ρ, and (b) the ratio of a representative wall thickness t to a representative cross-sectional radius r. The ratio r/ρ is of minor importance by itself but the combination of the two, namely $r^2/(\rho t)$, is the governing parameter. When $r^2/(\rho t)$ is small compared with unity the flattening effect is unimportant. When $r^2/(\rho t)$ is of the order of unity or large compared to unity, the flattening effect is important.

5.2. Procedures

To analyze the ovalization of FRP poles, two factors have to be considered. First, the poles are tapered, and second, materials are anisotropic. These two factors render that analytical method more difficult to apply. However, the basic formulations and finite element procedures discussed in Chapters 2 and 4 can be readily applied with some extensions.

Theoretically, the profile of a flattened circular cross-section is a complex pattern which may be represented with sufficient accuracy by Fourier expansions (Eqn. (2-53)) up to a particular order M_1. To simplify the analysis and capture the most important characteristics of the ovalization, it was assumed that ovalization of a circular cross-section can be modeled by the second-order Fourier terms. This assumption can be justified by observing the displacement patterns pertinent to $\cos 2\beta$ and $\sin 2\beta$ of the components of displacements u_2 and u_3. For example, $v^a_{32}\cos 2\beta$ is illustrated in Fig. 5-3. v^a_{32} is a constant value in relation to β and the sign of $v^a_{32}\cos 2\beta$ depends on the sign of $\cos 2\beta$. A positive value indicates a displacement away from the center point while a negative value indicates a displacement towards the center point.

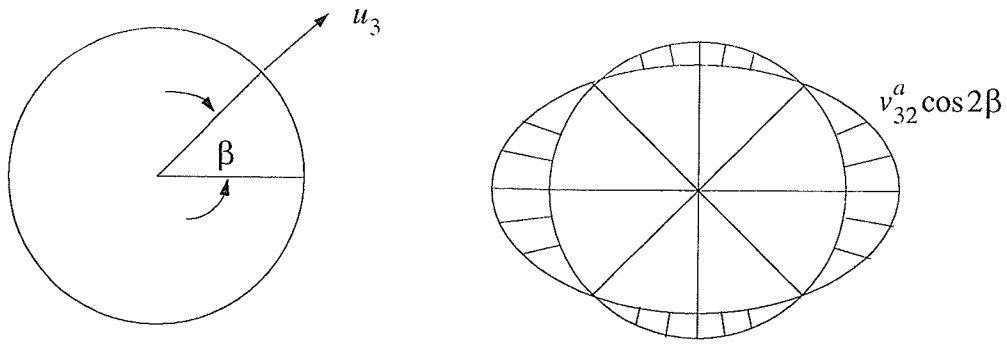

Fig. 5-3. Displacement component $v^a_{32}\cos 2\beta$

Careful examination of Eqns. (4-9) and (4-10) of the rigid-body rotation, shows that the equal amplitudes of the terms $v^a_{22}\sin 2\beta$ and $-v^a_{32}\cos 2\beta$ represent the rigid-body rotation (for a prismatic pole where $\psi = 0$) of a cross-section. Thus, only the difference of the amplitudes between $v^a_{22}\sin 2\beta$ and $-v^a_{32}\cos 2\beta$ represents the actual ovalization.

As mentioned earlier, the procedures and formulations discussed in Chapters 2 and 4 can be conveniently applied to the ovalization analysis provided all the second-order Fourier terms are included in accordance with the assumption made previously. Naturally, those second-order terms required by the rigid-body rotation are automatically included. Again, quadratic shape functions are used in the interpolation of v^a_{12}, ϕ^a_{12}, etc. The number of nodal displacements in an element, however, are increased from 39 to 54. The displacements u_1, u_2 and u_3 are expressed in the same

form as Eqns. (4-25), (4-26) and (4-27). These are:

$$u_1 = [\theta_1][\Gamma_1][N_1]q_e \tag{5-1}$$

$$u_2 = [\theta_2][\Gamma_2][N_2]q_e \tag{5-2}$$

$$u_3 = [\theta_3][\Gamma_3][N_3]q_e \tag{5-3}$$

where

$$q_e = \begin{bmatrix} q_i \\ q_k \\ q_j \end{bmatrix}. \tag{5-4}$$

$$q_m = \left[v^o_{1m}\ \phi^o_{1m}\ v^o_{2m}\ \phi^o_{2m}\ v^o_{3m}\ \phi^o_{3m}\ v^a_{11m}\ \phi^a_{11m}\ v^a_{21m}\ \phi^a_{21m}\ v^a_{31m}\ \phi^a_{31m}\ v^a_{12m}\ \phi^a_{12m}\ v^a_{22m}\ \phi^a_{22m}\ v^a_{32m}\ \phi^a_{32m} \right]^T \tag{5-5}$$

$$m = i, k, j$$

$$[\theta_1] = \begin{bmatrix} 1 & 1 & \cos\beta & \cos\beta & \cos 2\beta & \cos 2\beta \end{bmatrix} \tag{5-6}$$

$$[\theta_2] = \begin{bmatrix} 1 & 1 & \sin\beta & \sin\beta & \sin 2\beta & \sin 2\beta \end{bmatrix} \tag{5-7}$$

$$[\theta_3] = \begin{bmatrix} 1 & 1 & \cos\beta & \cos\beta & \cos 2\beta & \cos 2\beta \end{bmatrix} \tag{5-8}$$

$$\Gamma_1 = \Gamma_2 = \Gamma_3 = \begin{bmatrix} 1 & 0 & 0 & 0 & 0 & 0 \\ 0 & \gamma & 0 & 0 & 0 & 0 \\ 0 & 0 & 1 & 0 & 0 & 0 \\ 0 & 0 & 0 & \gamma & 0 & 0 \\ 0 & 0 & 0 & 0 & 1 & 0 \\ 0 & 0 & 0 & 0 & 0 & \gamma \end{bmatrix} \tag{5-9}$$

The shape function matrices $[N_i]$ $(i = 1, 2, 3)$ are given in Appendix D.

5.3. Example

Example 5-1: In this example, a thin-walled cylindrical tube is considered (Fig. 5-4). The dimensions of the tube are chosen in an attempt to clearly demonstrate the ovalization phenomena. As mentioned earlier, the ratio $r^2/(\rho t)$ governs the ovalization effect. An increase in this ratio

occurs if there is an increase in the radius of cross-section, a decrease in the thickness, or an increase in the length of the tube (so the radius of cuvatute decreases).

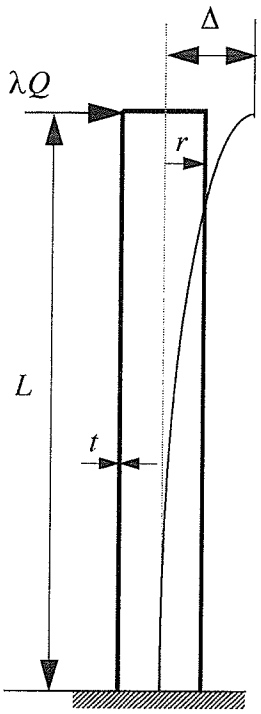

$$E = 24.04Gpa$$
$$G = 9.25Gpa$$
$$L = 2.4m$$
$$r = 72mm$$
$$t = 1mm$$
$$Q = 0.2262kN$$

Fig. 5-4. Thin-walled cylinder

In Fig. 5-5, the ovalization is represented by $v_E = \left|v_{32}^a\right| - \left|v_{22}^a\right|$. It can be seen that the ovalization is developed very quickly as the load reaches a certain level. The load starts to drop sharply after reaching a maximum. This behaviour indicates that the load carrying capacity decreases due to the ovalization effect. The load deflection curve is draw in Fig. 5-6. Contrary to the pure beam-type bending where a stiffening equilibrium path is obtained, a softening effect is observed because the decreasing of moment resistance. The maximum load point (limit point) determines the stability of the cylinder.The equilibrium is stable before the maximum load point and unstable after the maximum load point.

5.4. Discussion

The ovalization (Brazier effect) of cylindrical poles was investigated using the finite element method. All the second-order Fourier terms are included in the displacement functions. Procedures

for the implementation of the finite element method are similar to that of beam-type-bending. An example of a thin-walled cylinder is presented to demonstrate the ovalization effect. It is obvious that the load carrying capacity is strongly affected by the ovalization of the cross-section. A limit load point occurs when the ovalization reaches a certain point. Instability results after this point. The load deflection curve is quite different from that obtained in Chapter 4 (beam-type bending). The lateral load drops significantly after the limit point. This fact is important in the design of such poles where the ovalization might dominate.

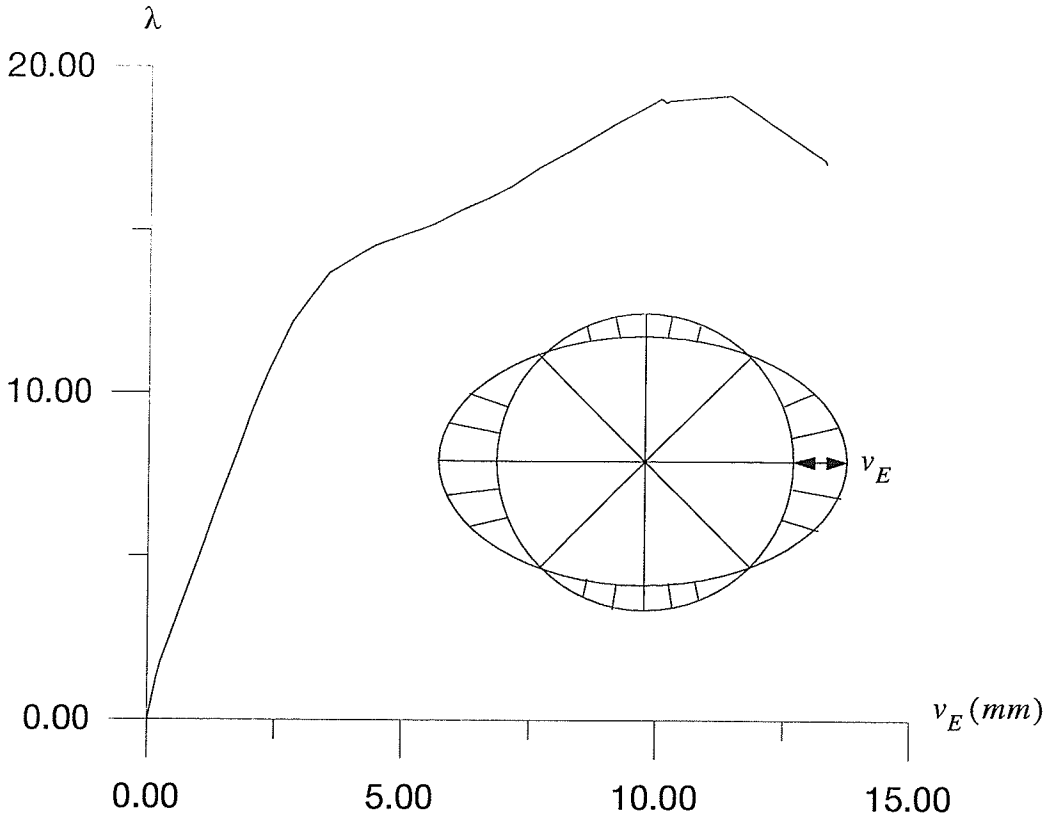

Fig. 5-5. Ovalization of thin-walled cylinder

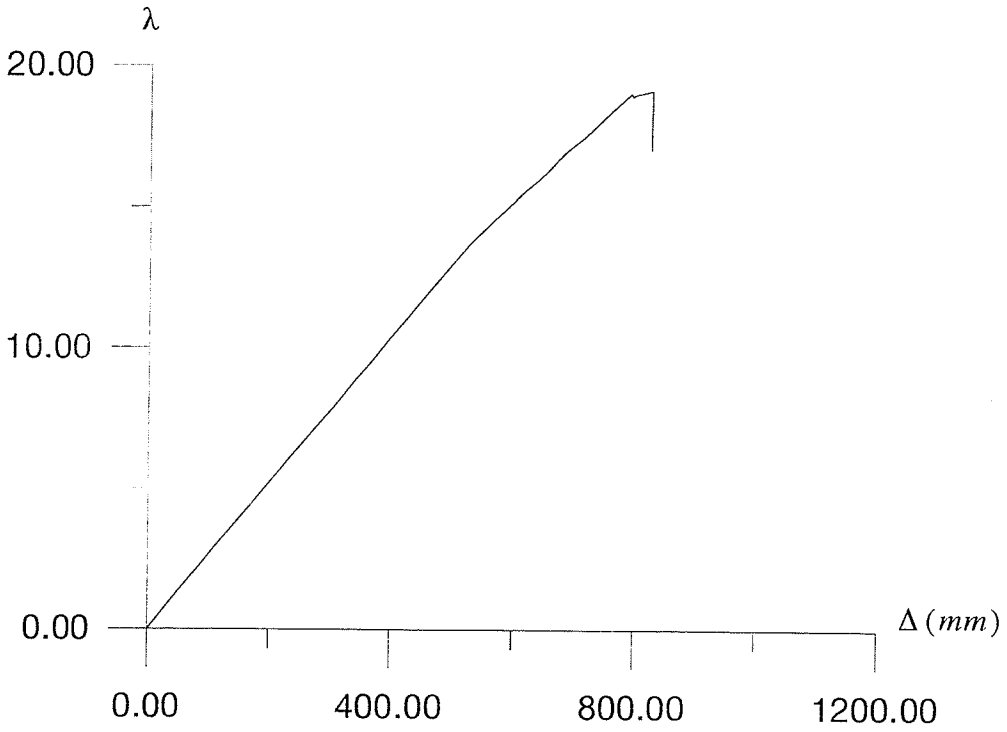

Fig. 5-6. Load-deflection curve of thin-walled cylinder

Chapter 6. Linear Buckling and $P-\Delta$ Analysis

The nonlinear analyses discussed in the previous chapters are based on the assumption that strains are small while displacements can be arbitrarily large. It is well known that the classical beam-column theory is based on the assumption that the displacements are small. If this assumption is retained and together with some other assumptions, the nonlinear equations can be degenerated into linear equations, namely, linear $P-\Delta$ analysis or linear buckling analysis depending on the loading conditions.

6.1. Assumptions and Derivations

For small displacements, the nonlinear strain $\{\varepsilon^N\}$ is small compared to linear strain $\{\varepsilon^L\}$. If $\{\varepsilon^N\}$ could be neglected but $\{\delta\varepsilon^N\}$ may not be neglected for the linear buckling and the $P-\Delta$ analyses in Eqns. (2-34) and (2-35). Also the nodal displacement vector q can be decomposed into axial symmetric part q^o and non-axially symmetric part q^a. Therefore, the nodal displacement vector of an element can be expressed as

$$q_e = \begin{bmatrix} q_e^o \\ q_e^a \end{bmatrix} \tag{6-1}$$

Accordingly, the external potential is

$$-W = \begin{bmatrix} (q^o)^T & (q^a)^T \end{bmatrix} \begin{bmatrix} f_o \\ f_a \end{bmatrix} \tag{6-2}$$

where f_o and f_a are axially symmetric and non-axially symmetric nodal load vectors, respectively. Further, by assuming that the nonlinear strain is caused by beam-type bending only, the system equations can be uncoupled in terms of q^o and q^a. To prove this, the variation of the strain energy of an element must be considered; i.e.,

$$\delta U_e = \int_v \{\delta\varepsilon^L\}^T \boldsymbol{D} \{\varepsilon^L\}\, dv + \int_v \{\delta\varepsilon^N\}^T \boldsymbol{D} \{\varepsilon^L\}\, dv \tag{6-3}$$

Eqns. (2-30) and (2-31) may be written in a decomposed form as

$$\{\varepsilon^L\} = \boldsymbol{B}^L \boldsymbol{q}_e = \left[\boldsymbol{B}_o^L \; \boldsymbol{B}_a^L\right] \begin{bmatrix} \boldsymbol{q}_e^o \\ \boldsymbol{q}_e^a \end{bmatrix}, \tag{6-4}$$

$$\{\delta\varepsilon^L\} = \boldsymbol{B}^L \delta\boldsymbol{q}_e = \left[\boldsymbol{B}_o^L \; \boldsymbol{B}_a^L\right] \begin{bmatrix} \delta\boldsymbol{q}_e^o \\ \delta\boldsymbol{q}_e^a \end{bmatrix} \tag{6-5}$$

$$\{\varepsilon^N\} = \frac{1}{2}\left[\boldsymbol{B}^N(\boldsymbol{q}_e)\right]\boldsymbol{q}_e = \frac{1}{2}\left[\boldsymbol{0} \; \boldsymbol{B}_a^N(\boldsymbol{q}_e^a)\right] \begin{bmatrix} \boldsymbol{q}_e^o \\ \boldsymbol{q}_e^a \end{bmatrix}, \tag{6-6}$$

$$\{\delta\varepsilon^N\} = \left[\boldsymbol{B}^N(\boldsymbol{q}_e)\right]\delta\boldsymbol{q}_e = \left[\boldsymbol{0} \; \boldsymbol{B}_a^N(\boldsymbol{q}_e^a)\right] \begin{bmatrix} \delta\boldsymbol{q}_e^o \\ \delta\boldsymbol{q}_e^a \end{bmatrix}. \tag{6-7}$$

Eqn. (6-3) becomes

$$\delta U_e = \left[(\delta\boldsymbol{q}_e^o)^T \; (\delta\boldsymbol{q}_e^a)^T\right] \left(\int_v \begin{bmatrix} (\boldsymbol{B}_o^L)^T \\ (\boldsymbol{B}_a^L)^T \end{bmatrix} \boldsymbol{D} \left[\boldsymbol{B}_o^L \; \boldsymbol{B}_a^L\right] dv + \int_v \begin{bmatrix} \boldsymbol{0} \\ (\boldsymbol{B}_a^N(\boldsymbol{q}_e^a))^T \end{bmatrix} \boldsymbol{D} \left[\boldsymbol{B}_o^L \; \boldsymbol{B}_a^L\right] dv \right) \begin{bmatrix} \boldsymbol{q}_e^o \\ \boldsymbol{q}_e^a \end{bmatrix} \tag{6-8}$$

Noting that $\boldsymbol{B}_o^L$ is a constant matrix with respect to β and $\boldsymbol{B}_a^L$ is linearly depended on $\cos\beta$ and $\sin\beta$, while, $\boldsymbol{B}_a^N(\boldsymbol{q}_e^a)$ is a function of $(\cos\beta)^2$ and $(\sin\beta)^2$, from the orthogonality of trigonometric functions (Zienkiewicz, 1971), the following relations are obtained.

$$\int_v (\boldsymbol{B}_o^L)^T \boldsymbol{D} \boldsymbol{B}_a^L dv = \boldsymbol{0} \tag{6-9}$$

$$\int_v (\boldsymbol{B}_a^L)^T \boldsymbol{D} \boldsymbol{B}_o^L dv = \boldsymbol{0} \tag{6-10}$$

$$\int_v (\boldsymbol{B}_a^N(\boldsymbol{q}_e^a))^T \boldsymbol{D} \boldsymbol{B}_a^L dv = \boldsymbol{0} \tag{6-11}$$

Eqn. (6-3) becomes

$$\delta U_e = (\delta\boldsymbol{q}_e^o)^T \int_v (\boldsymbol{B}_o^L)^T \boldsymbol{D} \boldsymbol{B}_o^L dv \boldsymbol{q}_e^o + (\delta\boldsymbol{q}_e^a)^T \int_v (\boldsymbol{B}_a^L)^T \boldsymbol{D} \boldsymbol{B}_a^L dv \boldsymbol{q}_e^a + (\delta\boldsymbol{q}_e^a)^T \int_v (\boldsymbol{B}_a^N(\boldsymbol{q}_e^a))^T \boldsymbol{D} \boldsymbol{B}_o^L dv \boldsymbol{q}_e^o \tag{6-12}$$

In the classical beam-column theory, the axial load is assumed to be fixed in the derivation of equi-

librium condition. This assumption is generalized so that the axially symmetric loads are kept constant and the state is equivalent to that when the axially symmetric displacement vector q_e^o is constant in Eqn. (6-12). The last term in Eqn. (6-12) can be put into the form

$$(\delta q_e^a)^T \int_v (B_a^N(q_e^a))^T D B_o^L dv q_e^o = (\delta q_e^a)^T \left[G_e(q_e^o)\right] q_e^a \tag{6-13}$$

where $\left[G_e(q_e^o)\right]$ is a matrix function of q_e^o only. Eqn. (6-13) holds true because $(B_a^N(q_e^a))$ is a linear function of q_e^a. If the following two equations are defined

$$K_e^o = \int_v (B_o^L)^T D B_o^L dv \tag{6-14}$$

$$K_e^a = \int_v (B_a^L)^T D B_a^L dv \tag{6-15}$$

then, the system of equations can be written in the form of two uncoupled equations; i.e.,

$$K_o q_o = f_o \tag{6-16}$$

$$[K_a + G(q_o)]\, q_a = f_a \tag{6-17}$$

In engineering practice, the matrix $G(q_o)$ usually appears in the form $G(\sigma_o)$ and the axially symmetric stress vector σ_o is evaluated according to q_o which is computed from Eqn. (6-16). Equations (6-16) and (6-17) form the basis for the $P-\Delta$ analysis since the axial load is included in f_o and its second order effect is reflected through the, so-called, initial stress stiffness matrix G. In the special case where $f_a = \{0\}$, Eqn. (6-17) can be cast into an eigenvalue problem as,

$$[K_a + \lambda G(q_o)]\, q_a = \{0\} \tag{6-18}$$

where, λ is the eigenvalue and q_a is the corresponding eigenvector. The critical load can then be determined by multiplying the lowest eigenvalue λ and the initial load f_o. This procedure is usually called linear stability analysis because both Eqns. (6-16) and (6-18) are linear. The process from Eqns. (6-16) to (6-18) implies that the displacement q_o is independent of q_a. This is an approximation and is valid only for the case of small lateral deflections.

Table 6-1 and Table 6-2 summarize the assumptions made for linear $P-\Delta$ analysis and linear stability analysis. The following examples are presented to show the applicability of the linear stability analysis and linear $P-\Delta$ analysis discussed in this chapter.

TABLE 6-1
Assumptions for $P-\Delta$ effect (small deflection)

Strains	Small
Deflection	Small
Load	General (Axial Symmetric Load and Transverse Load)
$\{\varepsilon^N\} \ll \{\varepsilon^L\}$	Yes
$\int_v \{\delta\varepsilon^L\}^T \boldsymbol{D} \{\varepsilon^N\}\, dv \ll \int_v \{\delta\varepsilon^L\}^T \boldsymbol{D} \{\varepsilon^L\}\, dv$	Yes
$\int_v \{\delta\varepsilon^N\}^T \boldsymbol{D} \{\varepsilon^N\}\, dv \ll \int_v \{\delta\varepsilon^N\}^T \boldsymbol{D} \{\varepsilon^L\}\, dv$	Yes

TABLE 6-2
Assumptions for Linear Stability

Strains	Small
Deflection	Small
Load	Axial Symmetric Only
$\{\varepsilon^N\} \ll \{\varepsilon^L\}$	Yes
$\int_v \{\delta\varepsilon^L\}^T \boldsymbol{D} \{\varepsilon^N\}\, dv \ll \int_v \{\delta\varepsilon^L\}^T \boldsymbol{D} \{\varepsilon^L\}\, dv$	Yes
$\int_v \{\delta\varepsilon^N\}^T \boldsymbol{D} \{\varepsilon^N\}\, dv \ll \int_v \{\delta\varepsilon^N\}^T \boldsymbol{D} \{\varepsilon^L\}\, dv$	Yes

6.2. Examples

Example 6-1: The homogeneous cylindrical tube shown in Fig. 6-1 is considered in this example. Material and geometric data are chosen as follows: modulus of elasticity $E = 24.04GPa$, shear modulus $G = 9.25GPa$, $r = 34.29mm$, $t = 5.08mm$, moment of inertia $I = 0.64 \times 10^6 mm^4$. The Euler buckling load according to beam-column theory (Chen and Lui 1987) is $P_e = (\pi^2 EI)/(4L^2) = 38.38kN$. The computed critical buckling load based on Eqns. (6-16) and (6-18) is $P_{cr} = 37.90kN$. $P-\Delta$ curves ($Q = 5.607kN$) are also drawn from Eqn. (6-16) and (6-17) to compare the computed results with that obtained from the beam-column theory (Chen and Lui 1987). The computed data are listed in Table 6-3. From Fig. 6-1 and Table 6-3 we see that the computed results are very close to the results obtained from beam-column theory in the reasonable range of displacement ($\Delta < L$). Unrealistic results of displacement are obtained when P/P_e approaches to unity.

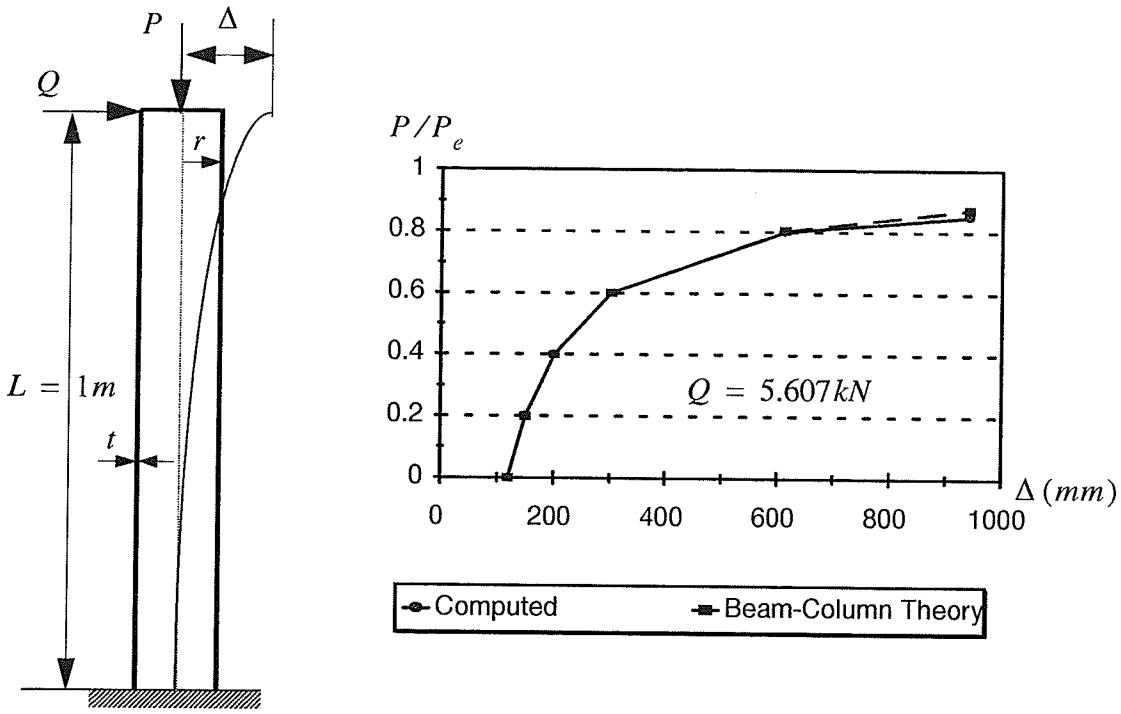

Fig. 6-1. Tip deflection vs. axial load of the cylindrical tube

TABLE 6-3
Comparison of Tip Deflection of the Cylindrical Tube

$\frac{P}{P_e}$	$\Delta\,(mm)$	
	Computed	Beam-Column Theory
0.0	120.8	120.0
0.2	150.9	150.0
0.4	201.1	200.0
0.6	302.5	300.0
0.8	613.5	600.0
0.9	1269.7	1200.0
0.95	2737.1	2400.0
1.00		∞

Example 6-2: In this example a tapered FRP pole with three layers (Fig. 6-2) is considered for the analysis of $P-\Delta$ effect and linear buckling. The material properties used are: modulus of elasticity in fiber longitudinal direction, $E_L = 38.0GPa$, modulus of elasticity in fibre transverse direction, $E_T = 6.832GPa$, the major Poisson's ratio, $\upsilon_{LT} = 0.3$, the minor Poisson's ratio, $\upsilon_{TT} = 0.49$, and in-plane shear modulus, $G_{LT} = 2.293GPa$. The fibres in the middle layers are oriented in meridional direction while the fibres in the inner and outer layers are oriented at ±3 degrees with respect to the circumferential direction.

The critical buckling load P_{cr} is obtained by solving an eigenvalue equation (Eqn. (6-18)) when the lateral load Q is equal to zero. The computed critical buckling load $P_{cr} = 104.69kN$. The $P-\Delta$ curves are obtained using the analysis discussed in this chapter (Eqns. (6-16) and (6-17)) when the lateral load is fixed ($Q = 19.63kN$ and $Q = 3.926kN$). These two curves are drawn from the computed data as listed in Table 6-4. A deflection modification factor is defined as

$$m_f = \frac{\Delta}{\Delta_0} \tag{6-19}$$

where Δ_0 is the deflection when $P/P_{cr} = 0$.

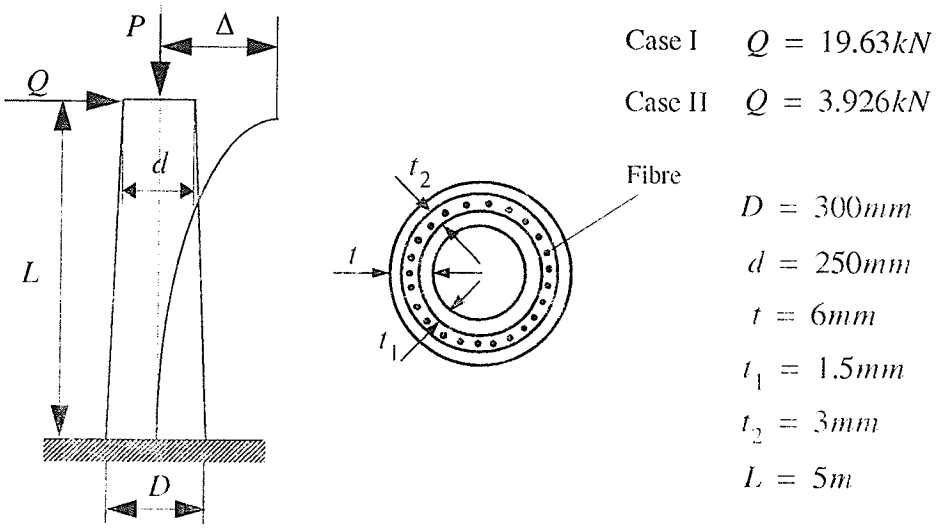

Fig. 6-2. A Tapered FRP pole with three layers

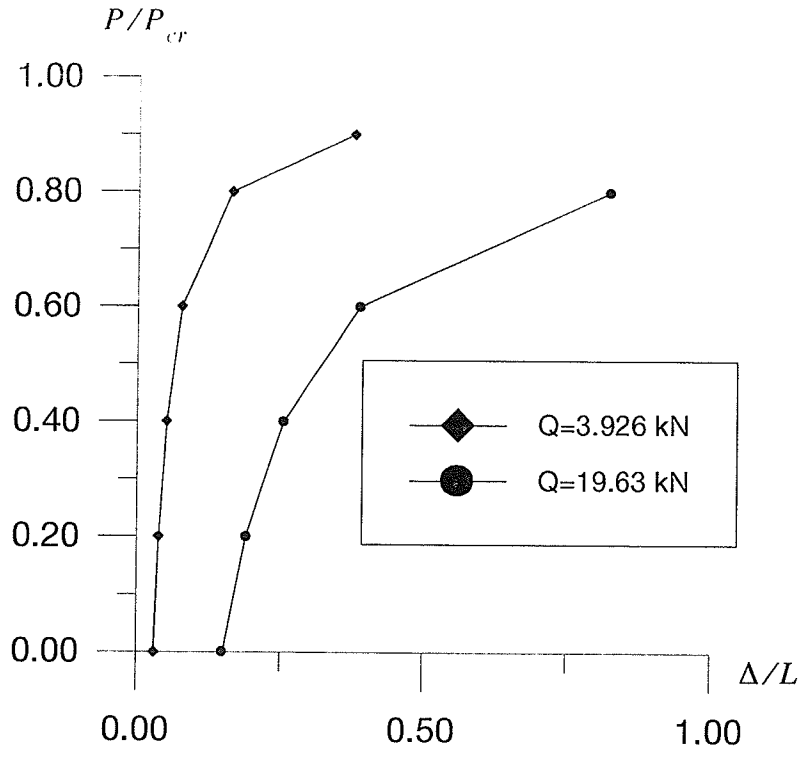

Fig. 6-3. $P-\Delta$ curves of tapered FRP pole

TABLE 6-4
Computed Tip Deflection of Tapered FRP Pole

$\frac{P}{P_{cr}}$	Δ/L		$m_f = \Delta/\Delta_0$	
	$Q = 19.63kN$	$Q = 3.926kN$	$Q = 19.63kN$	$Q = 3.926kN$
0.0	0.1520	0.0304	1.0	1.0
0.2	0.1904	0.0380	1.253	1.250
0.4	0.2554	0.0511	1.680	1.681
0.6	0.3892	0.0778	2.560	2.561
0.8	0.8246	0.1650	5.425	5.426
0.9	1.8872	0.3774	12.416	12.416
0.95	5.3534	1.0707	35.220	35.220
1.00				

As shown in Fig. 6-3, for different lateral load Q, different deflections are observed for the same level of axial load. When the axial load approaches the critical value, the deflection reaches infinity. This is not realistic and indicates that the $P-\Delta$ analysis, which is based on the assumption of small deflection, is not adequate for large displacements.

The results given in Table 6-4 show that the deflection modification factor m_f does not change drastically when the lateral load varies. In the classical beam-column theory, the deflection modification factor of prismatic homogeneous beam-columns depends on the axial load (P/P_{cr}) only. This is also true for tapered orthotropic FRP poles, where the deflection modification factor m_f still depends on the ratio (P/P_{cr}) only, as far as the linear $P-\Delta$ analysis is concerned. The modification factors for a given small lateral load Q can thus be computed. The deflections for different Q can then be obtained once Δ_0 has been computed.

6.3. Discussion

A number of assumptions were made in deriving the governing equations for the $P-\Delta$ analysis and the linear buckling analysis. The primary assumption is that the displacements are small. Therefore, it is reasonable to believe that at small displacements, the results from the $P-\Delta$ analysis is a good approximation to that of nonlinear analysis. When the displacements are large, the

$P-\Delta$ analysis is no longer accurate. It is not realistic to assume that the pole can deflect infinitely when the axial load approaches the critical value as shown in Fig. 6-3. However, if compared to the nonlinear analysis in which the pole always picks up load dramatically after a very large deflection, the $P-\Delta$ analysis is conservative as far as the design is concerned.

In addition to the assumption of small displacements, the assumption that the nonlinear strains are induced by the beam-type bending only is critical to the uncoupling of the system equations. The first equation (Eqn. (6-16)) is linear and involves only the axial symmetric displacement q_o. The second equation (Eqn. (6-17)) is a linear equation of displacement q_a. Although q_o is involved in Eqn. (6-17), it is presumed to be constant in the course of solving Eqn. (6-17). The procedure used is as follows: First Eqn. (6-16) is solved first; then q_o is used to compute the geometric matrix $G(q_o)$; for the $P-\Delta$ analysis, Eqn. (6-17) is solved directly. In the special condition where only axially symmetric loads are applied, an eigenvalue problem was derived. The linear buckling analysis consists of solving for the lowest eigenvalue (Eqn. 6-18). The critical axial load can be determined after the eigenvalue is obtained.

The $P-\Delta$ analysis is, computationally, more efficient than the full nonlinear analysis since no iteration is required to get a solution for a particular load level.

Chapter 7. Linear Static Analysis

For large displacements, the load-deflection curve obtained through the nonlinear analysis discussed in Chapter 4 deviates significantly from the linear curve. At small displacement ($\Delta/L < 0.25$), the linear solution is a good approximation of the nonlinear solution. Because the linear analysis is much easier to manipulate than the nonlinear analysis and the linear program is very efficient, most of the parameters incorporated in the analysis, such as taper-ratio and fibre-orientation, can be determined by performing a linear analysis in the design of FRP poles. Such an analysis could give reasonable results if $\Delta/L < 0.25$.

7.1. Formulations

The linear analysis can be manipulated in two ways. First, if neglecting all the nonlinear terms in the formulations developed in Chapter 2, the system of equations (Eqn. (2-47)) becomes

$$Kq = f \tag{7-1}$$

In Chapter 2, the displacement is assumed to be linearly distributed along the thickness direction. This approach conforms to the first order shear theory.

Since FRP usually has lower shear modulus, the transverse shear strains might have significant influence on the deformation and strength of FRP poles. In the second approach, a higher-order shear theory (Reddy and Liu 1985) is adopted to account for transverse shear strains. The main advantage of using high-order shear theory is that no correction to the shear strain is needed because at the edge of a shell wall, the zero shear strain is enforced. The manipulation of the linear analysis is accordingly different from that discussed in the previous chapters.

According to Reddy and Liu (1985), the displacement is assumed to be

$$u_1 = \bar{u}_1 + \gamma\bar{\phi}_{11} + \gamma^2\bar{\phi}_{12} + \gamma^3\bar{\phi}_{13} \tag{7-2}$$

$$u_2 = \bar{u}_2 + \gamma\bar{\phi}_{21} + \gamma^2\bar{\phi}_{22} + \gamma^3\bar{\phi}_{23} \tag{7-3}$$

$$u_3 = \bar{u}_3 \tag{7-4}$$

where $\bar{u}_1$, $\bar{u}_2$ and $\bar{u}_3$ are midsurface displacements in α, β and γ directions, respectively. $\bar{\phi}_{ij}$ $(i = 1,2;\ j = 1,2,3)$ are parameters to be determined.

In conical shells, by enforcing the linear transverse shear strains e_{23} and e_{31} to be zero at the edges ($\gamma = \pm\frac{h}{2}$, where h is the wall thickness) and by letting $\phi_1 = \bar{\phi}_{11}$, $\phi_2 = \bar{\phi}_{21}$, the following relationships are derived.

$$u_1 = \bar{u}_1 + \gamma\phi_1 + \frac{4\gamma^3}{3h^2}\left[-\phi_1 - \frac{\partial \bar{u}_3}{\partial\alpha}\right] \tag{7-5}$$

$$u_2 = \bar{u}_2 + \gamma\phi_2 + (\gamma^2 T_{22} + \gamma^3 T_{23})\left[\phi_2 - \frac{\bar{u}_2}{R_2} + \frac{\partial \bar{u}_3}{\partial\beta}\right] \tag{7-6}$$

$$u_3 = \bar{u}_3 \tag{7-7}$$

where, ϕ_1 is the rotation about the β axis, and ϕ_2 is the rotation about the α axis in the linear analysis, and

$$R_2 = r/(\cos\psi) \tag{7-8}$$

$$T_{22} = \frac{4R_2}{12R_2^2 - h^2} \tag{7-9}$$

$$T_{23} = \frac{-16R_2^2}{h^2(12R_2^2 - h^2)} \tag{7-10}$$

The midsurface displacements and rotations are,

$$\bar{u} = \left[\bar{u}_1\ \bar{u}_2\ \phi_1\ \phi_2\ \bar{u}_3\right]$$

$\bar{u}$ can be expanded into Fourier series in the circumferential direction, as follows:

$$\begin{bmatrix} \bar{u}_1 \\ \bar{u}_2 \\ \phi_1 \\ \phi_2 \\ \bar{u}_3 \end{bmatrix} = \begin{bmatrix} \bar{u}_1^o \\ \bar{u}_2^o \\ \phi_1^o \\ \phi_2^o \\ \bar{u}_3^o \end{bmatrix} + \sum_{l=1}^{M_l} \begin{bmatrix} \bar{u}_{1l}^a \cos l\beta \\ \bar{u}_{2l}^a \sin l\beta \\ \phi_{1l}^a \cos l\beta \\ \phi_{2l}^a \sin l\beta \\ \bar{u}_{3l}^a \cos l\beta \end{bmatrix} + \sum_{l=1}^{M_l} \begin{bmatrix} \bar{u}_{1l}^b \sin l\beta \\ \bar{u}_{2l}^b \cos l\beta \\ \phi_{1l}^b \sin l\beta \\ \phi_{2l}^b \cos l\beta \\ \bar{u}_{3l}^b \sin l\beta \end{bmatrix} \tag{7-11}$$

where, M_l is the highest order of Fourier series. Each coefficient in Eqn. (7-11) is a function of α only and will be interpolated in terms of nodal displacements. The superscript "o" denotes the

terms corresponding to axial symmetric displacements; superscript "a" denotes the terms corresponding to a symmetric (about $\beta = 0$) displacement pattern, and superscript "b" denotes the terms corresponding to an antisymmetric (about $\beta = 0$) displacement pattern.

For a linear static analysis, $\bar{u}^a_{1l}$, $\bar{u}^b_{1l}$, $\bar{\phi}^a_{1l}$, $\bar{\phi}^b_{1l}$ are assumed to be linear functions of α, and $\bar{u}^a_{2l}$, $\bar{u}^b_{2l}$, $\bar{\phi}^a_{2l}$, $\bar{\phi}^b_{2l}$, $\bar{u}^a_{3l}$ and $\bar{u}^b_{3l}$ are assumed to be quadratic functions of α. Taking the symmetric (about $\beta = 0$) displacements for example, the displacements u^a_{1l}, u^a_{2l} and u^a_{3l} can be expressed in a form similar to Eqns. (4-28), (4-29) and (4-30). That is,

$$u^a_{1l} = [\theta_{1l}]\,[\Gamma_1]\,[N_1]\,\{q_e\}^a_l \tag{7-12}$$

$$u^a_{2l} = [\theta_{2l}]\,[\Gamma_2]\,[N_2]\,\{q_e\}^a_l \tag{7-13}$$

$$u^a_{3l} = [\theta_{3l}]\,[\Gamma_3]\,[N_3]\,\{q_e\}^a_l \tag{7-14}$$

where

$$\{q_e\}^a_l = \left[(\bar{u}^a_{1l})_i\ (\bar{u}^a_{2l})_i\ (\bar{\phi}^a_{1l})_i\ (\bar{\phi}^a_{2l})_i\ (\bar{u}^a_{3l})_i\ (\bar{u}^a_{2l})_k\ (\bar{\phi}^a_{2l})_k\ (\bar{u}^a_{3l})_k\ (\bar{u}^a_{1l})_j\ (\bar{u}^a_{2l})_j\ (\bar{\phi}^a_{1l})_j\ (\bar{\phi}^a_{2l})_j\ (\bar{u}^a_{3l})_j\right]^T \tag{7-15}$$

$$[\theta_{1l}] = \left[\cos l\beta\ \sin l\beta\ \cos l\beta\ \sin l\beta\ \cos l\beta\right] \tag{7-16}$$

$$[\theta_{2l}] = \left[\cos l\beta\ \sin l\beta\ \cos l\beta\ \sin l\beta\ -\sin l\beta\right] \tag{7-17}$$

$$[\theta_{3l}] = \left[\cos l\beta\ \sin l\beta\ \cos l\beta\ \sin l\beta\ \cos l\beta\right] \tag{7-18}$$

$$[\Gamma_1] = \begin{bmatrix} 1 & 0 & 0 & 0 & 0 \\ 0 & 0 & 0 & 0 & 0 \\ 0 & 0 & \left(\gamma - \dfrac{4\gamma^3}{3h^2}\right) & 0 & 0 \\ 0 & 0 & 0 & 0 & 0 \\ 0 & 0 & 0 & 0 & \left(-\dfrac{4\gamma^3}{3h^2}\right) \end{bmatrix} \tag{7-19}$$

$$[\Gamma_2] = \begin{bmatrix} 0 & 0 & 0 & 0 & 0 \\ 0 & \left(1 - \frac{T_{22}\gamma^2}{R_2} - \frac{T_{23}\gamma^3}{R_2}\right) & 0 & 0 & 0 \\ 0 & 0 & 0 & 0 & 0 \\ 0 & 0 & 0 & \left(\gamma + \frac{T_{22}\gamma^2}{R_2} + \frac{T_{23}\gamma^3}{R_2}\right) & 0 \\ 0 & 0 & 0 & 0 & (T_{22}\gamma^2 + T_{23}\gamma^3) \end{bmatrix} \tag{7-20}$$

$$[\Gamma_3] = \begin{bmatrix} 0 & 0 & 0 & 0 & 0 \\ 0 & 0 & 0 & 0 & 0 \\ 0 & 0 & 0 & 0 & 0 \\ 0 & 0 & 0 & 0 & 0 \\ 0 & 0 & 0 & 0 & 1 \end{bmatrix} \tag{7-21}$$

where $[N_1]$, $[N_2]$ and $[N_3]$ are shape function matrices which are given in Appendix E.

The assembly of the system stiffness matrix follows standard finite element procedures (Weaver and Johnston 1985). The final system equation is

$$\boldsymbol{Kq} = \boldsymbol{f} \tag{7-22}$$

Due to the orthogonality of the integration of triangularmetric functions, i.e., for $(i, j = 1, 2, \ldots)$,

$$\int_0^{2\pi} \sin i\beta \sin j\beta d\beta = 0 \qquad (i \neq j) \tag{7-23}$$

$$\int_0^{2\pi} \sin i\beta \sin j\beta d\beta = \pi \qquad (i = j) \tag{7-24}$$

$$\int_0^{2\pi} \cos i\beta \cos j\beta d\beta = 0 \qquad (i \neq j) \tag{7-25}$$

$$\int_0^{2\pi} \cos i\beta \cos j\beta d\beta = \pi \qquad (i = j) \tag{7-26}$$

$$\int_0^{2\pi} \sin i\beta \cos j\beta d\beta = 0 \tag{7-27}$$

the system of equations Eqn. (7-22) are uncoupled in terms of the orders of Fourier series. Thus, for a given order l, if the displacement and the load terms corresponding to $\cos l\beta$ and $\sin l\beta$ are of interest, then the subset of the system of Eqn. (7-22) becomes,

$$K_l q_l = f_l \tag{7-28}$$

which can be independently solved.

7.2. Examples

Example 7-1. In this example, a long cylindrical tube of isotropic material was analyzed. Tip ring load is applied as shown in Table 7-1. This example is presented in order to demonstrate the accuracy of the finite element program. The tip displacement and the maximum stress obtained from the finite element analysis are compared with results obtained from the shell theory (Timoshenko and Woinowsky 1959). The computed displacement is 0.7 percent smaller than that of shell theory while the maximum stress is 5 percent larger than the maximum stress obtained from shell theory.

TABLE 7-1
Comparison of Computed Displacements and Stresses With Shell Theory

Example 7-1	Tip Displacement (mm)		Maximum Stress (MPa)	
	Computed	Shell Theory	Computed	Shell Theory
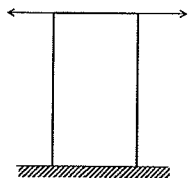 Tube with Ring Load	0.09706	0.09770	71.43	68.00

Example 7-2. In this example, a cylindrical tube with a tip load was analyzed. The material is assumed to be unidirectional FRP (one layer only). The tip displacement and the maximum stress obtained from the finite element method are shown in Table 7-2 along with the results from the beam theory. The results obtained from the finite element method are very close to the results

obtained from the beam theory (Chen and Lui 1987) since the relative differences is less than 1.0 percent.

TABLE 7-2
Comparison of Computed Displacements and Stresses With Beam Theory

Example 7-2	Tip Displacement (mm)		Maximum Stress (MPa)	
	Finite Element Method	Beam Theory	Finite Element Method	Beam Theory
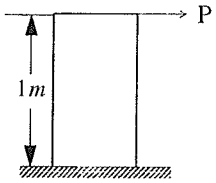 Tube with Tip Load	124.3	122.0	332	319

Example 7-3. In this example, four FRP poles which were tested to failure are analyzed. Those poles had three layers, as shown in Fig. 7-1, and fibres in the middle layer of each pole are oriented in the longitudinal direction while the fibres in inner and outer layers are oriented at an angle of 3° with respect to the horizontal plane. The test specimens and the experimental results are given in Appendix F. Some experimental results are included in Table 7-3 along with the displacements computed from the finite element program. The maximum difference between the two sets of results is about 29%. The differences between the computed and experimental results are believed to be due to the following factors: a) inaccurate manufacturing process; and b) inability to develop the designed strength without a plug (Specimen #1).

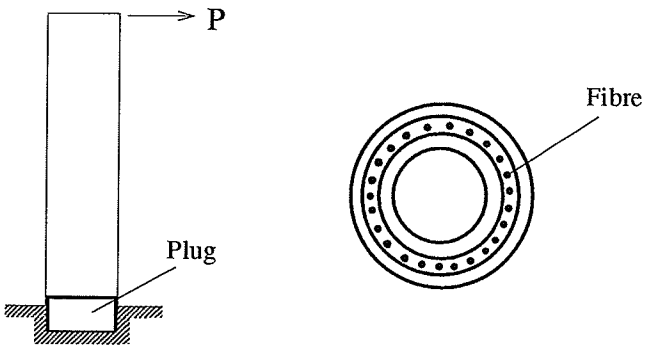

Fig. 7-1. FRP tube with three layers (Specimen #2)

TABLE 7-3
Comparison of Computed Maximum Lateral Deflections with the Experimental Results (mm)

Example 3	Computed Result	Experimental Result	Difference
Specimen #1	143.8	172.7	16.7%
Specimen #2	222.2	223.9	0.1%
Specimen #3	250.8	193.6	29.4%
Specimen #4	248.2	240.5	3.2%

The stress distribution at the various layers of Specimen #2 are presented in Fig. 7-2. As shown in this figure, the axial stress is the dominant stress, as expected, and the stress level in the middle layer is much higher than in the other two layers. The shear stresses, as well as the hoop stress in the three layers, are quite small.

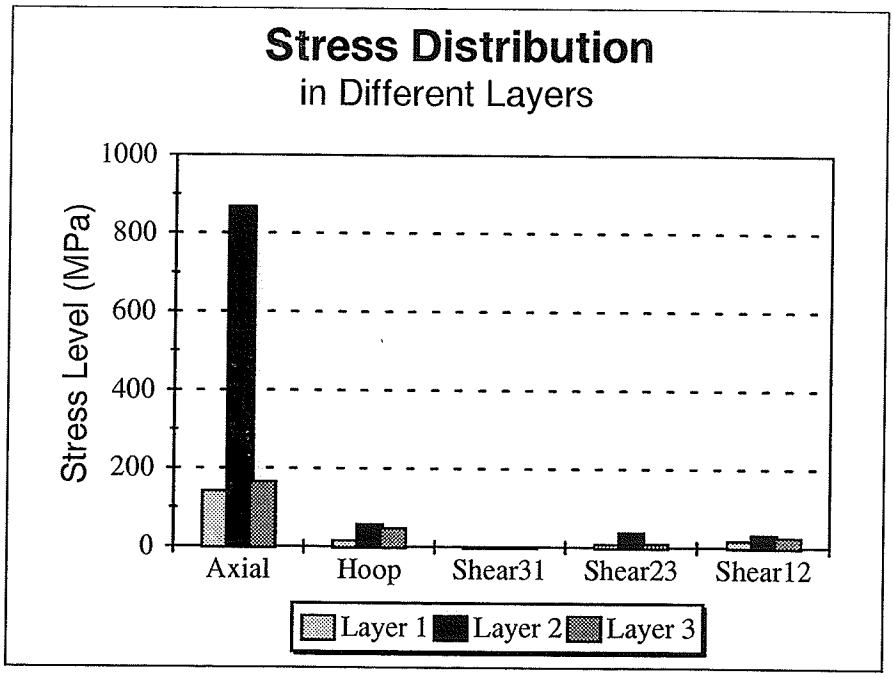

Fig. 7-2. Stress distribution in different layers

The optimum performance of the poles can be achieved by varying the fiber orientation in the inner and outer layers. Using Specimen #2 as an example, the lateral deflection and the maximum stress are computed as a function of the fibre orientation angles. The angles are referenced with

respect to the longitudinal direction. As shown in Table 7-4, an angle of 87°, actually used in fabricating this specimen, is not a good orientation because the displacement and stress are larger than those obtained using other orientations. By reducing the orientation angle, the performance of the pole can be improved. The improvement is minimal if the angle is larger than 45°. However, when the angle is decreased to 15°, the deflection and the maximum stress are reduced by more than 50%. It should be noted that torsional displacement effects are not considered in computing the results shown in Table 7-4.

TABLE 7-4
Lateral Deflection and Maximum Stress vs. Fibre Orientation

Fiber Orientation of Inner and Outer Layers	Lateral Deflection Under the Same Tip Load (mm)	Maximum Stress of Mid-Layer (MPa)
87°	222.2	868
60°	227.8	880
45°	222.4	830
30°	155.2	575
15°	104.8	392

Example 7-4. This example is used to demonstrate how the taper-ratio affects the performance of FRP poles. The configuration of layers and the material properties used in this example are the same as in Example 4-2. The volume of the pole varies with the taper ratio. The ratio of the applied load Q to the volume of the pole is used as an indicator of performance. The larger the ratio is, the better the design would be.

The load $\bar{Q}$ that would cause the maximum stress $\bar{\sigma}$ can be computed if the maximum stress σ under a load Q is known; i.e.,

$$\bar{Q} = \frac{\bar{\sigma}}{\sigma} Q \tag{7-29}$$

This relationship implies that the behaviour is linear. The volume V can be shown to be

$$V = \frac{2\pi t L}{\cos\psi}\left(\frac{d}{2} + \frac{\psi L}{2\cos\psi}\right) \tag{7-30}$$

where, ψ is the taper angle, d is the radius of the small end, L is the height of the pole, and t is the

wall thickness of the pole. For small value of ψ, which is the case in transmission poles, V can be approximated as

$$V = 2\pi tL\left(\frac{d}{2} + \frac{\psi L}{2}\right) \tag{7-31}$$

The load $\bar{Q}$, the volume V, and the ratio $(\bar{Q}/V)$, are listed in Table 7-5 as functions of ψ. The ratio $(\bar{Q}/V)$ is also shown in Fig. 7-4 as a function of ψ.

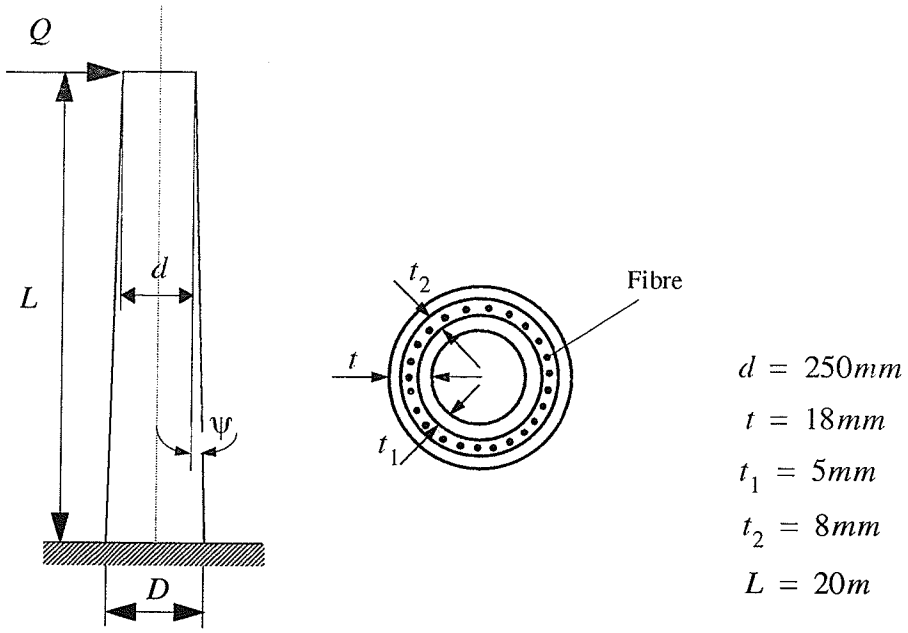

Fig. 7-3. Tapered FRP pole with three layers

The results shown in Table 7-5 and Fig. 7-4 indicate that the ratio Q/V increases with the increase of taper angle ψ for ψ up to 15°. Values of $\psi > 15°$ are not practically used in transmission poles. Thus, increasing the taper ratio will improve the performance of the FRP poles.

7.3. Discussion

A higher-order shear strain theory is employed in this Chapter to derive the linear system equations. The normal displacement u_3 is assumed to be constant in the thickness direction. This is based on the assumption that the normal strain is very small and can be neglected in the formulations.

TABLE 7-5
Performance Ratio $(\bar{Q}/V)$

$\psi°$	$\bar{Q}$ (kN)	$V\,(10^6 mm^3)$	$(\bar{Q}/V)$ $(10^{-3} kN/(mm)^3)$
0	1.0	282.75	3.537
1	7.748	677.47	11.437
2	19.25	1072.2	17.954
3	35.53	1467.1	24.218
4	55.25	1861.9	29.674
5	76.13	2121.1	33.892
6	100.46	2651.0	37.895
7	127.40	3046.9	41.813
8	157.19	3440.5	45.688
9	189.18	3836.4	49.312
10	224.10	4230.0	52.979
15	471.92	6204.8	76.057

Different orders of Fourier terms in the linear system of equations are uncoupled resulting in separate sets of equations. Each set of equations can be solved independently. A particular order of displacement and load that are of interest can be analyzed without any difficulty.

The linear finite element model developed has been tested through a number of examples. Comparisons with results obtained from the beam theory and the shell theory are made. It is shown that the finite element model can be used to perform linear analysis with good results. The numerical results are also compared with experimental results. The maximum difference between the analytical and experimental results is 29%.

For slender poles the transverse shear strains are not very significant. The stress and strain distribution at different layers depend on the fibre orientations at the various layers. For beam-type bending, it is ideally economical to design the fibre orientation in the longitudinal direction. If

hoop stresses and torsional stresses are present, the fibres in certain layers can be oriented at an angle varying of 0° to 90° with respect to the longitudinal direction.

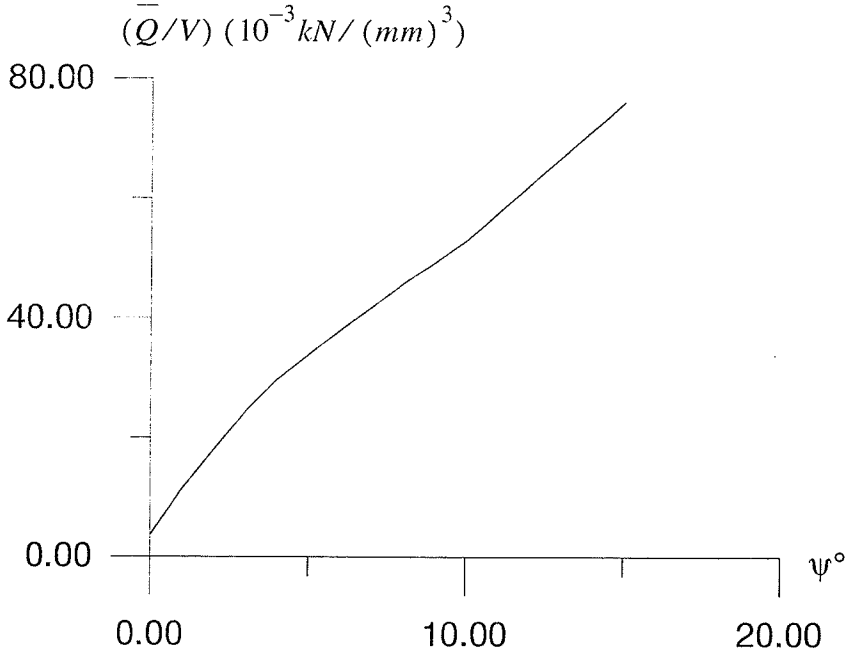

Fig. 7-4. Performance ratio $(\bar{Q}/V)$

In the practical range of taper ratios for transmission poles, it is demonstrated that the larger the taper ratio, the more economic the design is. This conclusion is drawn from results involving a concentrated load only, since this is the major case of loading in transmission poles. For other cases of loading, the influence of taper ratio can be analyzed using the computer program developed.

The computer program for linear analysis is very efficient. Nonlinear analyses are time consuming while linear analyses take only a few seconds to obtain the deflection curve for a single load case. If the maximum deflection of a FRP pole is less than 25% of its height, the linear analysis may be well employed to serve the design purpose.

Chapter 8. Conclusions and Recommendations for Future Work

8.1. General Conclusions

Fibre-reinforced plastic poles made of several layers are considered for the construction of transmission poles traditionally made of wood, steel and concrete. Fibre-reinforced plastic poles are anisotropic in nature but each layer of unidirectional reinforcement can be treated as an orthotropic material. The stress-strain relationship of orthotropic FRP and the transformation between material and system coordinates are used. Five engineering material constants are needed in the formulation of the governing equations. Four of these can be obtained from the fibre and matrix volume fraction.

The principle of stationary potential energy is employed for the analysis of FRP hollow tapered poles. Novozhilov's derivations of strains of general shells are used in the formulation process for the nonlinear finite element analysis. The use of Novozhilov's derivations results in a concise and compact expression for nonlinear strains and their first variations. When the information for computing linear strains is available, the nonlinear strains can then be computed. This is possible since the nonlinear strains are products of the linear strains. Therefore, the programming of nonlinear stiffness matrices can be systematically manipulated. The evaluation of the tangent stiffness matrices is discussed extensively. The relationships of nonlinear matrices, $H^* = H$ and $G = 2H^T$, can be employed to reduce computational time.

Methods for solving the nonlinear system of equations are presented. Based on the augmented equation method, external and internal potential control schemes are proposed and evolved into incremental work control and incremental strain energy control. These controls are shown to have good capability of traversing a limit point. It is suggested in this thesis that the coefficients in the augmented equations are considered as weighting factors, regardless the control methods used. Thus, different controls can be programed in a way that only the weight factors in the augmented equation need be evaluated differently. This approach provides the user of the computer program with the flexibility of selecting the proper control method during the analysis stages.

To model the beam-type bending of the poles, the second-order Fourier terms, which are necessary to model the rigid-body rotation, must be included in the displacement functions. A special displacement variable Φ_R is introduced to simplify the inclusion of rigid-body rotation. Other rigid-body motions, except the rigid-body rotation, are automatically included in the analysis though only zeroth-order and first-order Fourier terms are retained. This approach is shown to give

good results in a number of examples examined.

The nonlinear analysis of beam-type bending includes all the nonlinear strain and stress terms. If the displacement is very large, only nonlinear analysis can give a satisfactory theoretical solution. In an experimental program performed at University of Manitoba, scaled FRP poles failed at $\Delta/L \cong 30\%$. Thus, the nonlinear analysis must be used for very flexible poles. However, examples given in Chapter 4 show that poles possess post buckling resistance if they are still in the elastic range. In design, post buckling capacity may not be used because it can only be realized at very large deflections which may exceed the tolerance of serviceability.

The post-buckling behaviour of poles can be analyzed using the large displacement nonlinear analysis. Although transverse shear strains and hoop strains are included in the analysis, for slender poles, no significant effect is observed since the loading conditions considered are simple. The examples given in Chapter 4 show that the nonlinear finite element model gives accurate results even at very large deflections.

The ovalization effect is discussed in Chapter 5. The analysis presented is an extension of the beam-type bending analysis because all the second-order Fourier terms are included for the ovalization analysis while only terms necessary to model the rigid-body rotation of tapered poles are used for beam-type bending analysis. The ovalization analysis is based on the assumption that the ovalization of a circular cross-section can be represented by second-order Fourier expansions. This assumption is made in order to capture the most significant effect of ovalization while keeping the degrees-of-freedom to a reasonable number. An example of a thin-walled cylinder of isotropic material is presented to demonstrate the phenomenon of ovalization. The influence of the ovalization on the load carrying capacity is dramatic. Instability can occur if the ovalization reaches a critical level. Thus, inclusion of the ovalization behaviour is vital in the analysis and design of FRP poles.

In Chapter 6, a linear $P-\Delta$ analysis and a linear buckling analysis developed from a full nonlinear analysis using a number of assumptions are presented. The major assumption is that the displacement is small. With this assumption, the $P-\Delta$ analysis can be considered to be a good approximation to the nonlinear analysis. When the displacement is large, this conclusion is no longer valid. However, the $P-\Delta$ analysis predicts a lower axial load than the nonlinear analysis. This feature may be used in design since it results in a more conservative estimate of the failure load.

The linear buckling analysis may be used to predict, effectively, the critical axial buckling load of tapered poles. Because the theoretical value of critical buckling load of a tapered pole of orthotropic material is more difficult to obtain, a numerical prediction of such critical buckling load is indispensable in the design of FRP poles.

In the linear static analysis, a higher-order transverse shear strain theory is used and the displacement functions are derived. Results obtained from the linear static analysis are compared with those obtained from the beam and shell theories and very good agreements are observed. Computed displacements are also compared with experimental results of scaled poles and the maximum difference is about 29%.

Depending on the fibre orientations, the strains and stresses vary from layer to layer. The layer with the longitudinal fibre orientation will resist most of the load. Shear strains are not very significant if the pole is in bending.

The influence of fibre orientation is discussed in Chapter 7. In the simple case of beam-type bending, all fibres should be oriented in the longitudinal direction. In general, fibres oriented at an angle between 0 to 45 degree with respect to the longitudinal direction result in economic design.

The influence of taper is also investigated in Chapter 7. It is shown that in the practical range ($\psi < 15°$), the greater the taper ratio, the better the performance is. Here performance is measured by the ratio of the load carried by a pole when its maximum stress was specified to the volume of the pole.

The linear static analysis, the linear buckling analysis and the linear $P-\Delta$ analysis are applicable when the maximum deflection of a pole is less than 25% of the height. Ovalization analysis can be used to check the influence of the ovalization on the load carrying capacity in large displacement as well as in small displacement.

8.2. Recommendations for Future Research

One of the five engineering material constants of FRP, the minor Poisson's ratio, can not be determined by the volume fractions and material constants of fibres and matrix. A method to obtain this engineering material constant needs to be developed.

In this thesis, antisymmetric (about $\beta = 0$) loads and displacements are not considered. In the real design of FRP poles, antisymmetric loads and displacements may be combined with symmet-

ric loads and displacements. Although this combination may make the nonlinear analysis more complex, it would be beneficial in order to understand the nonlinear behaviour of FRP poles better.

The augmented equation method is a family of methods. Different control schemes play different roles in this method. More efficient and powerful control scheme should be pursued. Ideally, a control scheme should: a) allow the control parameter to increase monotonically (like arc length control); b) be easy to manipulate (such as load control and displacement control); and c) have a good capability to traverse a limit-point (such as arc length control and incremental work control).

Ovalization is a kind of local behaviour and is characterized by the second-order Fourier series. The local behaviour characterized by higher-order Fourier series is not considered in this thesis. The local buckling pertinent to those higher-orders and the interaction with ovalization could be an interesting topic to be investigated.

As indicated in Chapter 7, the taper-ratio should be increased as much as possible to gain better performance. But the taper-ratio is restricted by other factors such as manufacturing. An alternative to increasing performance is to vary the thickness of the poles. This should also be investigated by further studies.

References

Agarwal, B. D., (1980), *Analysis and Performance of Fibre Composites*, John Wiley & Sons, New York.

Ballinger, C., (1990), Structural FRP Composites, ASCE *Civil Engineering*, July 1990, pp.63-66.

Barten, H. J., (1945), "On the Deflection of a Cantilever Beam", *Q. Appl. Math.*, No. 2, pp. 168-171, and Q. Appl. Math., No. 2, pp. 275-276.

Bathe, K. J., Ramm, E. and Wilson, E. L., (1975), Finite Element Formulations for Large Deformation Dynamic Analysis, *Int. J. Num. Meth. Engng.*, Vol. 9, pp. 353-386.

Bathe, K. J. and Dvorkin, E. N., (1983), On the Automatic Solution of Nonlinear Finite Element Equations, *Computers & Structures*, Vol. 17, No. 5-6, pp. 871-879.

Batoz, J. L. and Dhatt, G., (1979), "Increment Displacement Algorithms for Nonlinear Problems", *Int. J. Numer. Meth. Engng.* 14, pp. 1262-1267.

Bisshopp, K. E. and Drucker, D. C., (1945), "Large deflection of Cantilever Beams", *Q. Appl. Math.*, No. 3, pp. 272-275.

Brush, D. O. and Almroth, B. O., (1975), *Buckling of Bars, Plates and Shells*, McGraw-Hill Book Co., New York.

Bushnell, D., (1984), Computerized Analysis of Shells Governing Equations, *Computers & Structures*, Vol. 18, No. 3, pp. 471-536.

Chen, W. F. and Lui, E. M., (1987), *Structural Stability, Theory and Implementation*, Elsevier Science publishing Co. Inc., New York.

Clark, R. A. and Reissner E., Bending of Curved Tubes, *Advances in Applied Mechanics*, Ed. R. V. Mises and T. V. Karman, Vol. 2, Academic Press Inc., New York, pp. 93-122.

Crisfield, M. A., (1981), "A Fast Incremental / Iterative Solution Procedure That Handles 'Snap-Through'", *Computers and Structures*, Vol. 13, pp. 55-62.

Escher, G. A., (1982), Design and Testing of an Optimum Fiberglass Reinforced Pole and Market Study on the Demand for Utility Poles in Canada, *Report for the Canadian Electrical Association*, Project 77-52A, Prepared by ABCO Plastics, Nova Scotia, Canada.

Felippa, C. A., (1986), Solution of Nonlinear Static Equations, *North-Holland Series on Computational Methods in Mechanics*, Volume on Large Deflection and Stability of Structures, ed. by K. J. Bathe, MIT, Cambridge, Mass, USA.

Fonder, C. A. and Clough, R. W., (1973), "Explicit Addition of Rigid-Body Motions in Curved Elements", *AIAA J.*, Vol. 11, No. 3, pp. 305-312.

Gelfand, I. M., Fomin, S. V., (1963), *Calculus of Variations*, Prentice-Hall, Inc.

Gould, P. L., (1985), *Finite Element Analysis of Shell of Revolution*, Pitman Publishing Inc., Lon-

don.

Gould, P. L. and Basu, P. K., (1977), Geometric Stiffness Matrices for the Finite Element Analysis of Rotational Shells, *J. Struct. Mech.*, Vol. 5, No. 1, pp. 87-105.

Green, A., (1987), Glass-Fibre-Reinforced Composite in Building Construction, *Transportation Research Record 1118.*

Haisler, W. E., Stricklin, J. A. and Key, J. E., (1977), Displacement Incrementation in Non-Linear Structural Analysis by the Self-Correcting Method, *Int. J. Numer. Meth. Engng.*, Vol. 11, pp. 3-10.

Holden, J. T., (1972), "On the Finite deflections of Thin Beams", *Int. J. Solids & Structures*, Vol. 8, pp. 1051-1055.

Holston, A. Jr., (1968), "Buckling of Filament-Wound Cylinders by Axial Compression", *AIAA J.*, Vol. 6, No. 5, pp. 935-936.

Jone, R. M., (1975), *Mechanics of Composite Materials*, Hemisphere publishing Corp., New York, N. Y.

Khdeir, A. A., Reddy, J. N. and Frederick, D., (1989), A Study of Bending, Vibration and Buckling of Cross-Ply Circular Cylindrical Shells with Various Shell Theories, *Int. J. Engne. Sci.*, Vol. 27, No. 11, pp. 1337-1351.

Lock, A. C. and Sabir, A. B., (1973), "Algorithm for the large Deflection Geometrically Nonlinear Plane and Curved Structures, *Proceedings of the Brunel Univ. Conference of the Institute of Mathematics and Its Applications held in April, 1972*, Edited by J. R. Whiteman, pp. 483-494.

Matin, J. D. and Richter, C. S., (1974), A Marketing Approach to the Development of the RP/C Lighting Pole Market, 29th Annual Technical Conference, 1974, Reinforced Plastics/Composites Institute, The Society of the Plastics Industry, Inc.

McClure, G. and Boire, L., (1992), Application of Advanced Composite Material in Overhead Power Lines and Telecommunications Structures, *Advanced Composite in Bridges and Structures*, Ed. K. W. Neale and P. Labossiere, Canadian Society for Civil Engineering, pp. 543-549.

Mebane, P. M. and Stricklin, J. A., (1971), Implicit Rigid Body Motion in Curved Finite Elements, *AIAA J.*, Vol. 9, No. 2, pp. 344-345.

Mufti, A. A., Erki, M-A, Jaeger, L. G., (1991), *Advanced Composite Materials (With Application to Bridges)*, CSCE, Montreal, Canada.

Navaratna, D. R., Pian, T. H. H. and Wittmer, E.A., (1968), "Stability Analysis of shell of Revolution by the Finite-Element Method", *AIAA J.*, Vol. 6, No. 2, pp. 355-360.

Noor, A. K., Burton, W. S. and Peters, J. M., (1991), Assessment of Computational Models for

Multilayered Composite Cylinders, *Int. J. Solids Structures*, Vol. 27, No. 10, pp. 1269-1286.

Novozhilov, V. V., (1961), *Theory of Elasticity*, Translated by J. K. Lusher, Pergamon Press, New York.

Park, K. C., (1982), A Family of Solution Algorithms for Nonlinear Structural Analysis Based on Relaxation Equations, *Int. J. Numer. Meth. Engng.*, Vol. 18, pp. 1337-1347.

Plecnik, J. M., (1992), Present and Possible Future Applications of Composite Materials for Infrastructure in USA, *Proc. of the 1992 NSF Structures, Geomechanics and Building Systems Grantees' Conference*, University of Puerto Rico, June 10-12, 1992, pp. 155-157.

Reddy, J. N. and Liu, C. F., (1985), "A Higher-Order Shear Deformation Theory of Laminated Elastic Shells", *Int. J. Engng. Sci.*, Vol. 23, No. 3, pp. 319-330.

Riks, E., (1979), "An Incremental Approach to the Solution of Snapping and Buckling Problems", *Int. J. Solids Structures*, Vol. 15, pp. 529-551.

Schwartz, M. M., (19), *Composite Materials Handbook*, McGraw-Hill Book Company, New York., USA.

Sharifi, P. and Popov, E. P., (1971), Nonlinear Buckling Analysis of Sandwich Arches, Journal of the Engineering Mechanics Division, ASCE, Vol. 97, No. EM5, pp. 1397-1412.

Sokol, T. and Witkowski, (1994), The Equilibrium Path Determination in Nonlinear Analysis of Structures, *Advances in Nonlinear Finite Element Methods*, Ed. B. H. V. Topping and M. Papadrakakis, Civil-Comp Press, Edinburgh, UK, pp. 35-45.

Stricklin, J. A. and Haisler, E. W., (1977), Formulations and Solution Procedures for Nonlinear Structural Analysis, *Computers & Structures*, Vol. 7, pp. 125-136.

Stricklin, J. A., et al, (1971), Nonlinear Dynamic Analysis of Shells of Revolution by Matrix Displacement Method, AIAA Journal, Vol. 9, No. 4, pp. 629-636.

Tang, R. C. and Adams, S. F., (1973), Application of Reinforced Plastics for Laminated Transmission Poles, *Forest Products Journal*, Vol. 28, No. 10.

Timoshenko, S. P. and Gere, J. M., (1961), *Theory of Elastic Stability*, McGraw Hill, Toronto.

Timoshenko, S. P. and Woinowsky-Kriegeri, S., (1959), *Theory of Plates and Shells*, McGraw-Hill Book Company, New York, USA.

Ugural, A. C. and Cheng, S., (1968) "Buckling of Composite Cylindrical Shells under Pure Bending", *AIAA J.*, Vol. 6, No. 2, pp. 349-354.

Vanderbuilt, M. D. and Criswell, M. E., (1988), Reliability Analysis of Pole-Type Transmission Structures, *Computer & Structures*, Vol. 28, No. 3, pp. 335-343.

Wang, T. M., (1969), "Non-Linear Bending of Beams with Uniformly Distributed Loads", *Int. J. Non-Linear Mechanics*, Vol. 4, pp. 389-395.

Wempner, G. A., (1971), Discrete Approximations Related to Nonlinear Theories of Solids, *In. J.*

Solids Structures, Vol. 7, pp. 1581-1599.

Weaver, W. Jr. and Johnston, P. R., (1985), *Finite Elements for Structural Analysis*, Prentice-Hall, Inc. Englewood Cliffs, New Jersey, U.S.A.

Wood, R. D. and Zienkiewicz, O. C., (1977), Geometrically Nonlinear Finite Element analysis of Beams, Frames, Arches and Axisymmetric Shells, *Computers & Structures*, Vol. 7, pp. 725-735.

Zienkiewicz, O. C., (1971), *The Finite Element Method in Engineering Science*, McGraw-Hill, London.

Zienkiewicz, O. C., (1971), Incremental Displacement In Non-Linear Analysis, *Int. J. Numer. Meth. Engng.*, Vol. 3, pp. 587-588.

Appendix A. Stress-Strain Transformation Matrix

Refer to Fig. 2-2, the stress vector in structural coordinates has the relationship with the stress vector in material coordinates,

$$\begin{bmatrix} \sigma_x \\ \sigma_y \\ \tau_{yz} \\ \tau_{zx} \\ \tau_{xy} \end{bmatrix} = [T]^{-1} \begin{bmatrix} \sigma_1^m \\ \sigma_2^m \\ \tau_{23}^m \\ \tau_{31}^m \\ \tau_{12}^m \end{bmatrix} \tag{A-1}$$

or

$$\{\sigma\} = [T]^{-1} \{\sigma^m\} \tag{A-2}$$

where

$$[T]^{-1} = \begin{bmatrix} \cos^2\theta & \sin^2\theta & 0 & 0 & -2\sin\theta\cos\theta \\ \sin^2\theta & \cos^2\theta & 0 & 0 & 2\sin\theta\cos\theta \\ 0 & 0 & \cos\theta & \sin\theta & 0 \\ 0 & 0 & -\sin\theta & \cos\theta & 0 \\ \sin\theta\cos\theta & -\sin\theta\cos\theta & 0 & 0 & \cos^2\theta - \sin^2\theta \end{bmatrix} \tag{A-3}$$

and

$$\begin{bmatrix} \varepsilon_1^m \\ \varepsilon_2^m \\ \frac{1}{2}\gamma_{23}^m \\ \frac{1}{2}\gamma_{31}^m \\ \frac{1}{2}\gamma_{12}^m \end{bmatrix} = [T] \begin{bmatrix} \varepsilon_x \\ \varepsilon_y \\ \frac{1}{2}\gamma_{yz} \\ \frac{1}{2}\gamma_{zx} \\ \frac{1}{2}\gamma_{xy} \end{bmatrix} \tag{A-4}$$

or

$$[C]\{\varepsilon^m\} = [T][C]\{\varepsilon^*\} \tag{A-5}$$

where

$$[T] = \begin{bmatrix} \cos^2\theta & \sin^2\theta & 0 & 0 & 2\sin\theta\cos\theta \\ \sin^2\theta & \cos^2\theta & 0 & 0 & (-2)\sin\theta\cos\theta \\ 0 & 0 & \cos\theta & -\sin\theta & 0 \\ 0 & 0 & \sin\theta & \cos\theta & 0 \\ -\sin\theta\cos\theta & \sin\theta\cos\theta & 0 & 0 & \cos^2\theta - \sin^2\theta \end{bmatrix} \tag{A-6}$$

$$[C] = \begin{bmatrix} 1 & 0 & 0 & 0 & 0 \\ 0 & 1 & 0 & 0 & 0 \\ 0 & 0 & \frac{1}{2} & 0 & 0 \\ 0 & 0 & 0 & \frac{1}{2} & 0 \\ 0 & 0 & 0 & 0 & \frac{1}{2} \end{bmatrix} \tag{A-7}$$

Using Eqn. (2-2) (rewrite it below),

$$\{\sigma^m\} = \boldsymbol{Q}\{\varepsilon^m\}$$

Eqn. (A-1) can be written as

$$\begin{bmatrix} \sigma_x \\ \sigma_y \\ \tau_{yz} \\ \tau_{zx} \\ \tau_{xy} \end{bmatrix} = [T]^{-1}[Q][C]^{-1}[T][C] \begin{bmatrix} \varepsilon_x \\ \varepsilon_y \\ \gamma_{yz} \\ \gamma_{zx} \\ \gamma_{xy} \end{bmatrix} \tag{A-8}$$

where

$$[C]^{-1} = \begin{bmatrix} 1 & 0 & 0 & 0 & 0 \\ 0 & 1 & 0 & 0 & 0 \\ 0 & 0 & 2 & 0 & 0 \\ 0 & 0 & 0 & 2 & 0 \\ 0 & 0 & 0 & 0 & 2 \end{bmatrix} \tag{A-9}$$

Comparing Eqn. (A-8) with Eqn. (2-14), the stress-strain transformation matrix can be expressed as:

$$\boldsymbol{D} = [T]^{-1}[Q][C]^{-1}[T][C] \tag{A-10}$$

Keeping in mind that matrix $[Q]$ is symmetric, matrix $\boldsymbol{D}$ can be proved to be symmetric because the following relationship

$$[T^{-1}]^{T} = [C]^{-1}[T][C]. \tag{A-11}$$

In the derivation of the above equations, matrices $[T]$ and $[T]^{-1}$ are pure geometric transformation matrices and can be derived directly from the geometric relation of stresses or strains in two coordinate systems. Part of the derivations may be found in the references (Jone 1975, Agarwal 1980).

Appendix B. Relationship of Nonlinear Strains and Nodal Displacements

In Chapter 2, the strains of shell of revolution are expressed as the sum of linear strains and nonlinear strains (Eqn. (2-15)),

$$\{\varepsilon^*\} = \{\varepsilon^L\} + \{\varepsilon^N\} \tag{B-1}$$

where

$$\{\varepsilon^L\} = \left[e_{11}\ e_{22}\ e_{23}\ e_{31}\ e_{12}\right]^T \quad \text{and} \quad \{\varepsilon^N\} = \left[\varepsilon_{11}\ \varepsilon_{22}\ \varepsilon_{23}\ \varepsilon_{31}\ \varepsilon_{12}\right]^T. \tag{B-2}$$

The linear strain components (e_{33} is given below because it will be used later in the expressions of nonlinear strains) are

$$e_{11} = \frac{1}{H_1}\frac{\partial u_1}{\partial \alpha} + \frac{1}{H_1 H_2}\frac{\partial H_1}{\partial \beta}u_2 + \frac{1}{H_1 H_3}\frac{\partial H_1}{\partial \gamma}u_3 \tag{B-3}$$

$$e_{22} = \frac{1}{H_2}\frac{\partial u_2}{\partial \beta} + \frac{1}{H_2 H_3}\frac{\partial H_2}{\partial \gamma}u_3 + \frac{1}{H_2 H_1}\frac{\partial H_2}{\partial \alpha}u_1 \tag{B-4}$$

$$e_{33} = \frac{1}{H_3}\frac{\partial u_3}{\partial \gamma} + \frac{1}{H_3 H_1}\frac{\partial H_3}{\partial \alpha}u_1 + \frac{1}{H_3 H_2}\frac{\partial H_3}{\partial \beta}u_2 \tag{B-5}$$

$$e_{23} = \frac{H_2}{H_3}\frac{\partial}{\partial \gamma}\left(\frac{u_2}{H_2}\right) + \frac{H_3}{H_2}\frac{\partial}{\partial \beta}\left(\frac{u_3}{H_3}\right) \tag{B-6}$$

$$e_{31} = \frac{H_3}{H_1}\frac{\partial}{\partial \alpha}\left(\frac{u_3}{H_3}\right) + \frac{H_1}{H_3}\frac{\partial}{\partial \gamma}\left(\frac{u_1}{H_1}\right) \tag{B-7}$$

$$e_{12} = \frac{H_2}{H_1}\frac{\partial}{\partial \alpha}\left(\frac{u_2}{H_2}\right) + \frac{H_1}{H_2}\frac{\partial}{\partial \beta}\left(\frac{u_1}{H_1}\right) \tag{B-8}$$

The nonlinear strain components are

$$\varepsilon_{11} = \frac{1}{2}\left[e_{11}^2 + \left(\frac{1}{2}e_{12} + \omega_3\right)^2 + \left(\frac{1}{2}e_{13} - \omega_2\right)^2\right] \tag{B-9}$$

$$\varepsilon_{22} = \frac{1}{2}\left[e_{22}^2 + \left(\frac{1}{2}e_{23} + \omega_1\right)^2 + \left(\frac{1}{2}e_{21} - \omega_3\right)^2\right] \tag{B-10}$$

$$\varepsilon_{23} = e_{22}\left(\frac{1}{2}e_{23} - \omega_1\right) + e_{33}\left(\frac{1}{2}e_{23} + \omega_1\right) + \left(\frac{1}{2}e_{21} - \omega_3\right)\left(\frac{1}{2}e_{31} + \omega_2\right) \tag{B-11}$$

$$\varepsilon_{31} = e_{33}\left(\frac{1}{2}e_{31} - \omega_2\right) + e_{11}\left(\frac{1}{2}e_{31} + \omega_2\right) + \left(\frac{1}{2}e_{32} - \omega_1\right)\left(\frac{1}{2}e_{12} + \omega_3\right) \tag{B-12}$$

$$\varepsilon_{12} = e_{11}\left(\frac{1}{2}e_{12} - \omega_3\right) + e_{22}\left(\frac{1}{2}e_{12} + \omega_3\right) + \left(\frac{1}{2}e_{13} - \omega_2\right)\left(\frac{1}{2}e_{23} + \omega_1\right) \tag{B-13}$$

where

$$\omega_1 = \frac{1}{2H_2H_3}\left[\frac{\partial}{\partial\beta}(H_3u_3) - \frac{\partial}{\partial\gamma}(H_2u_2)\right] \tag{B-14}$$

$$\omega_2 = \frac{1}{2H_1H_3}\left[\frac{\partial}{\partial\gamma}(H_1u_1) - \frac{\partial}{\partial\alpha}(H_3u_3)\right] \tag{B-15}$$

$$\omega_3 = \frac{1}{2H_1H_2}\left[\frac{\partial}{\partial\alpha}(H_2u_2) - \frac{\partial}{\partial\beta}(H_1u_1)\right] \tag{B-16}$$

In the finite element method, the linear strains are linear functions of element nodal displacements (Eqn. (2-30)),

$$\{\varepsilon^L\} = \boldsymbol{B}^L\boldsymbol{q}_e, \qquad \text{and} \qquad \{\delta\varepsilon^L\} = \boldsymbol{B}^L\delta\boldsymbol{q}_e \tag{B-17}$$

In expanded form,

$$e_{11} = \boldsymbol{B}_{11}^L\boldsymbol{q}_e \qquad \delta e_{11} = \delta\boldsymbol{q}_e^T(\boldsymbol{B}_{11}^L)^T \tag{B-18}$$

$$e_{22} = \boldsymbol{B}_{22}^L\boldsymbol{q}_e \qquad \delta e_{22} = \delta\boldsymbol{q}_e^T(\boldsymbol{B}_{22}^L)^T \tag{B-19}$$

$$e_{33} = \boldsymbol{B}_{33}^L\boldsymbol{q}_e \qquad \delta e_{33} = \delta\boldsymbol{q}_e^T(\boldsymbol{B}_{33}^L)^T \tag{B-20}$$

$$e_{23} = \boldsymbol{B}_{23}^L\boldsymbol{q}_e \qquad \delta e_{23} = \delta\boldsymbol{q}_e^T(\boldsymbol{B}_{23}^L)^T \tag{B-21}$$

$$e_{31} = \boldsymbol{B}_{31}^L\boldsymbol{q}_e \qquad \delta e_{31} = \delta\boldsymbol{q}_e^T(\boldsymbol{B}_{31}^L)^T \tag{B-22}$$

$$e_{12} = \boldsymbol{B}_{12}^{L} q_e \qquad \delta e_{12} = \delta \boldsymbol{q}_e^{T} (\boldsymbol{B}_{12}^{L})^{T} \tag{B-23}$$

$$\omega_1 = \boldsymbol{B}_{\omega 1}^{L} q_e \qquad \delta \omega_1 = \delta \boldsymbol{q}_e^{T} (\boldsymbol{B}_{\omega 1}^{L})^{T} \tag{B-24}$$

$$\omega_2 = \boldsymbol{B}_{\omega 2}^{L} q_e \qquad \delta \omega_2 = \delta \boldsymbol{q}_e^{T} (\boldsymbol{B}_{\omega 2}^{L})^{T} \tag{B-25}$$

$$\omega_3 = \boldsymbol{B}_{\omega 3}^{L} q_e \qquad \delta \omega_3 = \delta \boldsymbol{q}_e^{T} (\boldsymbol{B}_{\omega 3}^{L})^{T} \tag{B-26}$$

Substituting Eqns. (B-18) through (B-26) into Eqns. (B-9) through (B-13), the nonlinear strain vector and its variation can be proved to be the following expressions:

$$\varepsilon^{N} = \frac{1}{2}\left[\boldsymbol{B}^{N}(q_e)\right] q_e, \qquad \text{and} \qquad \delta\varepsilon^{N} = \left[\boldsymbol{B}^{N}(q_e)\right] \delta q_e. \tag{B-27}$$

where

$$\left[\boldsymbol{B}^{N}(q_e)\right] = \begin{bmatrix} \boldsymbol{q}_e^{T}\boldsymbol{B}_{11}^{N} \\ \boldsymbol{q}_e^{T}\boldsymbol{B}_{22}^{N} \\ \boldsymbol{q}_e^{T}\boldsymbol{B}_{23}^{N} \\ \boldsymbol{q}_e^{T}\boldsymbol{B}_{31}^{N} \\ \boldsymbol{q}_e^{T}\boldsymbol{B}_{12}^{N} \end{bmatrix} \tag{B-28}$$

In expanded form, Eqns. (B-27) are

$$\varepsilon_{11} = \frac{1}{2}\boldsymbol{q}_e^{T}\boldsymbol{B}_{11}^{N} q_e \qquad \delta\varepsilon_{11} = \boldsymbol{q}_e^{T}\boldsymbol{B}_{11}^{N}\delta q_e \tag{B-29}$$

$$\varepsilon_{22} = \frac{1}{2}\boldsymbol{q}_e^{T}\boldsymbol{B}_{22}^{N} q_e \qquad \delta\varepsilon_{22} = \boldsymbol{q}_e^{T}\boldsymbol{B}_{22}^{N}\delta q_e \tag{B-30}$$

$$\varepsilon_{23} = \frac{1}{2}\boldsymbol{q}_e^{T}\boldsymbol{B}_{23}^{N} q_e \qquad \delta\varepsilon_{23} = \boldsymbol{q}_e^{T}\boldsymbol{B}_{23}^{N}\delta q_e \tag{B-31}$$

$$\varepsilon_{31} = \frac{1}{2}\boldsymbol{q}_e^{T}\boldsymbol{B}_{31}^{N} q_e \qquad \delta\varepsilon_{31} = \boldsymbol{q}_e^{T}\boldsymbol{B}_{31}^{N}\delta q_e \tag{B-32}$$

$$\varepsilon_{12} = \frac{1}{2}\boldsymbol{q}_e^{T}\boldsymbol{B}_{12}^{N} q_e \qquad \delta\varepsilon_{12} = \boldsymbol{q}_e^{T}\boldsymbol{B}_{12}^{N}\delta q_e \tag{B-33}$$

where

$$B_{11}^{N} = (B_{11}^{L})^{T} B_{11}^{L} + p_{123}^{T} p_{123} + n_{312}^{T} n_{312} \tag{B-34}$$

$$B_{22}^{N} = (B_{22}^{L})^{T} B_{22}^{L} + p_{231}^{T} p_{231} + n_{123}^{T} n_{123} \tag{B-35}$$

$$B_{12}^{N} = (B_{11}^{L})^{T} n_{123} + n_{123}^{T} B_{11}^{L} + (B_{22}^{L})^{T} p_{123} + p_{123}^{T} B_{22}^{L} + n_{312}^{T} p_{231} + p_{231}^{T} n_{312} \tag{B-36}$$

$$B_{23}^{N} = (B_{22}^{L})^{T} n_{231} + n_{231}^{T} B_{22}^{L} + (B_{33}^{L})^{T} p_{231} + p_{231}^{T} B_{33}^{L} + n_{123}^{T} p_{312} + p_{312}^{T} n_{123} \tag{B-37}$$

$$B_{31}^{N} = (B_{33}^{L})^{T} n_{312} + n_{312}^{T} B_{33}^{L} + (B_{11}^{L})^{T} p_{312} + p_{312}^{T} B_{11}^{L} + n_{231}^{T} p_{123} + p_{123}^{T} n_{231} \tag{B-38}$$

where

$$p_{123} = \left(\frac{1}{2} B_{12}^{L} + B_{\omega 3}^{L}\right) \tag{B-39}$$

$$p_{231} = \left(\frac{1}{2} B_{23}^{L} + B_{\omega 1}^{L}\right) \tag{B-40}$$

$$p_{312} = \left(\frac{1}{2} B_{31}^{L} + B_{\omega 2}^{L}\right) \tag{B-41}$$

$$n_{123} = \left(\frac{1}{2} B_{12}^{L} - B_{\omega 3}^{L}\right) \tag{B-42}$$

$$n_{231} = \left(\frac{1}{2} B_{23}^{L} - B_{\omega 1}^{L}\right) \tag{B-43}$$

$$n_{312} = \left(\frac{1}{2} B_{31}^{L} - B_{\omega 2}^{L}\right) \tag{B-44}$$

To prove Eqns. (B-28) through (B-32), only two terms need to be selected to illustrate the procedures. Considering the term e_{11}^{2} and the cross-product term $e_{12}\omega_{3}$ in the right hand side of Eqn. (B-9), ε_{11} can be arranged as

$$\varepsilon_{11} = \frac{1}{2}\left[e_{11}^{T} e_{11} + \frac{1}{2} e_{12}^{T} \omega_{3} + \frac{1}{2} \omega_{3}^{T} e_{12} + \ldots\right] \tag{B-45}$$

Using Eqns. (B-18) through (B-26),

$$\varepsilon_{11} = \frac{1}{2}\left[\boldsymbol{q}_e^T (\boldsymbol{B}_{11}^L)^T \boldsymbol{B}_{11}^L + \frac{1}{2}\boldsymbol{q}_e^T (\boldsymbol{B}_{12}^L)^T \boldsymbol{B}_{\omega 3}^L + \frac{1}{2}\boldsymbol{q}_e^T (\boldsymbol{B}_{\omega 3}^L)^T \boldsymbol{B}_{12}^L + \ldots\right]\boldsymbol{q}_e \tag{B-46}$$

Similarly,

$$\delta\varepsilon_{11} = \left[e_{11}^T \delta e_{11} + \frac{1}{2}\omega_3^T \delta e_{12} + \frac{1}{2}e_{12}^T \delta\omega_3 + \ldots\right] \tag{B-47}$$

$$\delta\varepsilon_{11} = \left[\boldsymbol{q}_e^T (\boldsymbol{B}_{11}^L)^T \boldsymbol{B}_{11}^L + \frac{1}{2}\boldsymbol{q}_e^T (\boldsymbol{B}_{12}^L)^T \boldsymbol{B}_{\omega 3}^L + \frac{1}{2}\boldsymbol{q}_e^T (\boldsymbol{B}_{\omega 3}^L)^T \boldsymbol{B}_{12}^L + \ldots\right]\delta\boldsymbol{q}_e \tag{B-48}$$

If defining

$$\boldsymbol{B}_{11}^N = (\boldsymbol{B}_{11}^L)^T \boldsymbol{B}_{11}^L + \frac{1}{2}(\boldsymbol{B}_{12}^L)^T \boldsymbol{B}_{\omega 3}^L + \frac{1}{2}(\boldsymbol{B}_{\omega 3}^L)^T \boldsymbol{B}_{12}^L + \ldots \tag{B-49}$$

then Eqn. (B-29) have been proved, that is

$$\varepsilon_{11} = \frac{1}{2}\boldsymbol{q}_e^T \boldsymbol{B}_{11}^N \boldsymbol{q}_e \tag{B-50}$$

$$\delta\varepsilon_{11} = \boldsymbol{q}_e^T \boldsymbol{B}_{11}^N \delta\boldsymbol{q}_e \tag{B-51}$$

Similar procedure can be used to prove Eqns. (B-30) through (B-33).

Appendix C. Shape Function Matrices for Nonlinear Beam-Type Bending Analysis

If the following terms are defined:

$$\xi = \frac{\alpha_e}{L_e} \tag{C-1}$$

$$f_i = 1 - 3\xi + 2\xi^2 \tag{C-2}$$

$$f_k = 4\xi - 4\xi^2 \tag{C-3}$$

$$f_j = -\xi + 2\xi^2 \tag{C-4}$$

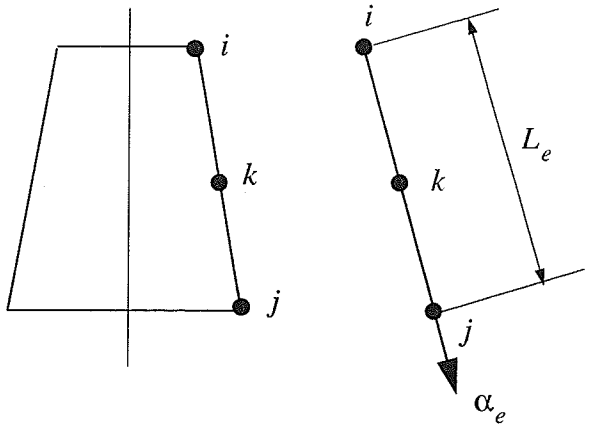

where L_e is the length of the element in α direction., then the shape function matrices are

$$N_1 = \begin{bmatrix}
f_i & 0 & 0 & 0 & 0 & 0 & 0 & 0 & 0 & 0 & 0 & 0 & f_k & 0 & 0 & 0 & 0 & 0 & 0 & 0 & 0 & 0 & 0 & 0 & f_j & 0 & 0 & 0 & 0 & 0 & 0 & 0 & 0 & 0 & 0 & 0 \\
0 & f_i & 0 & 0 & 0 & 0 & 0 & 0 & 0 & 0 & 0 & 0 & 0 & f_k & 0 & 0 & 0 & 0 & 0 & 0 & 0 & 0 & 0 & 0 & 0 & f_j & 0 & 0 & 0 & 0 & 0 & 0 & 0 & 0 & 0 & 0 \\
0 & 0 & 0 & 0 & 0 & 0 & f_i & 0 & 0 & 0 & 0 & 0 & 0 & 0 & 0 & 0 & 0 & 0 & f_k & 0 & 0 & 0 & 0 & 0 & 0 & 0 & 0 & 0 & 0 & 0 & f_j & 0 & 0 & 0 & 0 & 0 \\
0 & 0 & 0 & 0 & 0 & 0 & f_i & 0 & 0 & 0 & 0 & 0 & 0 & 0 & 0 & 0 & 0 & 0 & f_k & 0 & 0 & 0 & 0 & 0 & 0 & 0 & 0 & 0 & 0 & 0 & f_j & 0 & 0 & 0 & 0 & 0 \\
0 & 0 & 0 & 0 & 0 & 0 & 0 & 0 & 0 & 0 & 0 & 0 & f_i & 0 & 0 & 0 & 0 & 0 & 0 & 0 & 0 & 0 & 0 & 0 & f_k & 0 & 0 & 0 & 0 & 0 & 0 & 0 & 0 & 0 & 0 & f_j \\
0 & 0 & 0 & 0 & 0 & 0 & 0 & 0 & 0 & 0 & 0 & 0 & rf_i & 0 & 0 & 0 & 0 & 0 & 0 & 0 & 0 & 0 & 0 & 0 & rf_k & 0 & 0 & 0 & 0 & 0 & 0 & 0 & 0 & 0 & 0 & rf_j
\end{bmatrix} \tag{C-5}$$

$$N_2 = \begin{bmatrix}
0 & 0 & f_i & 0 & 0 & 0 & 0 & 0 & 0 & 0 & 0 & 0 & 0 & 0 & f_k & 0 & 0 & 0 & 0 & 0 & 0 & 0 & 0 & 0 & 0 & 0 & f_j & 0 & 0 & 0 & 0 & 0 & 0 & 0 & 0 & 0 & 0 \\
0 & 0 & 0 & f_i & 0 & 0 & 0 & 0 & 0 & 0 & 0 & 0 & 0 & 0 & f_k & 0 & 0 & 0 & 0 & 0 & 0 & 0 & 0 & 0 & 0 & 0 & f_j & 0 & 0 & 0 & 0 & 0 & 0 & 0 & 0 & 0 & 0 \\
0 & 0 & 0 & 0 & 0 & 0 & 0 & 0 & f_i & 0 & 0 & 0 & 0 & 0 & 0 & 0 & 0 & 0 & 0 & f_k & 0 & 0 & 0 & 0 & 0 & 0 & 0 & 0 & 0 & f_j & 0 & 0 & 0 & 0 & 0 & 0 & 0 \\
0 & 0 & 0 & 0 & 0 & 0 & 0 & 0 & 0 & f_i & 0 & 0 & 0 & 0 & 0 & 0 & 0 & 0 & 0 & 0 & f_k & 0 & 0 & 0 & 0 & 0 & 0 & 0 & 0 & 0 & f_j & 0 & 0 & 0 & 0 & 0 & 0 \\
0 & 0 & 0 & 0 & 0 & 0 & 0 & 0 & 0 & 0 & f_i & 0 & 0 & 0 & 0 & 0 & 0 & 0 & 0 & 0 & 0 & f_k & 0 & 0 & 0 & 0 & 0 & 0 & 0 & 0 & 0 & f_j & 0 & 0 & 0 & 0 & 0 \\
0 & 0 & 0 & 0 & 0 & 0 & 0 & 0 & 0 & 0 & 0 & rf_i & 0 & 0 & 0 & 0 & 0 & 0 & 0 & 0 & 0 & 0 & rf_k & 0 & 0 & 0 & 0 & 0 & 0 & 0 & 0 & 0 & rf_j & 0 & 0 & 0 & 0
\end{bmatrix} \quad \text{(C-6)}$$

$$N_3 = \begin{bmatrix}
0 & 0 & 0 & 0 & f_i & 0 & 0 & 0 & 0 & 0 & 0 & 0 & 0 & 0 & 0 & 0 & f_k & 0 & 0 & 0 & 0 & 0 & 0 & 0 & 0 & 0 & 0 & f_j & 0 & 0 & 0 & 0 & 0 & 0 & 0 & 0 & 0 \\
0 & 0 & 0 & 0 & 0 & f_i & 0 & 0 & 0 & 0 & 0 & 0 & 0 & 0 & 0 & 0 & f_k & 0 & 0 & 0 & 0 & 0 & 0 & 0 & 0 & 0 & 0 & f_j & 0 & 0 & 0 & 0 & 0 & 0 & 0 & 0 & 0 \\
0 & 0 & 0 & 0 & 0 & 0 & 0 & 0 & 0 & 0 & f_i & 0 & 0 & 0 & 0 & 0 & 0 & 0 & 0 & f_k & 0 & 0 & 0 & 0 & 0 & 0 & 0 & 0 & 0 & f_j & 0 & 0 & 0 & 0 & 0 & 0 & 0 \\
0 & 0 & 0 & 0 & 0 & 0 & 0 & 0 & 0 & 0 & 0 & f_i & 0 & 0 & 0 & 0 & 0 & 0 & 0 & 0 & f_k & 0 & 0 & 0 & 0 & 0 & 0 & 0 & 0 & 0 & f_j & 0 & 0 & 0 & 0 & 0 & 0 \\
0 & 0 & 0 & 0 & 0 & 0 & 0 & 0 & 0 & 0 & 0 & 0 & f_i & 0 & 0 & 0 & 0 & 0 & 0 & 0 & 0 & f_k & 0 & 0 & 0 & 0 & 0 & 0 & 0 & 0 & 0 & f_j & 0 & 0 & 0 & 0 & 0 \\
0 & 0 & 0 & 0 & 0 & 0 & 0 & 0 & 0 & 0 & 0 & rf_i & 0 & 0 & 0 & 0 & 0 & 0 & 0 & 0 & 0 & 0 & rf_k & 0 & 0 & 0 & 0 & 0 & 0 & 0 & 0 & 0 & rf_j & 0 & 0 & 0 & 0
\end{bmatrix} \quad \text{(C-7)}$$

Appendix D. Shape Function Matrices for Ovalization Analysis

In the following, the terms f_i, f_k and f_j are the same as defined in Appendix C.

$$N_1 = \begin{bmatrix} N_{1i} & N_{1k} & N_{1j} \end{bmatrix} \tag{D-1}$$

$$N_2 = \begin{bmatrix} N_{2i} & N_{2k} & N_{2j} \end{bmatrix} \tag{D-2}$$

$$N_3 = \begin{bmatrix} N_{3i} & N_{3k} & N_{3j} \end{bmatrix} \tag{D-3}$$

where

$$N_{1i} = \begin{bmatrix} f_i & 0 & 0 & 0 & 0 & 0 & 0 & 0 & 0 & 0 & 0 & 0 & 0 & 0 & 0 & 0 & 0 & 0 \\ 0 & f_i & 0 & 0 & 0 & 0 & 0 & 0 & 0 & 0 & 0 & 0 & 0 & 0 & 0 & 0 & 0 & 0 \\ 0 & 0 & 0 & 0 & 0 & 0 & f_i & 0 & 0 & 0 & 0 & 0 & 0 & 0 & 0 & 0 & 0 & 0 \\ 0 & 0 & 0 & 0 & 0 & 0 & 0 & f_i & 0 & 0 & 0 & 0 & 0 & 0 & 0 & 0 & 0 & 0 \\ 0 & 0 & 0 & 0 & 0 & 0 & 0 & 0 & 0 & 0 & 0 & 0 & f_i & 0 & 0 & 0 & 0 & 0 \\ 0 & 0 & 0 & 0 & 0 & 0 & 0 & 0 & 0 & 0 & 0 & 0 & 0 & f_i & 0 & 0 & 0 & 0 \end{bmatrix} \tag{D-4}$$

$$N_{1k} = \begin{bmatrix} f_k & 0 & 0 & 0 & 0 & 0 & 0 & 0 & 0 & 0 & 0 & 0 & 0 & 0 & 0 & 0 & 0 & 0 \\ 0 & f_k & 0 & 0 & 0 & 0 & 0 & 0 & 0 & 0 & 0 & 0 & 0 & 0 & 0 & 0 & 0 & 0 \\ 0 & 0 & 0 & 0 & 0 & 0 & f_k & 0 & 0 & 0 & 0 & 0 & 0 & 0 & 0 & 0 & 0 & 0 \\ 0 & 0 & 0 & 0 & 0 & 0 & 0 & f_k & 0 & 0 & 0 & 0 & 0 & 0 & 0 & 0 & 0 & 0 \\ 0 & 0 & 0 & 0 & 0 & 0 & 0 & 0 & 0 & 0 & 0 & 0 & f_k & 0 & 0 & 0 & 0 & 0 \\ 0 & 0 & 0 & 0 & 0 & 0 & 0 & 0 & 0 & 0 & 0 & 0 & 0 & f_k & 0 & 0 & 0 & 0 \end{bmatrix} \tag{D-5}$$

$$N_{1j} = \begin{bmatrix} f_j & 0 & 0 & 0 & 0 & 0 & 0 & 0 & 0 & 0 & 0 & 0 & 0 & 0 & 0 & 0 & 0 & 0 \\ 0 & f_j & 0 & 0 & 0 & 0 & 0 & 0 & 0 & 0 & 0 & 0 & 0 & 0 & 0 & 0 & 0 & 0 \\ 0 & 0 & 0 & 0 & 0 & 0 & f_j & 0 & 0 & 0 & 0 & 0 & 0 & 0 & 0 & 0 & 0 & 0 \\ 0 & 0 & 0 & 0 & 0 & 0 & 0 & f_j & 0 & 0 & 0 & 0 & 0 & 0 & 0 & 0 & 0 & 0 \\ 0 & 0 & 0 & 0 & 0 & 0 & 0 & 0 & 0 & 0 & 0 & 0 & f_j & 0 & 0 & 0 & 0 & 0 \\ 0 & 0 & 0 & 0 & 0 & 0 & 0 & 0 & 0 & 0 & 0 & 0 & 0 & f_j & 0 & 0 & 0 & 0 \end{bmatrix} \tag{D-6}$$

$$N_{2i} = \begin{bmatrix} 0 & 0 & f_i & 0 & 0 & 0 & 0 & 0 & 0 & 0 & 0 & 0 & 0 & 0 & 0 & 0 \\ 0 & 0 & 0 & f_i & 0 & 0 & 0 & 0 & 0 & 0 & 0 & 0 & 0 & 0 & 0 & 0 \\ 0 & 0 & 0 & 0 & 0 & 0 & 0 & 0 & f_i & 0 & 0 & 0 & 0 & 0 & 0 & 0 \\ 0 & 0 & 0 & 0 & 0 & 0 & 0 & 0 & 0 & f_i & 0 & 0 & 0 & 0 & 0 & 0 \\ 0 & 0 & 0 & 0 & 0 & 0 & 0 & 0 & 0 & 0 & 0 & 0 & 0 & f_i & 0 & 0 \\ 0 & 0 & 0 & 0 & 0 & 0 & 0 & 0 & 0 & 0 & 0 & 0 & 0 & 0 & f_i & 0 \end{bmatrix} \quad \text{(D-7)}$$

$$N_{2k} = \begin{bmatrix} 0 & 0 & f_k & 0 & 0 & 0 & 0 & 0 & 0 & 0 & 0 & 0 & 0 & 0 & 0 & 0 \\ 0 & 0 & 0 & f_k & 0 & 0 & 0 & 0 & 0 & 0 & 0 & 0 & 0 & 0 & 0 & 0 \\ 0 & 0 & 0 & 0 & 0 & 0 & 0 & 0 & f_k & 0 & 0 & 0 & 0 & 0 & 0 & 0 \\ 0 & 0 & 0 & 0 & 0 & 0 & 0 & 0 & 0 & f_k & 0 & 0 & 0 & 0 & 0 & 0 \\ 0 & 0 & 0 & 0 & 0 & 0 & 0 & 0 & 0 & 0 & 0 & 0 & 0 & f_k & 0 & 0 \\ 0 & 0 & 0 & 0 & 0 & 0 & 0 & 0 & 0 & 0 & 0 & 0 & 0 & 0 & f_k & 0 \end{bmatrix} \quad \text{(D-8)}$$

$$N_{2j} = \begin{bmatrix} 0 & 0 & f_j & 0 & 0 & 0 & 0 & 0 & 0 & 0 & 0 & 0 & 0 & 0 & 0 & 0 \\ 0 & 0 & 0 & f_j & 0 & 0 & 0 & 0 & 0 & 0 & 0 & 0 & 0 & 0 & 0 & 0 \\ 0 & 0 & 0 & 0 & 0 & 0 & 0 & 0 & f_j & 0 & 0 & 0 & 0 & 0 & 0 & 0 \\ 0 & 0 & 0 & 0 & 0 & 0 & 0 & 0 & 0 & f_j & 0 & 0 & 0 & 0 & 0 & 0 \\ 0 & 0 & 0 & 0 & 0 & 0 & 0 & 0 & 0 & 0 & 0 & 0 & 0 & f_j & 0 & 0 \\ 0 & 0 & 0 & 0 & 0 & 0 & 0 & 0 & 0 & 0 & 0 & 0 & 0 & 0 & f_j & 0 \end{bmatrix} \quad \text{(D-9)}$$

$$N_{3i} = \begin{bmatrix} 0 & 0 & 0 & 0 & f_i & 0 & 0 & 0 & 0 & 0 & 0 & 0 & 0 & 0 & 0 & 0 \\ 0 & 0 & 0 & 0 & 0 & f_i & 0 & 0 & 0 & 0 & 0 & 0 & 0 & 0 & 0 & 0 \\ 0 & 0 & 0 & 0 & 0 & 0 & 0 & 0 & 0 & f_i & 0 & 0 & 0 & 0 & 0 & 0 \\ 0 & 0 & 0 & 0 & 0 & 0 & 0 & 0 & 0 & 0 & f_i & 0 & 0 & 0 & 0 & 0 \\ 0 & 0 & 0 & 0 & 0 & 0 & 0 & 0 & 0 & 0 & 0 & 0 & 0 & 0 & f_i & 0 \\ 0 & 0 & 0 & 0 & 0 & 0 & 0 & 0 & 0 & 0 & 0 & 0 & 0 & 0 & 0 & f_i \end{bmatrix} \quad \text{(D-10)}$$

$$N_{3k} = \begin{bmatrix} 0 & 0 & 0 & 0 & f_k & 0 & 0 & 0 & 0 & 0 & 0 & 0 & 0 & 0 & 0 & 0 \\ 0 & 0 & 0 & 0 & 0 & f_k & 0 & 0 & 0 & 0 & 0 & 0 & 0 & 0 & 0 & 0 \\ 0 & 0 & 0 & 0 & 0 & 0 & 0 & 0 & 0 & f_k & 0 & 0 & 0 & 0 & 0 & 0 \\ 0 & 0 & 0 & 0 & 0 & 0 & 0 & 0 & 0 & 0 & f_k & 0 & 0 & 0 & 0 & 0 \\ 0 & 0 & 0 & 0 & 0 & 0 & 0 & 0 & 0 & 0 & 0 & 0 & 0 & 0 & f_k & 0 \\ 0 & 0 & 0 & 0 & 0 & 0 & 0 & 0 & 0 & 0 & 0 & 0 & 0 & 0 & 0 & f_k \end{bmatrix} \quad \text{(D-11)}$$

$$N_{3j} = \begin{bmatrix} 0 & 0 & 0 & 0 & f_j & 0 & 0 & 0 & 0 & 0 & 0 & 0 & 0 & 0 & 0 & 0 & 0 & 0 \\ 0 & 0 & 0 & 0 & 0 & f_j & 0 & 0 & 0 & 0 & 0 & 0 & 0 & 0 & 0 & 0 & 0 & 0 \\ 0 & 0 & 0 & 0 & 0 & 0 & 0 & 0 & 0 & 0 & f_j & 0 & 0 & 0 & 0 & 0 & 0 & 0 \\ 0 & 0 & 0 & 0 & 0 & 0 & 0 & 0 & 0 & 0 & 0 & f_j & 0 & 0 & 0 & 0 & 0 & 0 \\ 0 & 0 & 0 & 0 & 0 & 0 & 0 & 0 & 0 & 0 & 0 & 0 & 0 & 0 & 0 & 0 & f_j & 0 \\ 0 & 0 & 0 & 0 & 0 & 0 & 0 & 0 & 0 & 0 & 0 & 0 & 0 & 0 & 0 & 0 & 0 & f_j \end{bmatrix} \qquad \text{(D-12)}$$

Appendix E. Shape Function Matrices for Linear Analysis

Defining the following terms first (ξ is defined as in Appendix C),

$$f_1 = 1 - \xi \tag{E-1}$$

$$f_2 = \xi \tag{E-2}$$

$$f_3 = 1 - 3\xi + 2\xi^2 \tag{E-3}$$

$$f_4 = -\xi + 2\xi^2 \tag{E-4}$$

$$f_5 = -3 + 4\xi \tag{E-5}$$

$$f_6 = -1 + 4\xi \tag{E-6}$$

$$f_{k1} = 4\xi - 4\xi^2 \tag{E-7}$$

$$f_{k2} = 4 - 8\xi \tag{E-8}$$

then the shape function matrices used in Chapter 7 are

$$N_1 = \begin{bmatrix} f_1 & 0 & 0 & 0 & 0 & 0 & 0 & 0 & f_2 & 0 & 0 & 0 & 0 \\ 0 & f_3 & 0 & 0 & 0 & f_{k1} & 0 & 0 & 0 & f_4 & 0 & 0 & 0 \\ 0 & 0 & f_1 & 0 & 0 & 0 & 0 & 0 & 0 & 0 & f_2 & 0 & 0 \\ 0 & 0 & 0 & f_3 & 0 & 0 & f_{k1} & 0 & 0 & 0 & 0 & f_4 & 0 \\ 0 & 0 & 0 & 0 & f_5 & 0 & 0 & f_{k2} & 0 & 0 & 0 & 0 & f_6 \end{bmatrix} \tag{E-9}$$

$$N_2 = \begin{bmatrix} f_1 & 0 & 0 & 0 & 0 & 0 & 0 & 0 & f_2 & 0 & 0 & 0 & 0 \\ 0 & f_3 & 0 & 0 & 0 & f_{k1} & 0 & 0 & 0 & f_4 & 0 & 0 & 0 \\ 0 & 0 & f_1 & 0 & 0 & 0 & 0 & 0 & 0 & 0 & f_2 & 0 & 0 \\ 0 & 0 & 0 & f_3 & 0 & 0 & f_{k1} & 0 & 0 & 0 & 0 & f_4 & 0 \\ 0 & 0 & 0 & 0 & f_3 & 0 & 0 & f_{k1} & 0 & 0 & 0 & 0 & f_4 \end{bmatrix} \tag{E-10}$$

$$N_3 = \begin{bmatrix} f_1 & 0 & 0 & 0 & 0 & 0 & 0 & 0 & f_2 & 0 & 0 & 0 & 0 \\ 0 & f_3 & 0 & 0 & 0 & f_{k1} & 0 & 0 & 0 & f_4 & 0 & 0 & 0 \\ 0 & 0 & f_1 & 0 & 0 & 0 & 0 & 0 & 0 & 0 & f_2 & 0 & 0 \\ 0 & 0 & 0 & f_3 & 0 & 0 & f_{k1} & 0 & 0 & 0 & 0 & f_4 & 0 \\ 0 & 0 & 0 & 0 & f_3 & 0 & 0 & f_{k1} & 0 & 0 & 0 & 0 & f_4 \end{bmatrix} \quad \text{(E-11)}$$

Appendix F. Test Program

A limited test program was conducted in the Department of Civil and Geological Engineering at the University of Manitoba in 1993 in order to investigate the behaviour of scaled FRP models of a transmission pole under cantilever loading conditions. Four such scaled poles fabricated by FAROEX Ltd., Gimli, Manitoba were tested to failure. The test specimens, the test set-up, the loading procedures and the test results are presented in the following.

F.1. The Test Specimens

The four specimens tested are prismatic circular hollow sections. The geometry of the cross-section is shown in Fig. F-1. The outside diameter of the poles is 3 inches and the wall thickness is 1/4 inch. The material properties of resin and fibres are given in Table F-1 and Table F-2. The specimens were numbered as Specimen #1, #2, #3 and #4. Specimen #1 and Specimen #2 were each tested twice by reversing the fixed ends. According to the test sequence, these two tests were numbered as Test #1 and Test #2.

F.2. The Test Set-Up

The test set-up is illustrated in Fig. F-2. It consists of a rigid base in which the specimen was cast into with an epoxy. Then a load cell was connected to the specimen to monitor the loading. A hydraulic cylinder was used to control the deflection thus inducing the loads on the section. The deflection was monitored with the use of a string deflection meter. In order to enable the poles to develop their full strengths, Specimen #2, #3 and #4 were tested with a steel plug installed at the base. The plug was inserted into the poles at a length of 1.5 inches measured from the base.

F.3. The Loading Procedure

All the poles were tested as cantilever beams under concentrated transverse load. For Specimen #1, Test #1, the loading procedure was recorded in an observation list as shown in Table F-3. For Specimen #1, Test #2, the load was applied continuously until the section failed. For specimen #2, Test #1, the load was applied and stopped for a while. The load and the deflection dropped at this period. Then the load was applied until the pole failed. For Specimen #3 and #4, the loads were applied continuously until the poles are broken. The loading procedures were reflected in the load-deflection curves given in Figs. F-3 through F-8.

F.4. The Test Results

The load-deflection curves obtained from the six tests are given in Figs. F-3 to F-8. Partial results are listed in Table 7-3 in Chapter 7. Fig. F-9 combines all the six curves into one figure and provides an overall comparison for the curves obtained.

TABLE F-1
Resin Properties

Properties	Epoxy	
Tensile Modulus	$4.8 \times 10^5 psi$	$3.31 \times 10^3 MPa$

TABLE F-2
Fibre Properties

Properties	E-Glass	
Tensile Strength	$0.5 \times 10^6 psi$	$34.38 \times 10^3 MPa$
Tensile Modulus	$10.5 \times 10^6 psi$	$72.40 \times 10^3 MPa$
Elongation to Break	4.8%	

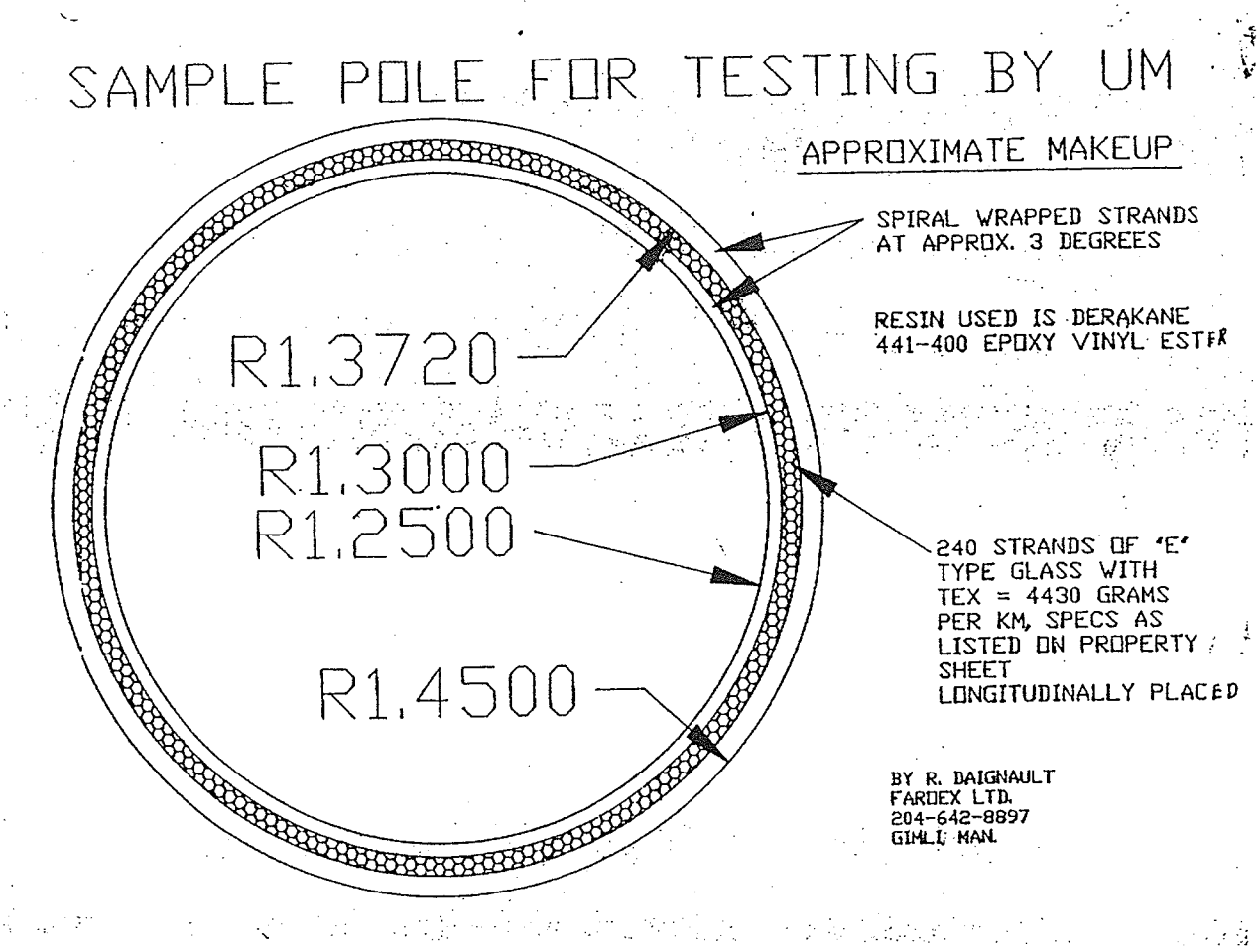

Fig. F-1. Cross-section of the test specimens

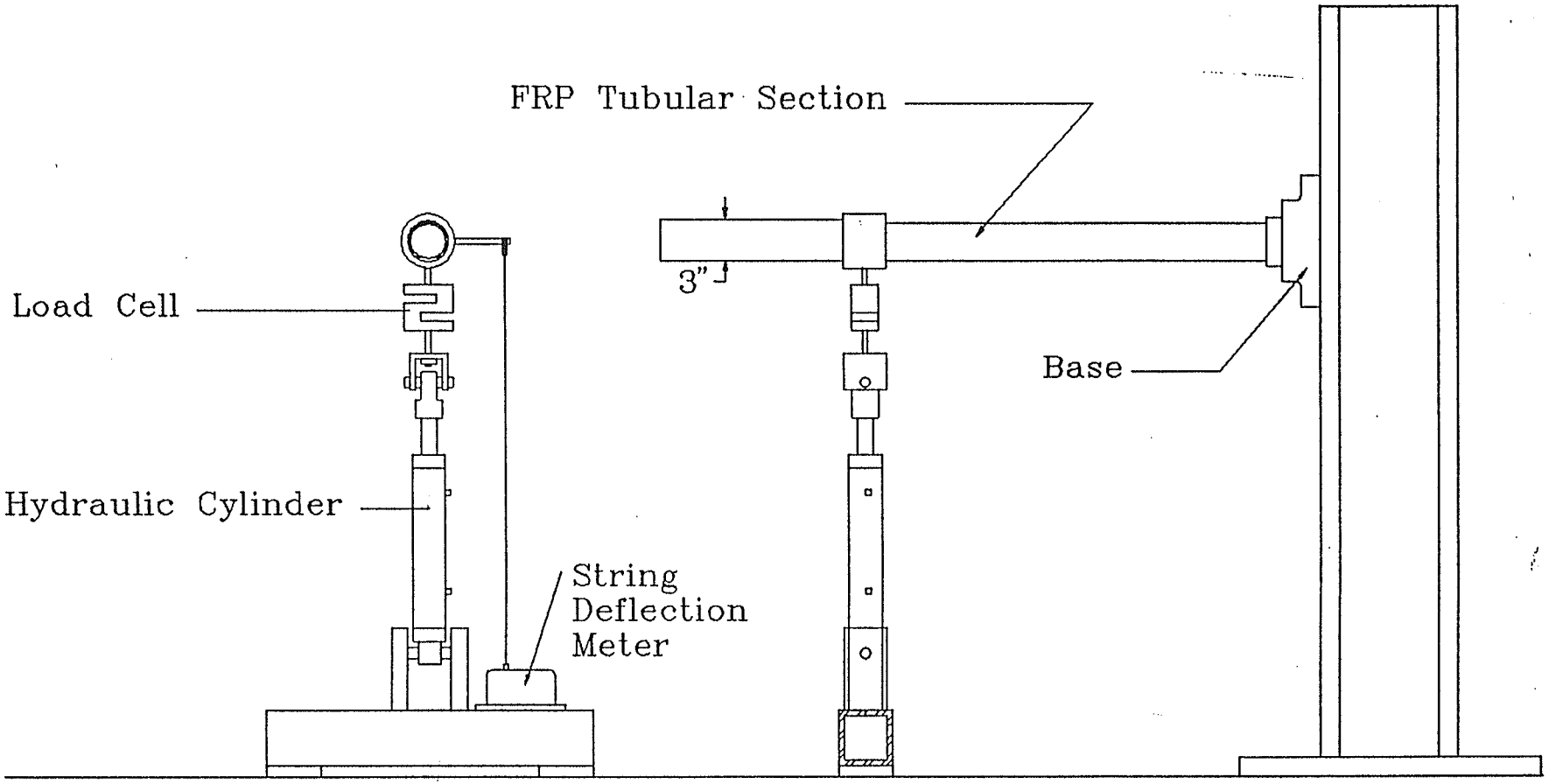
FRP Tubular Section
3"
Load Cell
Base
Hydraulic Cylinder
String
Deflection
Meter

Test Setup

List. F-1 Recorded Observations for Specimen #1, Test #1

- Initial checks made,
- Loadcell calibrated.....O.K.
- String deflection meter calibrated.....O.K.
- Preload to 100 lbs to ensure data acquisition system working properly.....O.K.
- Test Started.
- Halted test @ P=242.66 lbs, δ= 0.74 in.
  i) epoxy between collar and frp tube cracked.
- Test restarted.
- Halted test @ P=377.49 lbs, δ= 1.23 in.
  i) tube started to slip from the collar.
  ii) sounds of fibres breaking, no evidence.
- Restarted test
- Halted test @ P=466.07 lbs, δ= 1.53 in.
  i) more sounds of fibres breaking, no evidence.
- Test restarted.
- Halted test @ P=633.86 lbs, δ= 2.06 in
  i) Dr. Polyzois marked the slippage of the tube from collar.
- Restarted test.
- Halted test @ P=873.67 lbs, δ= 2.99 in.
  i) measured change in the outside diameter between the end and the base of the tube.
  Base, ϕ_b= 76.2 mm (3")
  End, ϕ_e= 75.2 mm (2.96")
- Test restarted.
- Slippage of the tube from the collar was observed
- Loading continued to P_{max}= 1211.28 lbs, δ_{max}= 5.42 in.
- Continued to induce more deflection, but the load plateaued after the maximum was reached.
- Test ended after the maximum stroke of the hydraulic cylinder was reached @ δ= 8.30 in.
- After the specimen was released from load, There was a permanent deformation observed of δ=3.25".
- End of test.

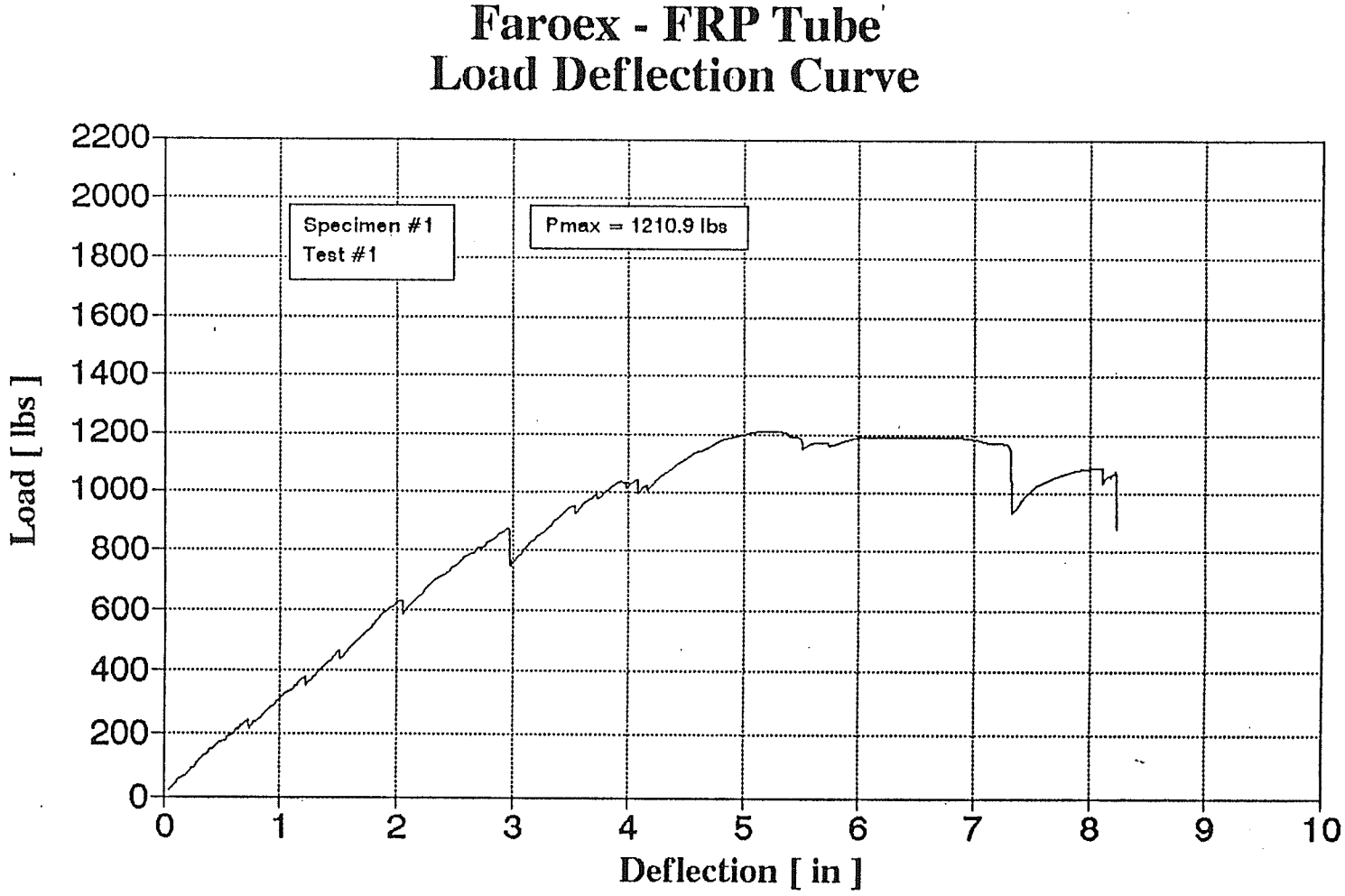

Fig. F-3. Load-deflection curve of Specimen #1, Test #1

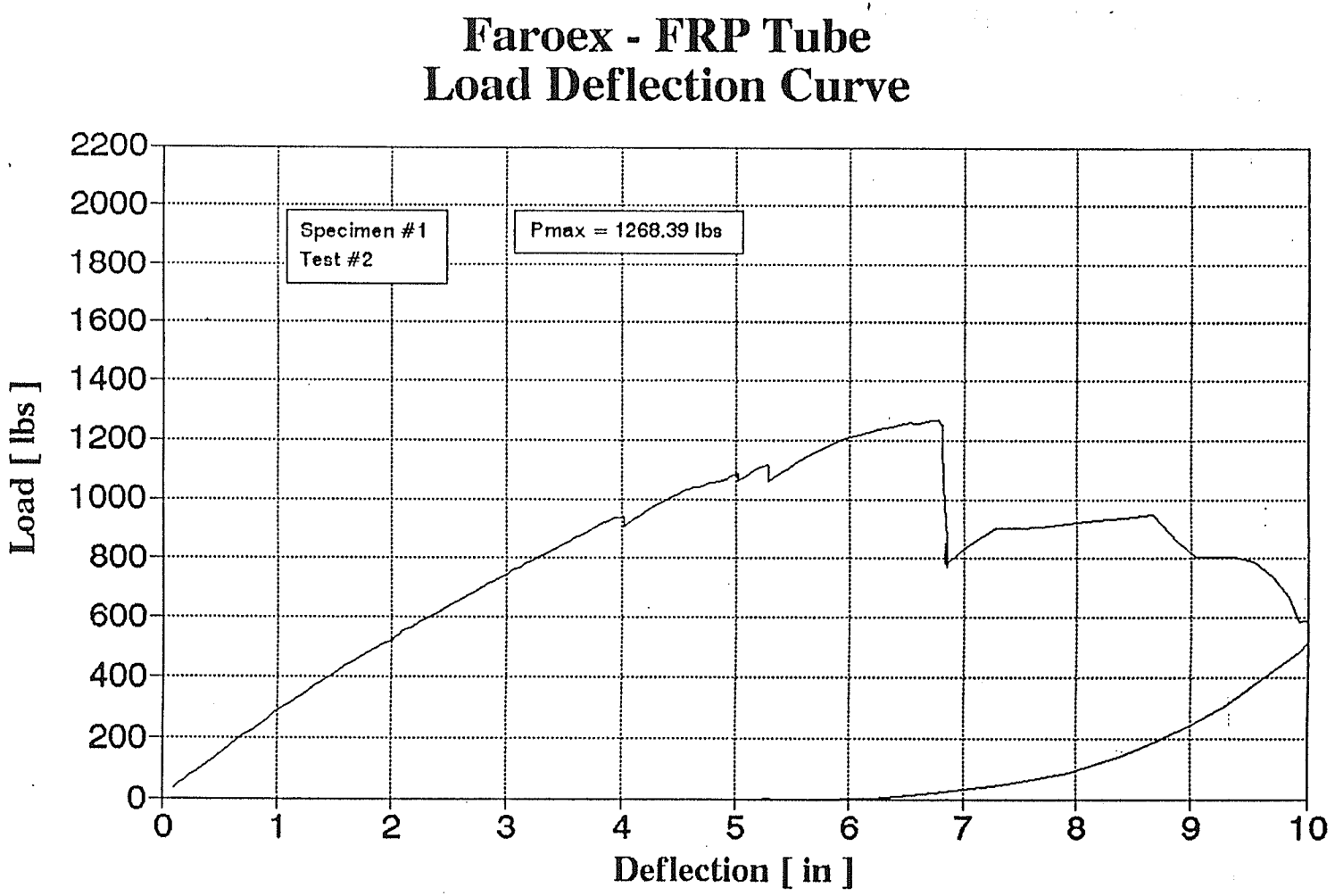

Fig. F-4. Load-deflection curve of Specimen #1, Test #2

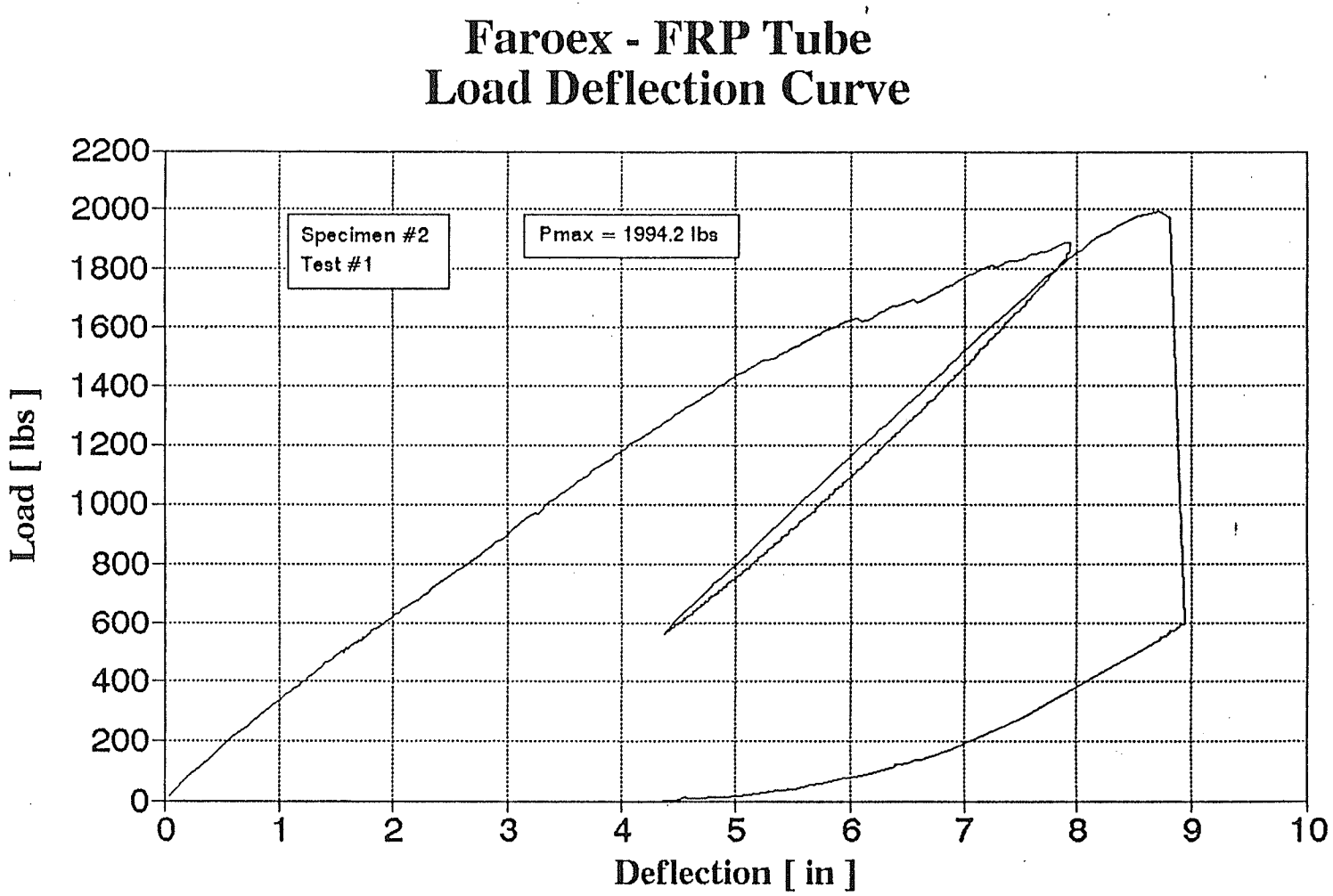

Fig. F-5. Load-deflection curve of Specimen #2, Test #1

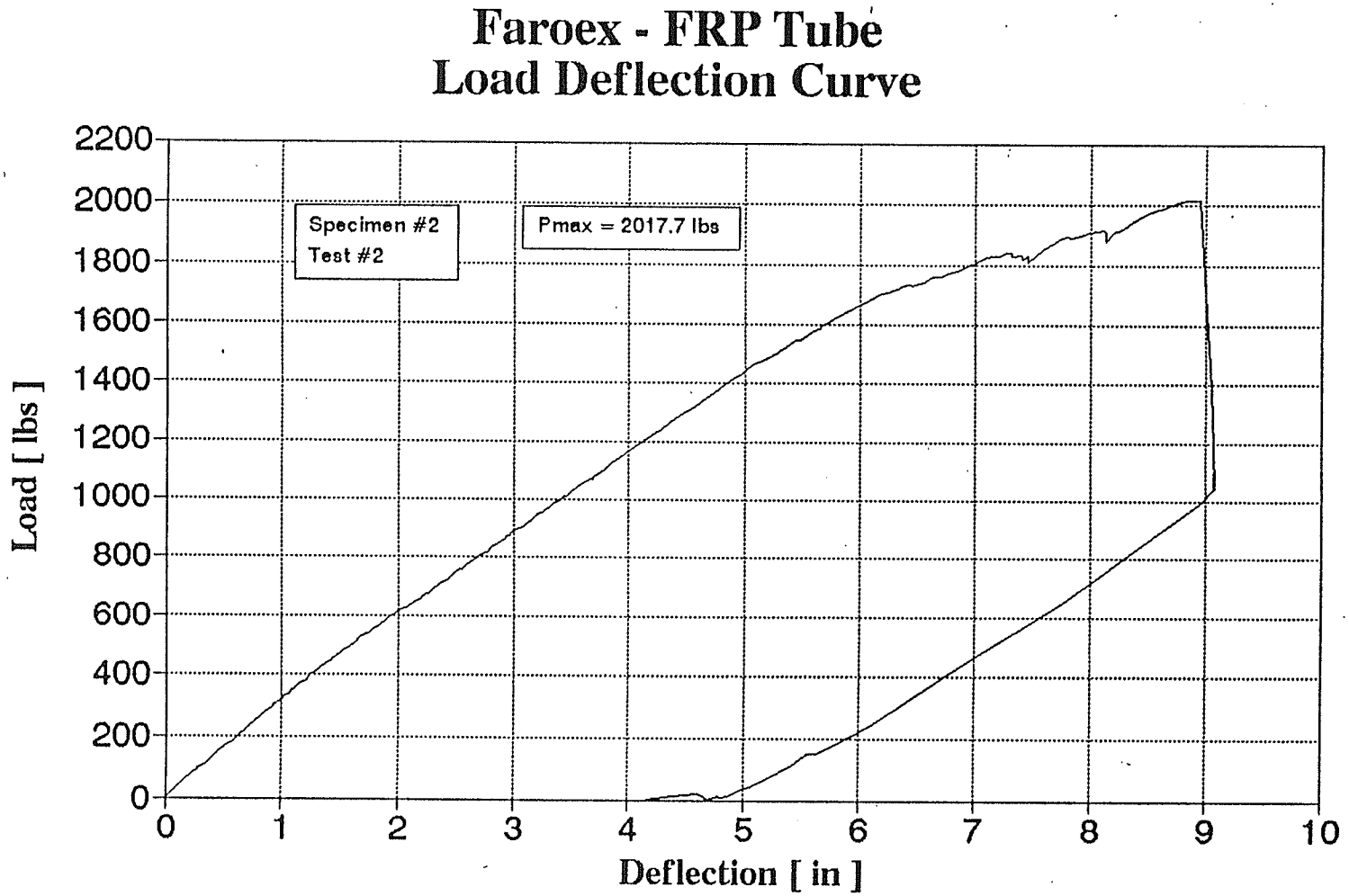

Fig. F-6. Load-deflection curve of Specimen #2, Test #2

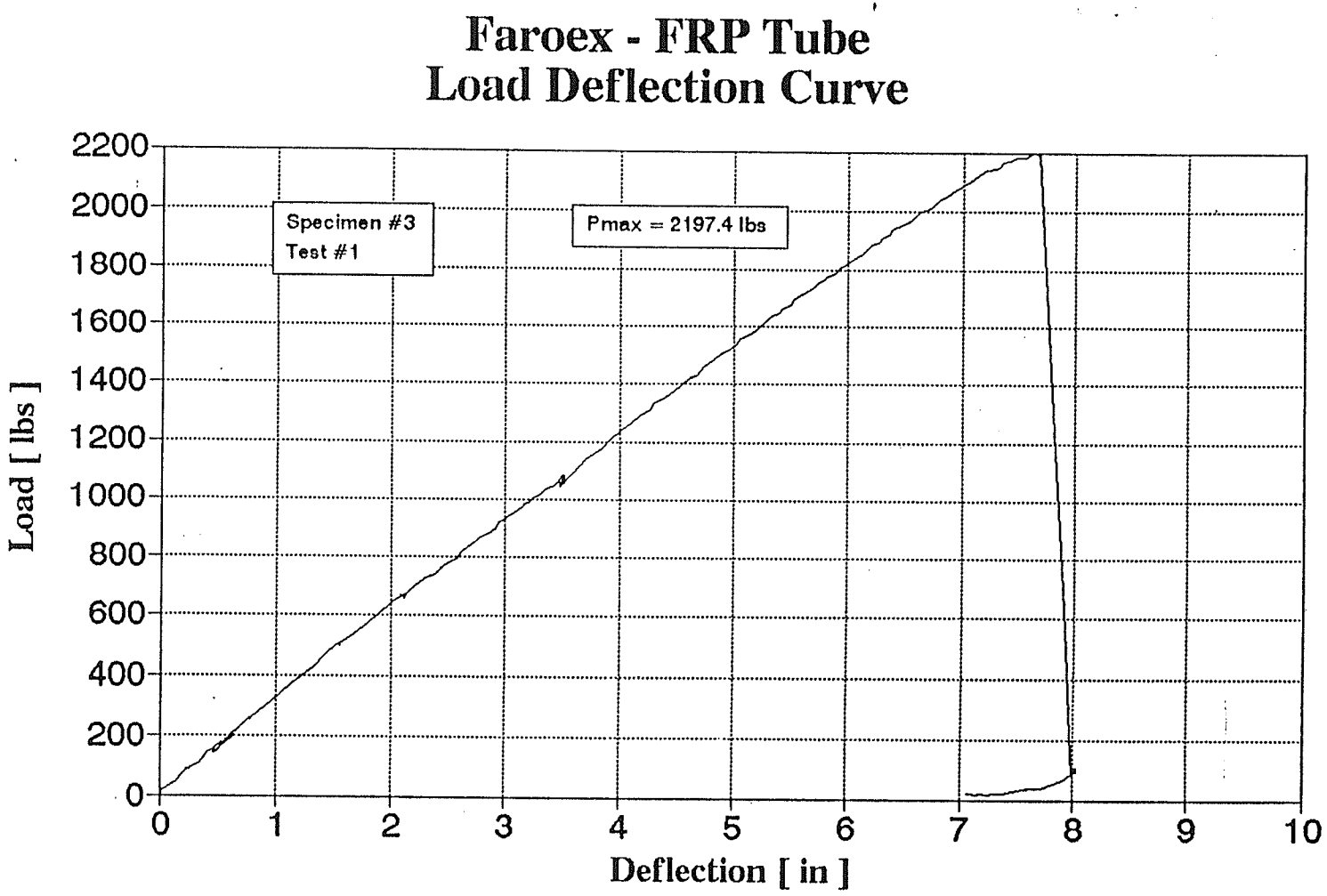

Fig. F-7. Load-deflection curve of Specimen #3

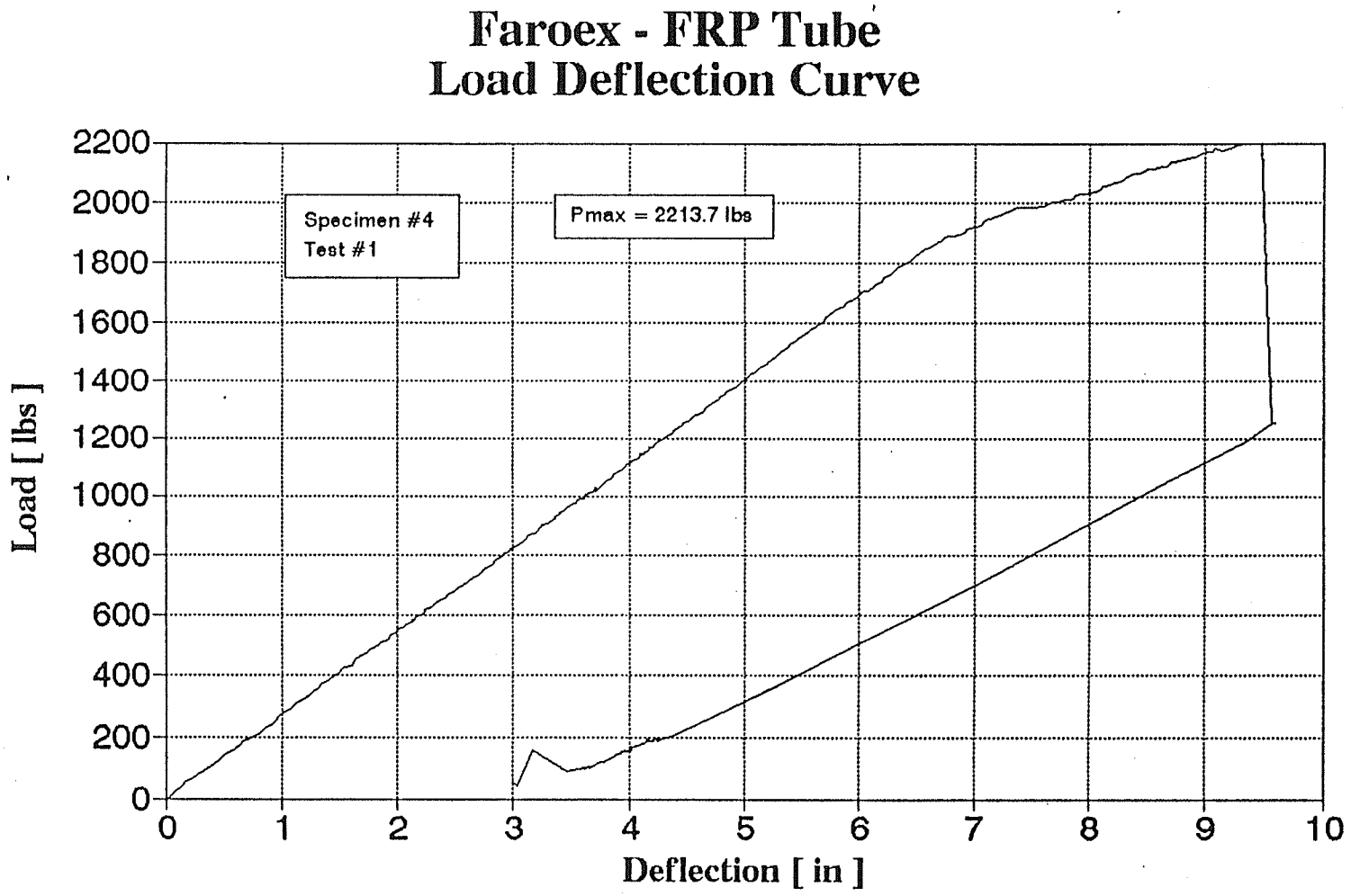

Fig. F-8. Load-deflection curve of Specimen #4

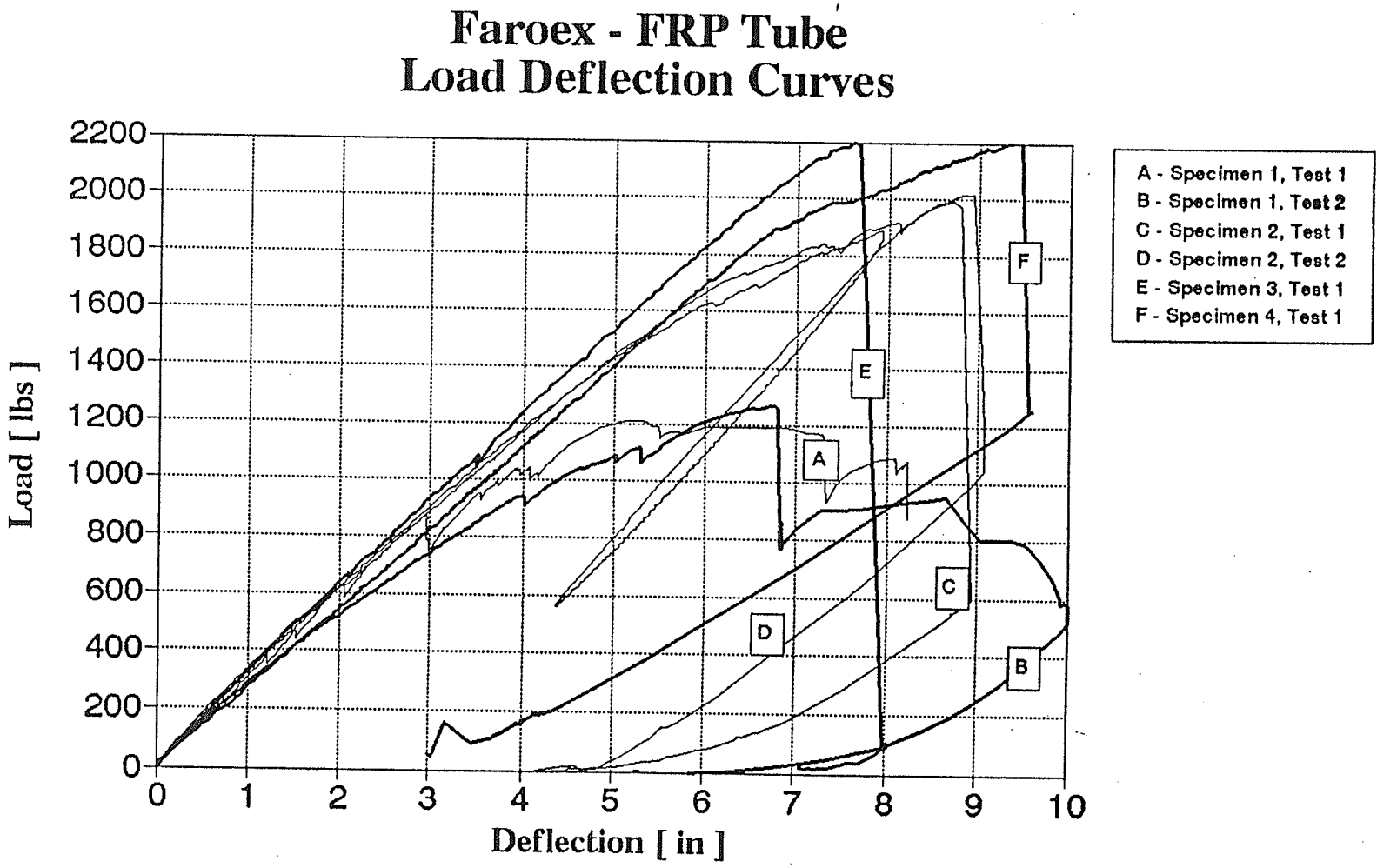

Fig. F-9. Load-deflection curves of all the six Specimens